A study of event-related electrocortical oscillatory dynamics associated with cued motor-response inhibition during performance of the Go/NoGo task within a sample of prenatally alcohol-exposed children and age-matched controls

Matthew M. Gerhold

Biomedical Engineering - Neuroscience

University of Cape Town

A thesis submitted for the degree of

Doctor of Philosophy

March 2017

Declaration

I, Matthew Michael Gerhold, hereby declare that this thesis is my own unaided work both in concept and execution and that apart from the normal guidance from my academic supervisors, I have received no assistance.

Signature of Candidate

Date

Acknowledgements

I would like to thank my thesis supervisor Prof Ernesta Meintjes for her encouragement throughout this project and for her financial support. I would also like to thank my co-supervisor Dr Colin Andrew for his support and guidance during the development of the analytical software used in this thesis, for his input and guidance through all of the analyses, and for assisting in the development of the manuscript. His attention to detail and depth of understanding in the field of biomedical engineering is remarkable. In addition, I would like to thank Profs Sandra and Joseph Jacobson for providing the demographic, psychometric and alcohol consumption data, as well as detailed information and insights regarding the participant sample. Profs Jacobson also assisted in developing the manuscript and provided expert advice related to fetal alcohol spectrum disorders. "The Jacobsons" are always willing to assist and I am very grateful for the contribution that they have made to this work. I would also like to thank Prof Chris Molteno for his input into the project. Last, but not least, I would like to extend my gratitude to students and friends in the Division of Biomedical Engineering—they made this journey a little easier.

Abstract

Fetal alcohol spectrum disorders (FASDs) are a spectrum of disorders that occur due to prenatal alcohol exposure (PAE). Response inhibition refers to the ability to inhibit/suppress a prepotent behavioural tendency set in motion during an experimental task. Our research explored neocortical processing in heavy-exposed children from Cape Town, South Africa, performing the Go/NoGo response inhibition task. We utilised event-related electroencephalographic methodologies to examine event-related potentials (ERP) and event-related changes in induced oscillatory power—event-related desynchronisation (ERD)/event-related synchronisation (ERS). Across visual and auditory Go/NoGo tasks, we observed equivalent levels of inhibitory control between heavy-exposed (HE) participants and normally-developing controls; however, HEs demonstrated significantly slower reaction times relative to the control group. In an auditory ERP study, we observed a number of alcohol-related changes in ERP waveform morphology, such as decreased P2 amplitude, reduced P3 amplitude, and longer P3 peak latency. In addition, within the HE group, late in the trials, a slow-wave component was observed in both experimental conditions. A significant difference in N2 amplitude across conditions that has consistently been observed in normally-developing samples was not observed in the HE group. We extended previous research findings in the visual domain by analysing induced oscillatory responses. We observed within the normally-developing sample: (1) in both experimental conditions, a frontal induced beta-band ERS related to decision-making; and (2) in the NoGo-condition, a frontal gamma-band ERS related to cognitive-control. Within the HE group, the beta-ERS was not observed in either of the experimental conditions, neither was the gamma-ERS observed in the NoGo-condition. Frontal induced beta-power was predictive of performance accuracy in the HE group, but not

in the control group. The observed alcohol-related effects were not explained and/or mediated by IQ (WISC-IQ), socio-economic circumstances, comorbid ADHD, or teratogenic effects related to postnatal lead exposure and prenatal cigarette-smoke exposure. Our results point to alterations in scalp-measured event-related neocortical oscillatory dynamics and slower processing of task demands due to heavy PAE. These alcohol-related effects are observable on ERP component measures, primarily related to conflict-monitoring and attention-based processing. PAE also affects induced classes of neocortical oscillatory dynamics related to decision-making and cognitive-control processes required to inhibit a prepotent motor-response.

Contents

4 The Effect of Heavy Prenatal Alcohol Exposure on Induced-Frontal Beta-Band Oscillations in Children Performing a Visual Go/NoGo Task

List of Figures

List of Tables

Abbreviations

Abbreviation	Description
AA	Absolute alcohol
AAR	Adaptive autoregression
ACC	Anterior cingulate cortex
ADHD	Attention deficit and hyperactivity disorder
AIC	Akaike's information criterion
AIC-AAR	AIC parametrised adaptive autoregressive model
AIC-C	Akaike's corrected information criterion
AR	Autoregression
AR-model	Autoregressive model
BCI	Brain computer interface
BIC	Bayesian information criterion
CDM	C.D. Molteno, Ph.D.
CI	Confidence interval
CMS	Common mode sense
CSD	Current source density
dB	Decibels
DBD	Disruptive behavioural disorders scale
DC	Direct current
DLPFC	Dorsolateral prefrontal cortex
DRL	Driven right leg

Abbreviation	Description
DSM-IV	The diagnostic and statistical manual of mental disorders 4th Ed.
DFT	Discrete Fourier transform
DTI	Diffusion tensor imaging
EEG	Electroencephalography
EP	Evoked potential
ERD	Event-related desynchronisation
ERP	Event-related potentials
ERS	Event-related synchronisation
FAS	Fetal alcohol syndrome
FASD	Fetal alcohol spectrum disorder
FDR	False discovery rate
fs	Sampling rate
G	Gain
Go/NoGo	Go NoGo response inhibition task
HE	Heavy exposed
HEH	H.E. Hoyme, M.D.
Hz	Hertz
JLJ	J.L. Jacobson, Ph.D.
ISI	Inter-stimulus interval
ITC	Inter-trial coherence
KLI	Kullback-Lieder Index
K-SADS	Schedule for affective disorders and schizophrenia for school aged children
LKR	L.K. Robinson, M.D.
log	Logarithmic
LPC	Late positive component

Abbreviation	Description
NK	N Khaole, M.D.
ML	Maximum likelihood
ms	Milliseconds
oz	Ounce
PAE	Prenatal alcohol exposure
PFAS	Partial fetal alcohol syndrome
PLV	Phase-locking value (inter-trial coherence measure)
POP	Preparing to overcome prepotency task
PPT	Progressive planning task
PSD	Power spectral density function
qEEG	Quantitative electroencephalography
REML	Restricted maximum likelihood
ROI	Region of interest
SES	Socio-economic status
SNR	Signal-to-noise ratio
STFT	Short-time Fourier transform
SWJ	S.W. Jacobson, Ph.D.
TFD	Time frequency distribution
TFR	Time frequency representation
uV^2	Microvolt
WCST	Wisconsin card sorting task
WISC-IQ	Wechsler's intelligence scale for children
Δ	Delta (difference between two numbers)

Preface

This thesis presents a series of event-related EEG studies that address the effect of prenatal alcohol exposure (PAE) on neocortical, event-related oscillatory dynamics during performance on the Go/NoGo response-inhibition task. The studies are a continuation/extension of previous work carried out by students, colleagues, and collaborators within the Division of Biomedical Engineering at the Department of Human Biology, University of Cape Town.

The thesis content consists of four independent articles that primarily address outcomes related to PAE within a developing sample. These articles explore event-related potentials in an auditory Go/NoGo study and build on published ERP findings using a visual Go/NoGo task. Our extensions using a visual task address hypotheses related to induced oscillations linked to cognitive processes that are pivotal for Go/NoGo task performance, such as decision-making and cognitive-control.

My contribution was in the form of developing a MATLAB based toolbox used for the analysis of experimental data. I also conceptualised all of the analyses, identified aims, and formulated hypotheses. I analysed the experimental data (and simulated datasets where applicable) and drew conclusions within each individual study, as well as drew overall conclusions based on the work as a whole. I also wrote and co-edited the manuscript.

I utilised the American Psychological Association's referencing system throughout the manuscript, but not its stylistic conventions. Due to the format of the thesis (a combination of independent articles) there is at times necessary repetition due to the recurring introduction, methods, results, and discussion sections. The thesis is structured as follows:

Chapter one states the main aims of the research and presents a literature review that covers key areas related to fetal alcohol syndrome, the experimental tasks used in the research, and the relationship between the disorder and performance on the experimental tasks. A summary of the methods and protocols are provided.

Chapter two is a simulation study wherein two time-varying spectral estimation routines are compared. The study deals with the estimation bias-variance trade-offs involved in time-frequency analysis. The analysis looks at condition contrasts and statistical masking applied to simulated and empirical EEG datasets, i.e. how condition contrasts are used to identify oscillatory features, and how different methodological approaches related to generating the contrasts can yield divergent results due to method-specific bias-variance trade-offs.

Chapter three is a study of induced gamma-band dynamics during performance on a visual Go/NoGo task. The study utilises the signal processing methodology presented in Chapter two. Induced gamma-band oscillations are linked to sub-processes of executive control that are responsible for the allocation of cognitive resources during task performance. We investigate the impact of PAE on cognitive-control linked scalp-measured gamma oscillations.

Chapter four is a study of induced beta-band dynamics during performance on a visual Go/NoGo task. The study utilises the signal processing methodology presented in Chapter two. Induced beta-band oscillations have been linked to decision-making processes during performance on the Go/NoGo task. We investigate the impact of PAE on decision-making linked scalp-measured beta oscillations.

Chapter five is an ERP study using an auditory Go/NoGo task. This study looks at event-related potentials (ERP), a different class of neocortical electrical activity. The study demonstrates the effect of PAE on ERP waveform morphology. The observed alcohol-related changes on ERP component measures provide an

understanding of the impact of PAE on executive functions involved in response-inhibition tasks.

Chapter six discusses the outcomes of the research across the different studies. The discussion deals with research outcomes in relation to previously published findings, and draws conclusions related to the impact of PAE on the electrical dimensions of human brain function—specifically in connection with performance on the Go/NoGo response inhibition task. We also provide suggestions for future studies, so as to address a number of limitations that became apparent during the course and scope of this research.

Parts of this work were presented at a regional biomedical engineering conference in the Western Cape in 2016:

> Gerhold, M. M., Jacobson, J. L., Jacobson, S. W., Meintjes, E. M. and Andrew, C. M. (2016, March). *A comparison of non-parametric and parametric spectral estimators*. Oral presentation at the 2nd South African Biomedical Engineering Conference, Stellenbosch University.
>
> Gerhold, M. M., Jacobson, J. L., Jacobson, S. W., Meintjes, E. M. and Andrew, C. M. A. (2016, March). *The effect of heavy prenatal alcohol exposure on induced gamma band oscillations in a developing sample performing the Go/NoGo task*. Poster session presented at the 2nd South African Biomedical Engineering Conference, Stellenbosch University.

Chapter 2 is currently under review at the *Journal of Computational Neuroscience*:

> Gerhold, M. M., Jacobson, J. L., Jacobson, S. W., Meintjes, E. M. and Andrew, C. M. (under review). A comparative analysis of time-varying Fourier and AIC-parametrised autoregressive spectral estimation methods applied to EEG event-related data. *Journal of Computational Neuroscience*.

Chapter 5 was published in January 2017 in *Alcoholism: Clinical and Experimental Research*:

> Gerhold, M. M., Jacobson, S. W., Jacobson, J. L., Molteno, C. D., Meintjes, E. M., & Andrew, C. M. (2017). An ERP study of response inhibition in the auditory domain in children with fetal alcohol spectrum disorders. *Alcoholism: Clinical and Experimental Research*, *41*, 96–106.

Chapter 1
Introduction

1.1 Prenatal Alcohol Exposure

Fetal alcohol spectrum disorder (FASD) is an umbrella term used to describe the range of disorders that have been linked to maternal alcohol consumption during pregnancy. Fetal alcohol syndrome (FAS) is the most severe manifestation along the spectrum and was first described by Kenneth Jones and David Smith in 1973. Jones and Smith describe FAS as a syndrome characterised by: central nervous system deficits, growth deficiencies, and craniofacial dysmorphologies (Jones & Smith, 1973). Facial dysmorphologies include: a flattened philtrum, a thin upper lip, flattened midface, and shortened palpabral fissures; thus, FAS patients have a unique and distinctive appearance. These distinctive dysmorphologies are coupled with a range of behavioural and cognitive deficits (Chudley *et al.*, 2005; Hoyme *et al.*, 2005) as well as changes in cortical structure and function (De Guio *et al.*, 2014; Fan *et al.*, 2016). In milder cases along the spectrum, the facial dysmorphologies do not present themselves, but cognitive-behavioural deficits occur in the context of altered/compensatory neurophysiological function (Fryer *et al.*, 2012; Mattson & Riley, 1998).

1.1.1 Executive Functions and Prenatal Alcohol Exposure

Executive functions are a collection of cognitive operations controlled from the prefrontal and frontal lobes of the brain that allow for intelligent, goal-directed behaviours. Throughout the research literature, FASD participants consistently show deficits on tasks that assess different aspects of executive function, such as planning, verbal fluency, attention, and working memory (Burden, Jacobson, & Jacobson, 2005; Kodituwakku, 2009; Spohr & Steinhausen, 2008). For example, Burden *et al.*, (2005) demonstrated that executive function as assayed by *The Wisconsin Card Sorting Task* (WCST) was significantly affected in the instance of FAS. Kodituwakku (2009) reported PAE related impairment on the *Progressive Planning Task* (PPT), a task that relies heavily on executive functions, specifically working memory function. The literature points to the fact that key cortical areas supporting executive functions within the frontal, temporal and parietal regions are often underdeveloped in the FAS population, accompanied by changes in regional metabolite utilisation during performance of cognitive tasks (Archibald *et al.*, 2001; Kodali *et al.*, 2017; Sowell *et al.*, 2002; Sowell *et al.*, 2001). Animal models of prenatal alcohol exposure (PAE) demonstrate ethanol induced lengthening of the cell-cycle linked to microencephaly and cortical hypoplasias at later stages of development (Gohlke, Griffith, & Faustman, 2008). In addition, a specific sensitivity of serotonergic-dependent frontal brain structures and associated pathways as well as serotonergic thalamocortical projections have been demonstrated in a rodent animal model of PAE (Zhou, Sari, & Powrozek, 2005). Serotonergic signalling in the frontal lobes is important to decision-making processes, a large component of executive function. In humans, changes in the features of the cerebral cortex related to cortical folding (less complex folding with wider sulci) have also been observed in heavy exposed participants (De Guio *et al.*, 2014). In addition, diffusion tensor imaging (DTI) studies have revealed changes in instances of heavy PAE within the structure of a number of cortical white-matter fibre tracts (Fan *et al.*, 2016). These fibre tracts play a pivotal role in functional integration within the

cerebral cortex during performance on experimental tasks (Wang, Li, Metzak, He, & Woodward, 2010; Wang, Zhang, & Liu, 2015). Cortical structural serotonergic frontal pathways and related brain structures are important to our research, as they are known to play a role in decision-making , an important feature in a number of executive control tasks and pivotal to performance on the Go/NoGo response inhibition task (Eagle, Bari, & Robbins, 2008; Eagle & Baunez, 2010; Homberg, 2012).

1.1.1.1 Response Inhibition and Prenatal Alcohol Exposure

Response inhibition (or more generally, inhibitory control) is a component of executive function and refers to a participant's ability to inhibit/suppress a response when cued to do so. The research findings are mixed in terms of the effect of PAE on inhibitory control. A study by Kodituwakku, Handmaker, Cutler, Weathersby, & Handmaker (1995) demonstrated that high-functioning children with FAS can perform as well as controls on simple versions of the Go/NoGo task, a response inhibition task with heavy dependence on conflict-monitoring, cognitive-control, and decision-making processes (Botvinick, Braver, Barch, Carter, & Cohen, 2001; Donkers & van Boxtel, 2004; Eagle *et al.*, 2008). Other studies have linked PAE to impairment of response inhibition on more challenging measures of inhibitory control, such as the Stroop Color-Word Test (Connor *et al.*, 2000; Mattson *et al.*, 1999). Studies by Burden *et al.* (2009, 2011) using a visual Go/NoGo task, demonstrated comparable inhibitory control between the FAS/PFAS and control groups; although within the FAS/PFAS group, significant amplitude and latency differences on a number of event-related potential (ERP) components were observed.

Burden *et al.* (2009, 2011) demonstrated PAE effects on the P2 ERP component. Differences in component amplitude between the Go- and NoGo-conditions were observed for normally-developing controls, but not for FAS/PFAS participants. In addition, FAS/PFAS participants had significantly longer P2-component latency (Burden *et al.*, 2009). This ERP component has been linked to processes that facilitate

discrimination between basic symbols. The N2 ERP component is also affected in the FASD population. Typically, the amplitude of the N2 ERP component is larger for the NoGo-condition than the Go-condition; however, this was not observed in Burden *et al.*, (2009): the N2 component amplitude was significantly reduced in the NoGo-condition within the FAS/PFAS group. The N2 ERP component is linked to response inhibition and conflict monitoring (Botvinick *et al.*, 2004; Donkers & van Boxtel, 2004). A non-human primate study conducted by Sasaki, Gemba, & Tsujimoto (1989) localised the current source-generator of the N2 ERP component to the bilateral prefrontal regions. In humans, the right ventrolateral prefrontal cortical regions have been cited as pivotal in response inhibition, while the preSMA and ACC are implicated in conflict monitoring processes (Chikazoe, 2010; Ipser, 2011; Mostofsky & Simmonds, 2008).

In Burden *et al.* (2009, 2011), the well-known P300 ERP component demonstrated the usual increased amplitude effects in the NoGo-condition compared to the Go-condition for FAS/PFAS participants and controls. The P300 is linked to attention and working-memory function (Polich, 2007). The P300 is also known to be a sensitive biomarker for alcoholism (Bauer, 2001; Begleiter, Porjesz, Bihari, & Kissin, 1984; Viana-Wackerman *et al.*, 2007). Burden *et al.*, (2009) observed that the P300 persisted as a late slow wave component in the heavy-exposed group. This was attributed to "increased cognitive effort", but is also likely to play a role in resetting of frontal-parietal attentional networks in preparation for the next trial.

The ERP waveform is known to arise from strongly phase-locked oscillatory activity across experimental trials. Other classes of cortical electrical activity exist, where changes in signal power are observed with inconsistent oscillatory phase across trials (weak phase-locking). These power changes in the EEG do not contribute to ERP waveform magnitudes and are referred to as *induced* oscillatory activity. The frequency and spatial-temporal properties of event-related induced oscillatory dynamics covary with a number of different cognitive functions (Klimesch, 1999; Klimesch, 2012;

Klimesch, Sauseng, & Hanslmayr, 2007). To-date, no studies have explored induced oscillatory power changes in the FASD population during performance on any experimental task. There are, however, studies in healthy adult samples performing the Go/NoGo task and within clinical populations characterised by frontal lobe dysfunction (Alegre *et al.*, 2004; Alegre *et al.*, 2006a; Alegre *et al.*, 2006b; Cho, Konecky, & Carter, 2006; Kieffaber & Cho, 2010; Minzenberg *et al.*, 2010; Shibata *et al.*, 1999). The studies of Alegre *et al.* (2004, 2006a) elicited an induced beta oscillation over the frontal regions of the scalp in both conditions of the Go/NoGo task. The authors linked the beta oscillation to decision-making processes. The studies of Cho *et al.* (2006), Kieffaber and Cho (2001), Minzenberg *et al.* (2010), and Shibata *et al.*, (1999) point to frontal induced gamma-band oscillations when inhibiting or selecting against a prepotency. These oscillations are not observed on the scalp of patients with frontal lobe dysfunction. As PAE is associated with underdeveloped structures and features of the cerebral cortex, and animal models point to changes in serotonergic dependent structures in the frontal regions as well as in thalamocortical relay circuitry, it is likely that the frontal beta oscillations are affected in the instance of PAE. As FAS patients have remarkable changes in frontal lobe structure and cortical white-matter, as well as demonstrate deficits on tasks that require frontal-lobe function, it is likely that cognitive-control linked induced gamma oscillations will also be affected by PAE.

1.2 Thesis Scope and Aims

The study of event-related neocortical oscillatory dynamics within the FASD population has focused exclusively on event-related potentials. The reported response inhibition/conflict-monitoring and attention linked ERP findings are all specific to the visual domain. Thus, it is not clear whether the reported ERP findings are modality specific, or are a more general class of observation independent of stimulus modality. Nothing is known about how PAE affects the neural mechanisms involved in generating induced scalp-measured oscillatory activity: there are no published

findings in this area. As the frequency and spatial-temporal properties of induced oscillatory activity are intimately tied to distinct cognitive processes, such studies are needed in addition to ERP research in order to better understand the impact of PAE on executive functions in general, but more specifically in relation to processes that support response-inhibition. Thus, we seek to: (1) assess if Burden *et al.*'s ERP findings are specific to the visual domain; (2) extend event-related induced oscillatory findings from healthy adult samples performing the Go/NoGo task into normally-developing preadolescent/adolescent samples—this is to verify the presence of these oscillations at earlier stages of human development; (3) based on extensions of induced oscillatory findings into normally-developing samples, we intend to assess if these oscillations are affected by PAE; and (4) we also intend to see if alcohol-related effects are independent of other confounding and/or mediating effects, such as intellectual abilities, socio-economic circumstances, comorbidity, and the effects of other teratogens such as postnatal lead (Pb) exposure and prenatal cigarette smoke exposure.

1.3 Methods

1.3.1 Participants

Our participants (children and mothers) were sampled from the Cape Coloured community in Cape Town, South Africa. Cape Town, and South Africa in general, has one of the highest prevalence rates of FAS in the world (Popova *et al.*, 2017). The Cape Coloured are descendants from a mixed ancestral lineage including European colonists, Malaysian slaves, Khoisan aboriginals, and the African Nguni ethnic group. Poor socio-economic circumstances and historical practices of compensating farm labour (in-part) with wine have contributed to a tradition of heavy recreational weekend binge drinking in a portion of this population. The specific characteristics of the samples (measurements associated with the children and mothers) are provided within the respective studies.

1.3.2 Tasks and EEG Recording

The experiments were simple implementations of the Go/NoGo experimental paradigm. Two versions of the experiment were used: visual and auditory. The details of the exact implementations of either task are provided within the methodology section of the respective chapters.

1.3.3 Independent Variables and Covariates

1.3.3.1 Prenatal Alcohol Exposure

Alcohol exposure was determined by an interview with the mother in her primary language (Afrikaans or English) regarding her alcohol consumption during pregnancy using a timeline follow-back approach (Jacobson, Chiodo, Sokol, & Jacobson, 2002). Volume was recorded for each type of beverage consumed on a daily basis, converted to absolute alcohol (AA), and averaged to provide a summary measure of alcohol consumption during pregnancy (AA/day). Based on alcohol consumption, our experimental groups were defined as: (1) *normally-developing, minimally-exposed controls* whose mothers did not drink during pregnancy or consumed alcohol less than one to two days per month and less than two standard drinks on any single occasion; and (2) *heavy-exposed* participants whose mothers drank heavily during pregnancy averaging 12 – 13 standard drinks per occasion, binging heavily over the weekend. The exception was the heaviest drinker who drank 19.2 standard drinks on a daily basis.

1.3.3.2 Movement versus Motor Response Inhibition

Our implementations of the Go/NoGo task consist of two experimental conditions: (1) the Go-condition (movement), wherein participants were required to press a button with their right index finger when cued to do so, and (2) the NoGo-condition (motor response inhibition), wherein participants are required to inhibit/withhold the motor-response.

1.3.3.3 Covariates and Additional Fixed Effects

Additional continuous measures and nominal categorical variables were included as control variables for potential confounding and possible mediating effects related to PAE: (1) child's age at EEG recording (in years); (2) ADHD diagnosis; (3) IQ assessed by Wechsler Intelligence Scale for Children (WISC-IQ); (4) mother's age at delivery (in years); (5) primary caregiver's education (in years); (6) postnatal lead exposure (Pb; μg/dl); (7) socio-economic status; (8) mother's marital status (married/not married), and (9) mother's cigarettes smoking during pregnancy (cigarettes per day).

1.3.4 EEG Event-Related Oscillatory Brain Measurements

1.3.4.1 Event-Related Potentials and Evoked Power

Evoked power changes are stimulus-locked changes in spectral power that arise due to strongly phase-locked activity across multiple experimental trials: within each single-trial, the phase of on-going neocortical oscillatory activity is reset relative to stimulus onset. Thus, across multiple trials one observes consistency of the oscillatory phase within certain frequency bands. This phase reset of the neocortical oscillation is spatially widespread across the cerebral cortex, thus distant cortical regions (via mechanisms of the thalamocortical relay circuitry) oscillate in-phase for a brief period of time resulting in the scalp-measured ERP waveform. The ERP waveform is the time-domain representation of a broad band, event-related evoked power response. On a cellular level, evoked oscillations arise from afferent innervation of cortical pyramidal cells from thalamic projections, leading to formation of cortical local field potentials based on the summation of excitatory post-synaptic potentials (Handy, 2004; Luck, 2012; Pfurtscheller & Lopes da Silva, 1999; Schomer & Silva, 2012).

In this study peak amplitude and latency measures of the P2-N2-P3 ERP waveform complex are utilised. Where peaks are not well-defined (specifically in the instance of late slow wave activity) we use an average within a predefined time-window. In

specific instances, we also utilise an ERP area measure, this measure is known to be more robust against noise compared to peak measures (Luck, 2012). We do not analyse evoked power, as analysis of evoked power does not offer any further discriminatory power between groups over and above the information in the ERP waveform (Andrew & Fein, 2010a).

1.3.4.2 Induced Power Features

An induced power change refers to a change in oscillatory power that is time-locked, but not phase-locked to stimulus onset; thus, across multiple experimental trials the phase at a given time-frequency point can be inconsistent. Event-related changes in induced oscillatory power are spatially well-circumscribed in comparison to the spatially widespread evoked-power/ERP changes. Rather than being driven by afferent innervation of the neocortex, changes in induced oscillatory power arise due to changes in membrane potential within the deep-brain components of the thalamocortical relay circuitry. Thus, deep-brain neural electrical activity modulates on-going oscillatory patterns within the cerebral cortex (Pfurtscheller, 2006; Suffczynski, Kalitzin, Pfurtscheller, & Lopes da Silva, 2001). Induced oscillatory power varies independently from evoked power and associated ERP time-domain measures, it is thus a distinct class of event-related neocortical oscillatory activity that provides unique information regarding the electrical dimension of human brain function (Andrew & Fein, 2010b). Induced power has been shown to covary with a number of cognitive processes including memory and attention (Klimesch, 1999; Klimesch, 2012).

In this study, induced oscillatory power is derived from an average of single-trial time-frequency distributions for each participant as well as for each experimental group. Our averaged time-frequency distributions are baseline corrected to reflect changes in oscillatory power relative to prestimulus baseline, i.e. we analyse relative power changes; these changes are referred to as "power changes" or changes in signal "power". The time-frequency distributions are derived using a short-time Fourier

transform and an adaptive autoregressive model (see Chapter Two for a detailed description of our use of these methods). In conjunction with the power analysis, we also analyse inter-trial coherence (ITC) measures to assess the strength of phase-locking underlying the observed changes in oscillatory power.

1.3.4.3 Inter-Trial Coherence Features

Phase information can be extracted from Fourier or wavelet coefficients (Delorme & Makeig, 2004; Tallon-Baudry, Bertrand, Delpuech, & Pernier, 1996). Using oscillatory phase information it is possible to compute univariate, inter-trial phase coherence (ITC) values in the form of an inter-trial phase-locking value—also known as a phase-locking factor (Tallon-Baudry *et al.*, 1996). This measure provides a normalised measure of the strength of phase-locked oscillatory activity across multiple trials at a given time-frequency point. The measure ranges from 0 – 1: 0 indicating no-phase locking and 1 indicating consistent phase across all trials. ITC is used to distinguish between induced and evoked power changes, i.e. strong phase-locked activity indicates an evoked response, while weak or no phase-locking provides evidence for an induced oscillation (Makeig, Debener, Onton, & Delorme, 2004).

In this study ITC measures are derived from an average of single-trial time-frequency distributions for each participant as well as across each experimental group. Our averaged time-frequency distributions are baseline corrected to reflect changes in ITC relative to pre-stimulus baseline.

Chapter 2

A Comparative Analysis of Time-Varying Fourier and AIC-Parametrised Autoregressive Spectral Estimation Methods applied to EEG Event-Related Data

Matthew M. Gerhold[1], Joseph L. Jacobson[1,2,3], Sandra W. Jacobson[1,2,3], Ernesta M. Meintjes[1] and Colin M. Andrew[1,4]

[1]Division of Biomedical Engineering, Department of Human Biology, University of Cape Town, South Africa; [2]Department of Psychiatry and Behavioural Neurosciences, Wayne State University School of Medicine, Detroit, MI, United States; [3]Department Psychiatry and Mental Health, University of Cape Town; South Africa; [4]Essentric Technology, Cape Town, South Africa.

Abstract

There are a host of methods, non-parametric and parametric, available to researchers for the purposes of EEG event-related spectral analysis. However, these methods provide varying degrees of time-frequency resolution, leading to different representations of the signal's components in time and frequency. In order to understand how differences in component representations can contribute to statistical outcomes in an EEG event-related analysis, our study compares and contrasts time-

frequency distributions from a short-time Fourier transform (STFT) and an adaptive autoregressive (AAR) model parametrised using Akaike's information criterion (AIC). We utilise simulated data and analyse the resultant distributions of spectral power in terms of: (1) the estimation bias-variance trade-offs that are made and (2) how these trade-offs influence component representations in time and frequency, demonstrating that the AIC-AAR model, relative to the non-parametric STFT estimator, provides better frequency resolution but poorer temporal resolution. We then perform an analysis of EEG event-related data from participants performing the Go/NoGo task. Within our empirical data analysis, we show that due to the enhanced frequency resolution and reduced temporal resolution, the AIC-AAR model can suppress important short-duration, narrow-band oscillatory events that differentiate experimental conditions; alternatively, it can enhance trivial oscillatory bouts, in both instances leading to errors in statistical inferences. We conclude that when performing spectral analysis in the context of EEG event-related studies, researchers need to exercise an awareness of the many trade-offs offered by a chosen method; specifically, how these trade-offs influence component representations and downstream statistical inferences.

2.1 Introduction

A research area within EEG signal-processing that has received some amount of attention is the comparison of linear parametric and non-parametric approaches to EEG event-related spectral analysis (Allen & MacKinnon, 2010; Principe & Brockmeier, 2015; Tarvainen, Hiltunen, Ranta-aho, & Karjalainen, 2004; Wang, Veluvolu, & Lee, 2013; Zhang, Hung, & Chan, 2011). These studies emphasise the improvements made with parametric approaches relative to existing non-parametric methods, but do not necessarily explore potential issues related to statistical inferences when time-frequency distributions (TFDs) of spectral power from multiple experimental conditions are compared. We seek to address this niche, answering questions regarding comparative representations of signal components in time and frequency, and time-frequency properties of composite distributions used to compare two experimental conditions, such as distributions of difference scores (Condition 2 – Condition 1) and associated probabilities. For instance, if we assume linear dependencies across time in the electroencephalogram, appropriate parametrisation (in terms of model order selection for parametric approaches), and equivalent scaling of power spectral densities yielded by either approach, are the time-frequency distributions of autoregressive spectra parametrised using Akaike's information criterion (AIC) and time-varying Fourier-based estimates equivalent? Specifically, (1) are the same components represented in the time-frequency distribution and (2) are common components represented equivalently in time and frequency? In the instance of datasets where two experimental conditions are present and time-frequency contrasts between conditions are analysed, (3) are there differences between the composite distributions yielded by the two approaches? If differences exist, (4) what are they and how do they potentially affect study outcomes?

In the instance of EEG event-related analysis, one is faced with the analysis of a non-stationary stochastic process (Glavinovic, Gooria, Aristizabal, & Taghirad, 2008;

Kaplan, Fingelkurts, Fingelkurts, Borisov, & Darkhovsky, 2005; Thakor & Tong, 2004; Ting, Salleh, Zainuddin, & Bahar, 2011). Quantitative approaches to electroencephalography predominantly focus on spectral content in terms of power spectral densities. Amongst a host of methods, sliding window parametric and non-parametric approaches are available for such analysis (Cohen, 2014; Delorme & Makeig, 2004; Florian & Pfurtscheller, 1995; Kiebel, Tallon-Baudry, & Friston, 2005; Oostenveld *et al.*, 2010; Pardey, Roberts, & Tarassenko, 1996). These approaches involve windowing local regions of the signal to ensure stationarity and then conducting some form of spectral decomposition on the windowed signal. The analytical window is slid across the signal to yield a time-frequency distribution of spectral power. In these approaches, the choice of window length is key, as it effects a trade-off between the temporal and frequency resolution of the resultant time-frequency distribution: short-window lengths provide high temporal resolution while yielding low frequency resolution, lengthening the window leads to the opposite effect. In signal processing this trade-off is referred to as the *uncertainty principle* and is a pivotal factor in spectral analysis of non-stationary data (Gabor, 1946; Marple, 1986; Sörnmo & Laguna, 2005).

Sliding window autoregressive approaches have additional parameters that lead to estimation bias-variance trade-offs and contribute to the localisation of components in time and frequency. For instance, selecting an appropriate model order is a matter of negotiating an estimation bias-variance trade-off that takes place within the frequency domain, but can also affect the temporal dimension of the signal. Higher model orders provide reduced bias, greater dynamic range, and enhanced frequency resolution relative to a spectrogram computed from the same windowed data wherein a taper has been applied. However, excessively high model orders can result in overfitting, leading to shifting and splitting of peaks as well as introducing spurious peaks into the spectra. Low model orders may lead to narrow band phenomena being smoothed

out in the resultant spectra. This is due to a large estimation bias that leads to reduced dynamic range and poor resolution (Sanei & Chambers, 2007).

EEG event-related spectral analysis is primarily concerned with changes in neocortical oscillatory dynamics elicited by a repetitive stimulus that requires the participant to respond according to a predefined stimulus-response set. Often a stimulus-response set will define multiple experimental conditions across which behavioural responses and changes in spectral power are compared. Event-related changes in spectral power are referred to as *event-related desynchronisation* (ERD) or *event-related synchronisation* (ERS). The latter refers to an increase in spectral power relative to prestimulus baseline, while the former, a decrease (Hu, Xiao, Zhang, Mouraux, & Iannetti, 2014; Pfurtscheller & Lopes da Silva, 1999). Changes in spectral power can be further classified as *evoked* or *induced.* Evoked power changes are stimulus-locked increases in spectral power that arise from strongly phase-locked activity across multiple trials within a single channel. The alignment of phase across trials within a given frequency band results in an observed increase in band power; these spectral perturbations are observed as widespread across the scalp. An induced power change refers to a change in oscillatory power that is time-locked, but not phase-locked to stimulus onset; they arise from changes in deep brain control parameters that regulate neocortical oscillatory activity (Pfurtscheller, 1992; Pfurtscheller & Lopes da Silva, 1999). Evoked and induced classes of neocortical oscillatory activity are believed to arise due to different underlying neurophysiological processes. Evoked oscillations arise from afferent innervation of cortical pyramidal cells, leading to formation of local field potentials based on the summation of excitatory post-synaptic potentials (Handy, 2004; Luck, 2012; Schomer & Silva, 2012). Induced oscillations arise due to changes in membrane potential within the deep-brain components of the thalamocortical relay circuitry, resulting in changes in oscillatory patterns within the neocortex (Pfurtscheller, 2006; Suffczynski *et al.*, 2001).

A short-time Fourier transform (STFT) is a non-parametric approach to time-frequency analysis and has been widely utilised throughout the literature in the analysis of EEG event-related datasets. When applying a STFT, the overall signal is divided up into smaller, stationary, fixed-length segments that may or may not be overlapping. This is achieved by applying a fixed length window at the start of the signal and sliding the window across the length of the entire signal. In the process, complex-valued Fourier coefficients are derived from the windowed segments by applying a discrete Fourier transform (DFT). Non-parametric Fourier-based spectral estimation may require the application of a taper function to the data within the sliding window. This brings into play an estimation bias-variance trade-off wherein incurring bias influences frequency resolution and dynamic range over-and-above the choice of window length. This yields a time-frequency distribution of spectral power that is referred to as a *spectrogram*. One may choose to express the spectrogram in linear or log scales (Sörnmo & Laguna, 2005). Often in EEG event-related analysis multiple trials are available and time-varying estimates are averaged across trials; such averaging provides a reduction in the variance of the spectral estimates. Within the sliding window based approaches to ERD/ERS analysis, besides window length providing a trade-off between temporal and frequency resolution, it also sets the lower bound of the analytical bandwidth: at least one cycle of the lowest frequency must be represented in the windowed segment to allow for meaningful analysis.

Phase information can be extracted from the Fourier coefficient matrix obtained from the sliding window spectral decomposition (Delorme & Makeig, 2004; Tallon-Baudry *et al.*, 1996). Using phase information it is possible to compute univariate, inter-trial phase coherence (ITC) values in the form of a phase-locking value or coefficient. This measure provides an index of the strength of phase-locked activities across multiple trials at a given time-frequency point. The measure ranges from 0 – 1: 0 indicating no-phase locking and 1 indicating consistent phase across all trials. ITC is used to distinguish between induced and evoked power changes: strong phase-locked

activity indicates an evoked response, while weak or no phase-locking across trials provides evidence for an induced oscillation (Makeig *et al.*, 2004).

Adaptive autoregression (AAR) is a parametric-based approach to time-frequency analysis wherein linear dependencies across time within a locally windowed signal are modelled as a finite set of coefficients. The coefficients are allowed to vary with time by estimating a set of AR-parameters within consecutive fixed-length, stationary segments (Florian & Pfurtscheller, 1995). Autoregressive modelling of stationary, windowed time series data requires one to estimate the order of the model, and then to compute the model coefficients and residual errors using one of a number of different algorithms, such as Ordinary Least-Squares, Levinson-Durbin Recursion, or Burg's algorithm (Pardey *et al.*, 1996; Sörnmo & Laguna, 2005). The power spectral densities for each window are computed from the AR-coefficients as well as the estimated variance of the model's residual errors (Florian & Pfurtscheller, 1995; Pardey *et al.*, 1996; Thakor & Tong, 2004; Zetterberg, 1969). In the AAR approach, the model order parameter can be related to how many spectral peaks are available in the resultant AR spectrum to represent the underlying spectral components of the signal: increments of two in model order add an additional spectral peak to the AR spectrum (Sörnmo & Laguna, 2005). Thus, an order of 20 would yield an AR spectrum with ten available peaks to represent the spectral components of the modelled signal. The upper bound for model order is based on a heuristic: $p < N/3$, where p is model order and N is signal length; however, in practice, the estimated model order is normally much lower than the prescribed upper bound (Marple, 1986). For example, brain computer interface (BCI) applications that classify estimated AR-coefficients (as opposed to spectral features) use lower model orders, $p = 5$ or $p = 6$, to model slow changing properties of the electroencephalogram (Anderson, Stolz, & Shamsunder, 1998; Keirn & Aunon, 1990; Schlögl, Flotzinger, & Pfurtscheller, 1997). Sörnmo & Laguna (2005, *p.* 119) recommend using higher model orders when more detailed (higher resolution) spectra are required, as in the instance of event-related spectral analysis. There are a

number of approaches to model order selection including information theoretic approaches and cross-validation (Bergmeir & Benítez, 2012; Costa & Hengstler, 2011; Hastie, Tibshirani, & Friedman, 2009). Information theoretic approaches are often utilised in quantitative electroencephalography (qEEG). These can include, but are not limited to: Akaike's information criterion (AIC), Akaike's information criterion corrected (AIC-C), and Bayesian information criterion (BIC) (Akaike, 1974; Schwarz, 1978; Sugiura, 1976).

Akaike's information criterion is an information criterion that is rooted in asymptotic theory. Formally, AIC is an asymptotically unbiased estimator of the expected *Kullback-Liedler index* (KLI) of the estimated model. Under asymptotic approximations AIC is an accurate estimator of KLI, however, this estimate becomes inaccurate for finite samples, more so with increasingly complex models (De Waele, 2003). In finite samples, AIC's deviation from its asymptotic expected behaviour is known as the *finite-sample effect*. Specifically, AIC underestimates KLI and as such misrepresents the quality of the estimated model, i.e. how well the estimated model describes the true data-generating process. Practically speaking, such parametrisation in finite samples leads to an over-fitted model. It results in greatly reduced residual variance, but increases the out-of-sample prediction errors beyond the bounds of what would be considered objectively as an optimal prediction. In the frequency domain, this overfitting has an impact on bias-variance trade-offs related to estimation of spectral quantities. Overfitting in terms of spectral estimates results in peaks within the spectrum splitting and shifting as well as the introduction of spurious peaks. Often a correction is implemented to counteract finite sample effects associated with AIC in the form of the corrected Akaike's information criterion (AIC-C), which can provide a more accurate estimate of KLI in finite-samples.

In this study, our intention is to compare Fourier and AIC-parametrised autoregressive spectral estimation approaches. This intention translates into two main aims. The first main aim is to compare and contrast the properties of STFT and AIC-

AAR time-frequency distributions using a multi-trial simulated dataset, wherein a ground-truth is clearly defined in order to understand the relative properties of each distribution. Specifically, how each estimator represents simulated signal components along: (1) the frequency dimension, in terms of representative bandwidth vs actual simulated bandwidth; and (2) the temporal dimension, in terms of rise and decay times relative to a simulated benchmark. This will enable us to better understand and interpret time-frequency distributions of electrophysiological data acquired under experimental conditions. In these instances, a ground-truth is not available and researchers may not be fully aware of how a specific spectral estimator may shape and influence analytical outcomes. A focus on statistical outcomes using empirical data from participants performing an event-related behavioural task (the Go/NoGo task) translates into our second main aim: to compare and contrast event-related spectral power between experimental conditions (Go vs NoGo) using short-time Fourier transform and univariate, Akaike-parametrised adaptive autoregressive (AIC-AAR) time-frequency estimators. We look at the data in terms of time-frequency distributions of difference scores (NoGo - Go) as well as look at probability contrasts based on paired-sample *t*-tests within the time-frequency domain. We compare and contrast the oscillatory components that differentiate experimental conditions across methods. Our goal is to compare methods in terms of the spectral components estimated, in order to assess if the information obtained from each method is comparable, and to what extent the two methods differ.

We expect that the two methods will estimate common oscillatory information; however, components identified by either method will have different specifications in time and frequency. Either method may produce Type I or Type II statistical errors in their respective probability contrasts (NoGo - Go) due to different specification of components in time and frequency.

2.2 Simulated Data Analysis

2.2.1 Simulated Data

We followed a similar simulation approach used in Allen & MacKinnon (2010) and Zhang *et al.* (2011). Two datasets were synthesised, each containing one-hundred 1750 millisecond trials at a sampling rate of 128Hz. Within the trials, an imaginary stimulus onset occurred at 750ms, thus dividing the simulated trials into a 750ms "baseline-period" followed by 1000ms of "post-stimulus" activity (see Table 2.1 for details of the simulated datasets).

Table 2.1: Signal components in the simulated datasets.

Condition	Component	Frequency	Power Change	Onset (seconds)	Offset (seconds)
1	1	10Hz	↑	0.250	0.750
	2	15Hz	↓	0.750	1.250
	3	35Hz	↑	0.000	1.000
	4	55Hz	↑	0.250	1.250
2	1	4Hz	↑	0.000	1.000
	2	25Hz	↑	0.250	1.250
	3	40Hz	↑	0.875	1.180
	4	45Hz	↓	0.500	0.875

Note: Onset and offset times are in seconds, formatted in decimal. Onset and offset times are measured relative to "stimulus-onset". Power changes are measured as a change relative to baseline power levels.

Each trial was composed of four sinusoidal components whose initial-phase was randomised across trials as well as within each trial: phase was randomised between 0 to 2π following a uniform distribution. The components were synthesised in such a manner that they had a sudden onset and sudden offset and a mixture of increases and decreases in spectral power occurring relative to the baseline period within each trial. The resultant signals have Gaussian white-noise added to them to yield an SNR of

approximately 5 dB. The time course of each trial is structured as follows (see Figure 2.1. Templates for the simulated datasets).

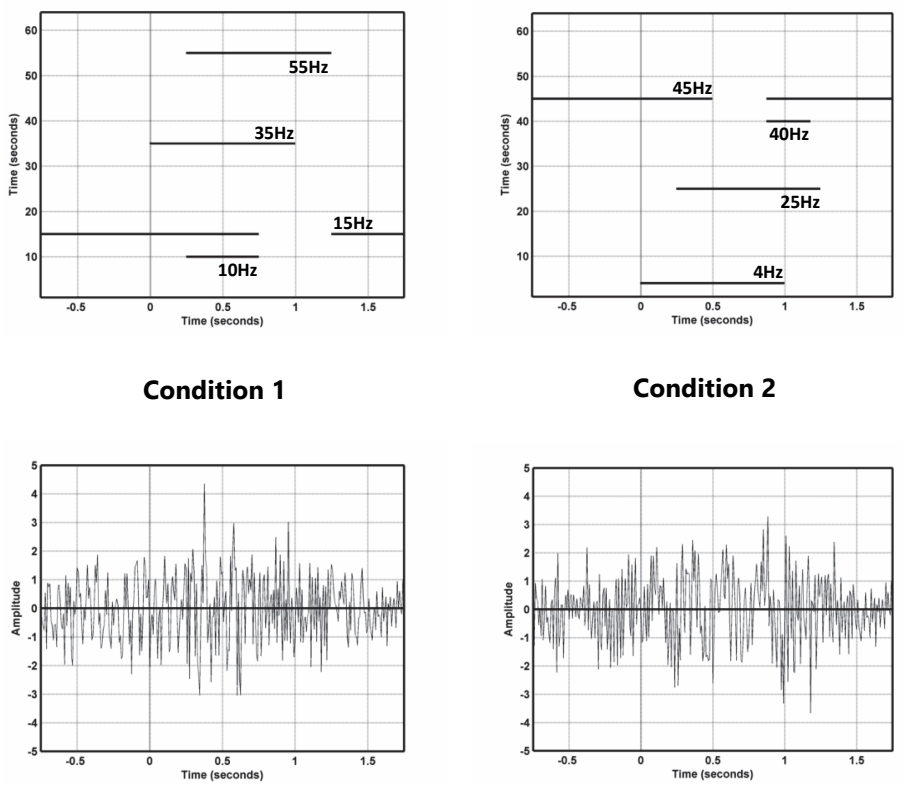

Figure 2.1: Templates for the simulated datasets. The upper left panel contains the template for the trials for Condition 1; the lower left panel contains a single realisation from the simulated dataset. The upper right panel contains the template for the trials for Condition 2; the panel beneath it contains a single realisation from the simulated dataset.

2.2.2 Time-Frequency Analysis

Single-trial short-time Fourier transform (STFT) and AIC-adaptive-autoregressive (AIC-AAR) time-frequency distributions were generated using an in-house MATLAB based toolbox. The toolbox implements a number of different time-frequency estimation algorithms for the purposes of EEG event-related analysis. For the STFT and AIC-AAR-based approaches, 500ms windows were used with the window slid by a single sample point. When using the STFT approach, a hamming window was

applied to the data. No windowing was applied to the data when using the AAR-based approach as the power spectral density (PSD) estimates are derived from the model coefficients and not from the data itself; thus discontinuities at the start and end of data segments do not influence the PSD estimates as they would in a STFT approach (Marple, 1986; Pardey *et al.*, 1996). In the instance of the AAR time-frequency distributions, wherein model order must be estimated, the minimum AIC taken across multiple intra-trial time-windows was used to determine model order. Power spectral densities were extracted for each single-trial, converted to logarithmic scale (relative power) and baseline corrected; single-trial data was then averaged across trials.

2.2.2.1 AAR Model Order Selection

The AIC taken across multiple intra-trial time-windows as well as the distribution of AIC minima across all windows for both simulated conditions are presented in Figure 2.2. The minima identified across all windows for Condition 1 was p = 20 (AIC = -11.07), which also equates to the mode of the distribution of AIC minima across all windows tested. We tested to see that closely spaced components were resolved and if any shifting and splitting of spectral peaks had occurred within the frequency domain by checking spectra generated using model orders around the selected order, i.e. p = 16, p = 18, p = 22, and p = 24. None of the higher order models (p > 20) changed the locations of the spectral peaks within the frequency domain—there was no splitting of spectral peaks. The only observable difference was that the closely spaced components appeared to be better resolved. For the lower model orders, closely spaced components were not as well resolved (see Appendix A – Compare Peaks AIC-AAR). It is also evident when consulting the plot in the top left panel of Figure 2.2, at around a sixth order model (AIC = -5.63), much of the variance in the data could be explained; however, such a parametrisation would only provide three spectral peaks within the AR spectra to represent the simulated signal's components.

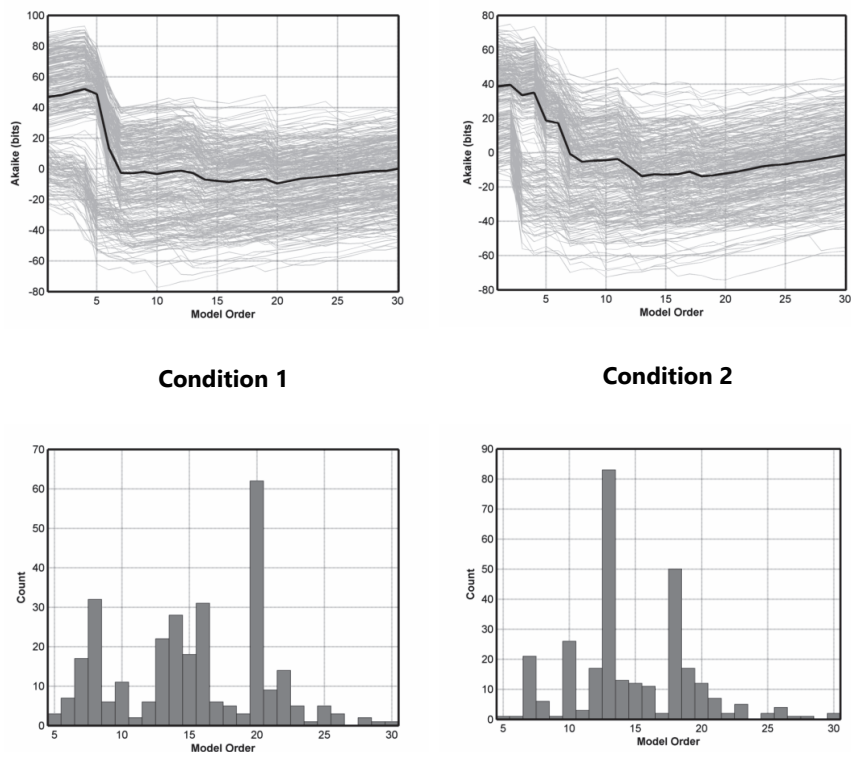

Figure 2.2: Results of the model order selection routine using AIC. The left column is the AIC-criterion for simulated Condition 1: (top left panel) AIC computed across a range of model orders for each window (grey lines) and the average criterion across all windows (black line); (bottom left panel) the distribution of AIC minima across the range of model orders tested. The right column is the AIC-criterion for simulated Condition 2: (top right panel) AIC computed across a range of model orders for each window (grey lines) and the average criterion across all windows (black line); (bottom right panel) the distribution of AIC minima across the range of model orders tested.

In the Condition 1, three spectral peaks would not allow one to resolve the closely spaced components at 10Hz and 15Hz. Additional lags must be added to the model to be able to resolve these closely spaced components; thus, the necessity for a higher model order, as indicated when using the AIC criterion for model order selection. Based on the above observations, an adequate parametrisation that allows one to resolve closely spaced components is situated between p = 16 – 20; although, higher model orders that were checked (p > 20) did not cause observable changes in component spectral peak locations due to bias-variance trade-offs within the frequency domain.

In terms of Condition 2, the minima identified across all windows was p = 18 (AIC = -14.8). This value was higher than any of the descriptive statistics characterising the central tendency of the distribution of AIC-minima across windows. For example, the median AIC-minima was p = 13, the mode of the distribution was also p = 13. We checked to see if this model order was adequate—even though it was not the AIC-minima. We observed that such a model order did not allow us to resolve closely spaced components at 40Hz and 45Hz. The AIC minima (p = 18) allowed for closely spaced components to be resolved; however, the lower peak at 40Hz in the simulated data was represented at 39.5Hz. A model order of p = 20 allowed for the components to be resolved with peak locations specified in-line with the simulated components. We further checked peak locations for p = 22 and p = 24 and no splitting of shifting of components in the frequency domain was observed. These higher model orders (p > 20) allowed closely spaced components at 40Hz and 45Hz to be better resolved.

Given the observations of the AIC-minima for Condition 1 and Condition 2, and the necessity to select a single model order for the time-varying AR estimates for both conditions, the model order p = 20 was adequate, although higher model orders may also have been used without affecting the location of the component peaks in the derived spectra. The chosen model order provided an adequate reduction in estimation bias, so as to distinguish closely spaced components. The chosen order did not affect bias-variance trade-offs related to statistical uncertainties such that locations of identified peaks were greatly biased relative to the simulated ground-truth examples; neither did the estimated components split, nor were spurious components observed within the spectra.

2.2.2.2 Time-Varying AIC-AAR Model Validation

In order to validate the time-varying AIC-AAR model, we tested for model stability and whiteness of residuals. As our approach utilised single-trial spectral estimates, we assessed model validity on a trial-by-trial basis within each time-window. We tested for stability by solving for the characteristic roots of the polynomial acquired through the model fitting procedure and investigated the modulus of each of the characteristic roots: we tested to see if the maximum of the moduli was less than one. In such instances the local model was stable. One-hundred percent of all local models were stable under Condition 1 and Condition 2, partly owing to the use of the Burg parameter estimation routine that guarantees a stable model.

We tested for whiteness using Li-McLoed's test for residual whiteness (McLoed & Li, 1983); we utilised a lag of 50, which was smaller than the length of the windowed signal. As with stability, whiteness was tested on a trial-by-trial basis within each time-window. We tested for whiteness across all models at $\alpha = 0.05$, $\alpha = 0.01$ and $\alpha = 0.001$. The majority of models (99.54%) were white at $\alpha = 0.01$ under Condition 1, as was the case for Condition 2 (99.5%). We computed spectral averages across trials including and excluding models with non-white residuals. The resultant averaged spectral estimates were not significantly different when excluding non-white models compared to when they were included. There was a slight variability in the spectral estimate when excluding models with non-white residuals, but this variability did not exceed the 95% confidence intervals of the spectral estimates derived when all windows (white and non-white) were included in the average. The small insignificant amount of variability caused as a result of non-white models was counteracted by the decrease in variability owing to averaging over trials.

2.2.2.3 Time-Frequency Distribution Analysis

Prior to applying the preprocessing steps involved in EEG event-related analysis, we compared cross-sections of the time-frequency distributions yielded by either methodology. Figure 2.3 depicts a cross-section in the frequency domain taken at 1.25 seconds from the averaged time-frequency distributions produced by either method under Condition 1.

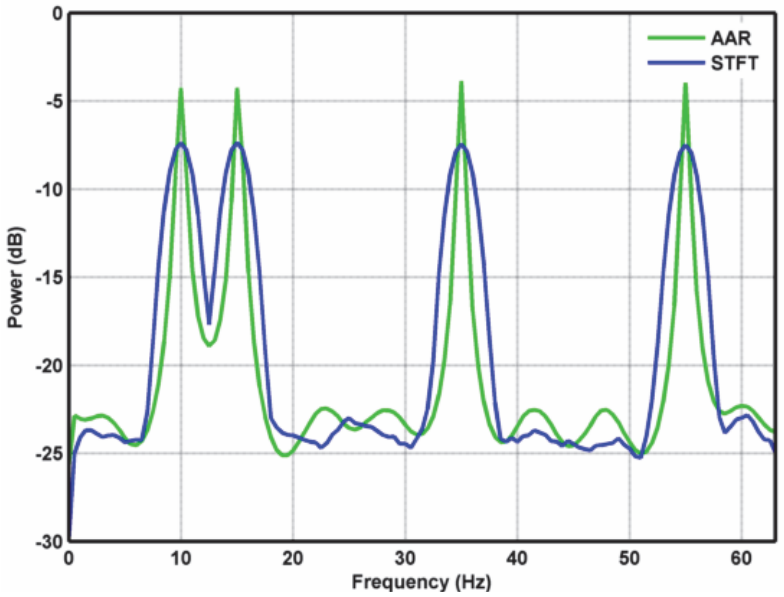

Figure 2.3: Spectral power at 1.25 seconds for each of the time-frequency distribution under Condition 1.

In-line with known properties of the estimators, the AAR-estimated components are more well-defined in frequency when compared to the STFT components, where components are characteristically more rounded due to the application of the taper. The two closely spaced components at 10Hz and 15Hz are resolved both in the STFT and AIC-AAR time-frequency distributions.

We also compared rise and decay times of the components in the time-frequency distributions. In Figure 2.4, we present a cross-section in the time domain at 35Hz.

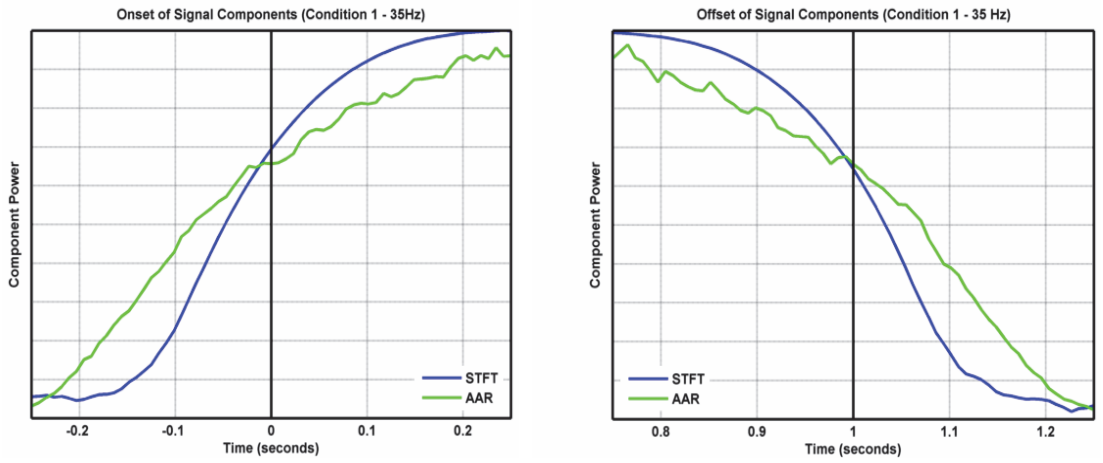

Figure 2.4: Component onset/offset at 35Hz compared against ground-truth (vertical solid black line).

Across the analytical bandwidth (DC-Nyquist) the AIC-AAR estimated component time series demonstrate extended length rise and decay times relative to STFT-estimated component time series. Due to variable residual error within each local AR model, the AIC-AAR component power jitters across time. The rise/decay times of either estimator do not differ from low to high frequencies due to fixed time-frequency resolution of either estimator.

2.2.2.4 Single-Trial Time-Frequency Estimates

The TFDs generated by either methods were baseline corrected by subtracting the average baseline power (-500ms -100ms) from each time point of the single-trial time-frequency representations. Baseline confidence intervals were then derived using bootstrap resampling procedures applied to the baseline corrected data: we resampled the mean baseline power at each frequency 400 times and computed the upper and lower bounds of the 95th percentile range of the bootstrapped distribution. Each time-frequency point within each single-trial TFD was then compared to the adjusted baseline confidence interval at 95% (CI = 95%), where the adjustment was made by computing a false discovery rate (FDR) significance threshold using methods presented in Durka, Zygierewicz, Klekowicz, Ginter, and Blinowska (2004). This

yielded baseline corrected time-frequency representations for both algorithms wherein non-significant time-frequency points were set to zero.

2.2.2.5 Time-Frequency Condition Contrasts

We formed condition contrasts by computing multiple paired-samples *t*-tests for each time-frequency point for the baseline-corrected STFT and AIC-AAR log power representations; a *p*-value for each time-frequency point was stored to provide a time-frequency probability representation. As the TFD data was log-transformed and approximately normal, the *t*-test is cited as the appropriate test (Kiebel *et al.*, 2005; Zhang *et al.*, 2011). The time-frequency probability representations were masked using a Bonferonni threshold.

The condition time-frequency distributions and condition contrasts for the STFT spectral-estimator are presented in Figure 2.5. The components that differentiate the two simulated conditions are identified within the time-frequency contrasts and are numbered according to their condition of origin. Consulting the time-frequency distributions on the first row of Figure 2.5, one notices that the component onsets/offsets are not strictly aligned with the ground-truth: components appear to have a gradual onset and slow rolling offset instead of the true simulated on/off effect. This is most appreciable for components with onsets at the point of "stimulus-onset" — the 35Hz component in Condition 1 and the 4Hz component in Condition 2 — although the same applies to all other components within the distributions owing to the existence of a constant time-frequency resolution. In addition, the distribution of spectral power along the frequency dimension is not well localised to the frequency bands of the simulated components, rather components are represented with a wider bandwidth relative to the ground-truth.

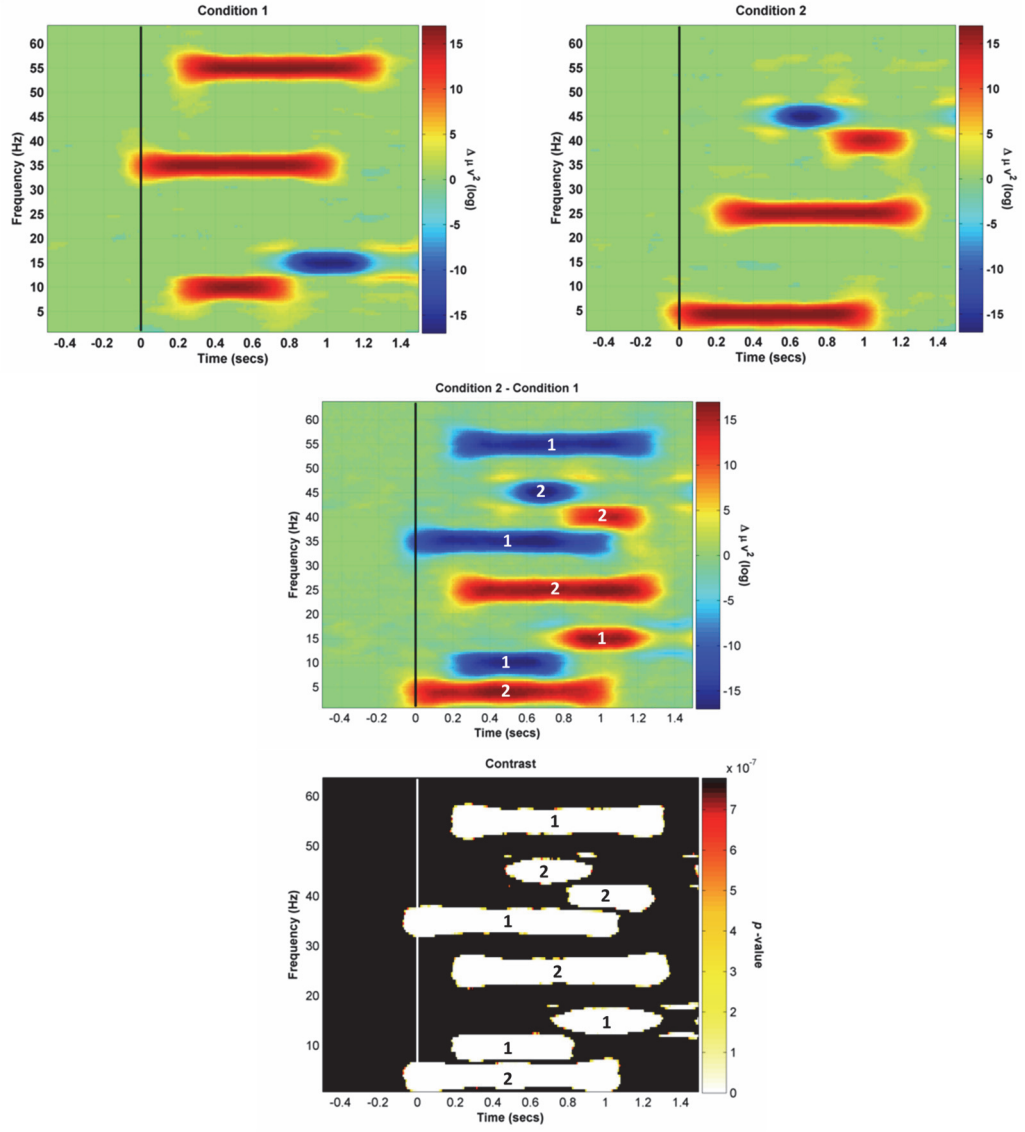

Figure 2.5: Contrasts from the two simulated conditions using STFT-based representations. The top two panels in the first row are time-frequency distributions: the left panel displays Condition 1 and the right panel displays Condition 2. The middle panel is the contrast between conditions expressed as differences in baseline corrected log-power. Components that lead to differences in the time-frequency contrasts are numbered according to their respective condition of origin. The bottom-panel is the probability time-frequency contrast (FDR threshold = 7.7809e-07). Components that lead to significant differences in the time-frequency contrasts are numbered according to their respective condition of origin.

Due to a small sample of datum-points representing the signal components at the points of onset and offset, the estimates in these time-frequency regions are biased due

to small sample properties of the estimator and are thus not well-defined in frequency. When the component is represented within the centre of the sliding window, the component is represented at a given bandwidth set by the window length and associated taper; the estimates are relatively unbiased—the estimator is asymptotically unbiased; however, in finite samples, the bias can be reduced by increasing the number of component sample points within the sliding window. In the instance of the ERDs, where the baseline components are subtracted from a given band across time, the broader edges of the biased estimates of the component remains in the time-frequency distribution.

The centre panel in Figure 2.5 contains the condition contrasts formed by subtracting Condition 1 from Condition 2. As such, red represents time-frequency regions where Condition 2 > Condition 1. This can be due to an ERS in Condition 2 or an ERD in Condition 1. Blue represents time-frequency regions where Condition 1 > Condition 2 due to an ERS in Condition 1 or ERD in Condition 2. The condition contrast provides a useful representation to identify components that differentiate experimental conditions, although statistical thresholding is needed to determine random variability around zero-mean differences and significant changes in spectral power owing to differences in experimental conditions.

The bottom panel in Figure 2.5 is the masked probability contrast, where the significance threshold is set according to the Bonferroni correction (we tested a number of thresholding procedures. Refer to Supplementary Materials B – Statistical Thresholds for Simulated Data for a comparison of these procedures). Within the probability contrast, significant oscillatory events are identified, we have numbered the events according to their condition of origin for ease of reference. The essential nature of the STFT component representation is demonstrated in this contrast, i.e. the uncertainty of ground-truth onset and the wide component bandwidth. The subtraction artefacts are also present in the probability contrast, even when using a conservative multiple comparison correction procedure such as the Bonferonni

correction. The condition time-frequency distributions and condition contrasts for the AIC-AAR spectral-estimator are presented in Figure 2.6.

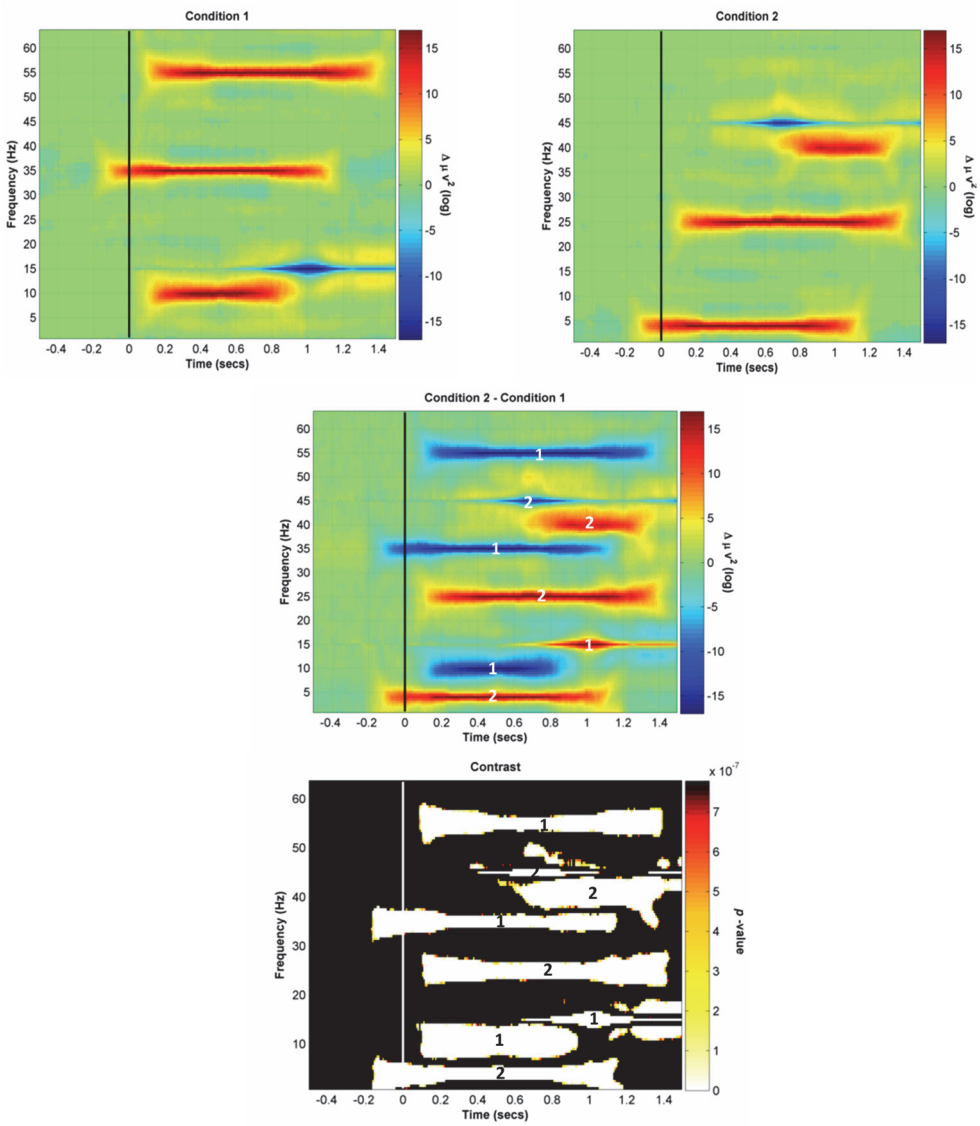

Figure 2.6: Contrasts from the two simulated conditions using AIC-AAR-based representations. The top two panels in the first row are time-frequency representations from either condition: the left panel displays Condition 1 and the right panel displays Condition 2. The middle panel is the contrast between conditions expressed as differences in baseline corrected log-power. Components that lead to differences in the time-frequency contrasts are numbered according to their respective condition of origin. The bottom-panel is the probability time-frequency contrast (FDR threshold = 7.7809e-07). Components that lead to differences in the time-frequency contrasts are numbered according to their respective condition of origin.

Looking at the condition contrasts and the probability contrasts, as with the STFT distributions, subtraction artefacts are present within both of the time-frequency distributions; although the AIC-AAR model appears to be more affected by this. As with the STFT probability contrasts, we utilised the Bonferroni correction to set the significance threshold.

2.3 Discussion - Simulation Study

Differences in representations of simulated signal components in time and frequency were observed across methods. The AIC-AAR model was adequately fitted and thus the observed differences arose due to bias-variance trade-offs related to common elements of either method, such as the choice of window length, but also due to trade-offs specific to each estimation routine: the application of tapers when using a STFT and the estimation of the model order parameter for the AIC-AAR methodology. The method-specific choices involving bias-variance trade-offs in the frequency domain in turn affect the time resolutions of either distribution despite using a common window length of 500ms. We discuss the general methodological decisions related to window length and the method specific trade-offs below.

The first point to consider is the length of the sliding window, the main control parameter for the time-frequency resolution trade-off. Generally speaking, window length sets the time-frequency resolution. Short-windows offer enhanced temporal resolution at the cost of frequency resolution, while the opposite is true for longer windows. An important yet often neglected fact is that when window lengths are shortened in AAR and STFT spectral estimation, greater bias can be incurred within the spectral estimate despite the specific estimation routine being asymptotically unbiased, the degree to which is dependent on the relative small sample properties of each specific estimator. Such methodological realities can mean that despite using the same window length across methodologies, different estimators can lead to different specifications of components in time and/or frequency. These observations are driven

by estimator bias and how these biases translates into changes in overall resolution and dynamic range within the frequency domain, affecting resolvability of closely spaced peaks as well as localisation of components in time and frequency.

The second consideration is the application of tapers: in the instance of the STFT distributions we used a hamming window. For a non-parametric approach, such as the spectrogram, a rectangular window leads to discontinuities at the edges of the sliding window—the DFT assumes all values outside the window are zero. This results in side-lobe leakage, due to the manner in which the Fourier transform relates the auto-covariance sequence to the Fourier coefficients, i.e. the sudden step-up/step-down in the auto-covariance sequence to/from zero at the edges results in the leakage effect that necessitates enforcing converges to zero at the edge of the data sequence. Tapering suppresses side-lobe leakage and increases the dynamic range of the resultant spectra; however, some estimation bias is incurred and the resolution of the spectrum decreases. Thus, estimation bias-variance trade-offs are directly related to the resolution of the estimated spectrum. The applied taper in the STFT also has an impact on the temporal dimensions of the time-frequency distribution. The signal components will only appear to rise from the noise-bed when a sufficient amount of sample points are represented within the centre region of the tapered sliding window. This is due to the fact that the leading and trailing edges of the sliding window are weighted down when tapers are applied. Thus, even when component sample points are included at the leading edge of the sliding window, the component will not appear to rise from the noise bed within the time-frequency distribution. Similar reasoning applies to component offset. This offers a different temporal-frequency specification of signal components in comparison to when one utilises a rectangular window, where components would appear to rise from the noise bed earlier when sample points are present within the unweighted leading edge of the sliding window, leading to greater temporal uncertainty with better frequency resolution.

For AAR spectral estimation, it is not necessary to taper the sliding windows as it is with a spectrogram, as the auto-covariance sequence can be extrapolated outside the data-window and is assumed to be non-zero. Thus, discontinuities at the edge of the windowed signal and the manner in which these affect the transformation from time domain to frequency domain in a spectrogram are not encountered in AAR spectral estimation. The reason is that spectral estimates are based on a finite set of estimated coefficients of a given order p, where the order of the model is normally determined using one or more information criteria, although there are number of other available methods for this purpose. The estimated coefficients represent the underlying system. By solving for the roots of the polynomial formed from these coefficients, the peak positions and magnitudes within the AR spectra are derived, rather than estimating spectral power in each frequency bin based on the data sequence as with a STFT. Thus, time and frequency resolution are affected across estimators, not as a result of window length, but as a consequence of bias-variance trade-offs.

Another important factor that affects time-frequency resolution through bias-variance trade-offs is that AAR-models require parametrisation: a model order must be determined using one of a number of methods. Thus, the model order parameter creates an additional trade-off in the analysis. When the selected model order is too low, the resultant spectrum is biased: closely spaced peaks cannot be resolved and there is low dynamic range; while too high model order results in overfitting and leads to a highly variable spectral estimate, wherein component peaks can split and shift, thus introducing spurious components into the spectral estimate. Reducing bias at the cost of incurring greater variance is the key trade-off. The ability to adequately resolve closely spaced components is dependent upon this trade-off through the impact that decreasing bias has on resolution and dynamic range. AIC-AAR time-frequency resolution is directly affected by the bias-variance trade-off related to model order.

One must also take into consideration that we were averaging time-varying spectra over trials, where each trial is considered a realisation of an underlying data-

generating process. It is well-known that the Fourier spectrum is an inconsistent estimator on a single-trial basis. The estimate is asymptotically unbiased, however, the variance of the estimate does not converge to zero as the number of datum-points increases, or even if the number of datum-points tends towards infinity; whereas the auto-regressive spectral estimates are consistent on a single-trial basis. The averaging process in the instance of a STFT yields consistent estimates of the true spectrum by reducing the variance of the estimated quantity; however, this is accompanied by a slight increase in estimation bias when dealing with finite samples. The change in bias results in differences in component bandwidth when considering single-trial estimates versus the averaged periodogram. The single-trials are less biased, essentially due to their narrower component main lobe within the frequency domain, while the averaged periodogram has a slightly larger main lobe due to an increase in estimation bias. Thus, the bias-variance trade-off related to averaging affects the frequency resolution further, over-and-above window length and tapers; however, this is distinct from the time-frequency trade-off related to window length.

2.4 EEG Event-Related Data Analysis

2.4.1 Participants

Six right-handed children were selected from a sample of children recruited from the Cape Coloured community in Cape Town, South Africa, to participate in a broader research programme into fetal alcohol spectrum disorders (Burden *et al.*, 2009; Jacobson *et al.*, 2011). Mothers were interviewed about their alcohol consumption during pregnancy using a timeline follow-back approach (Jacobson *et al.*, 2002). In our analysis, we utilised a sample of minimally alcohol-exposed children performing the Go/NoGo task. These were children of mothers who abstained or consumed amounts not know to be harmful to the developing foetus: two drinks per occasion on a monthly basis. Participants' mean age in years was 12.06 (SD±1.08), ranging from 11.07-13.62.

All mothers/primary caregivers provided written informed consent; all children provided oral assent. Each mother received a small monetary compensation for her participation and each child was given a small gift. All protocols were approved by the Wayne State University and the University of Cape Town institutional review boards.

2.4.2 Go/NoGo Task

The experimental task was administered using E-Prime® 2.0 Professional Edition (Psychological Software Tools, Pennsylvania, USA). The Go/NoGo task is a cognitive-behavioural experimental paradigm that provides a measure of inhibitory control. In the Go/NoGo task, a motor response (button press) is cued during a large proportion of the trials (Go-condition), interspersed with a limited number of cues to withhold the response (NoGo-condition). One assays behavioural performance in terms of errors-of-omission (leaving out a response when one is cued), errors-of-commission (responding when inhibition is cued), and reaction times under the Go-condition. In our version of the task, each participant was instructed to press a button with the index finger of the right hand in response to a letter that appeared on the screen (the "Go" trials) with the exception of "X" (the "NoGo" trials). Inter-stimulus intervals were constant through the sessions (ISI = 5500ms), with the stimulus centered on screen for 500ms followed by a blank screen for 5000ms. Go and NoGo stimuli were alternated randomly within five consecutive blocks of 30 trials each (20 Go, 10 NoGo) for a total of 150 trials. We placed a two-minute rest period between blocks. The entire task, including instructions and practice items, took approximately 20 minutes to complete.

2.4.3 EEG Data-Acquisition

EEG data was acquired using an active-electrode Biosemi ActiveTwo EEG system (BioSemi, Netherlands, Amsterdam). A Common Mode Sense (CMS) and Driven Right Left (DRL) reference/ground scheme was used for data-acquisition with an on-line band-pass filter set at DC-400Hz. Data were acquired at a sampling rate of 512Hz at 24-bit resolution. Thirty-four electrodes were placed according to 10/10 electrode placement system (Jurcak, Tsuzuki, & Dan, 2007). We placed the electrodes on the participant's head using a tight-fitting elasticised cap; a conductive gel was injected into the gel cavity of each electrode to form a conductive bridge between the scalp and measurement electrode. Measurement electrodes fitted in the cap were placed over the following regions: anterior-frontal (AF3, AF4, Fp1, Fp2), frontal (F3, F4, F7, F8, Fz), frontal-central (FC1, FC2, FC5, FC6), central (C3, C4, Cz), central-parietal (CP1, CP2, CP5, CP6), parietal (P3, P4, P7, P8, Pz), parietal-occipital (PO3, PO4), temporal (T7, T8), occipital (O1, O2, Oz), and mastoids (M1, M2). In addition, two sets of bipolar pairs were placed: (1) above and below the right eye and (2) near the outer canthus of the left and right eye. These bipolar pairs recorded vertical and horizontal eye-movements, respectively. An additional channel was used to record participant behaviour, i.e. a button press made during the experimental task. Data was stored off-line in the *.bdf file format.

2.4.4 EEG Data-Processing

All preprocessing was performed within the MATLAB computing environment using custom scripts built upon functions provided by the EEGLAB toolbox (Delorme and Makieg, 2004). Time-frequency distributions were generated using our in-house MATLAB toolbox.

2.4.4.1 Preprocessing

Data were imported into EEGLAB, re-referenced to a linked Mastoid reference, and filtered using a band-pass filter from 0.5Hz – 45Hz. Recordings were scanned for gross-movement artefacts, and those portions of data containing artefacts were excluded from the datasets. The two-minute rest periods between blocks were also excluded from further analysis. Noisy channels were identified and replaced by interpolated values. Data were then segmented relative to stimulus onset: 750ms prior to stimulus onset and 1750ms post-stimulus onset. The epoched data were submitted to a *blind source separation* (BSS) algorithm: the *adapted infomax* algorithm within EEGLAB. Derived components were visually scanned for evidence of artefact and those components that were indicative of oculargenic artefact and myogenic artefact were removed. Components were projected back onto the scalp to form an artefact-free dataset. Epochs were then submitted to a time-domain thresh-holding algorithm: any epoch with extreme values exceeding 50μV was excluded from further analysis. The epochs were then scanned for behavioural response data using custom software written within the MATLAB computing environment (The MathWorks Inc., Natick, MA, USA). The software classified and stored information associated with the following responses: correct Go, correct NoGo, incorrect Go, and incorrect NoGo. The behavioural response data was used for further analysis of participant behaviour under experimental conditions. The data tables containing the behavioural response data formed the basis for automated epoch rejection, whereby error-trials were removed from further analysis. We considered analysing error trials, however, commission and omission error rates were low due to the relative ease of this specific version of the Go/NoGo task. Thus, there were too few trials to perform an analysis.

2.4.4.2 Time-Frequency Analysis

We used the same approach as applied to the simulated datasets outlined in a previous section (2.2.2 Time-Frequency Analysis).

2.4.4.2.1 Autoregressive Model Order Selection

We selected the model order for the AR-based approach using the Burg algorithm for coefficient estimation and AIC as well as AIC-C approaches to model order selection. As per the suggestion in Florian and Pfurtscheller (1995) and Mullen (2014), we utilised a subset of data segments taken across trials and across time-windows within trials. We randomly sampled 10% of trials and 3 x (500ms 0% overlapping time-windows) within each sampled trial. Estimates using each of the information criteria were computed across a range of model orders ranging from 1 – 30; these estimates were computed separately for each of the sampled segments and then stored for further analysis. In order to derive an estimate of model order, we took the median measure for each information criterion across all data segments for which we estimated a model order. As the distributions were skewed for these metrics, a median offered the best measure of central tendency.

AIC yielded an estimate across segments of $p = 28$. AIC-C provided an estimation of model order slightly lower than that of AIC, $p = 23$. An optimal model order was selected within a range defined by median AIC and median AIC-C minima, $p = 26$. Model orders within this range provided sufficient detail (reduced bias and enhanced frequency resolution) within the time-frequency distributions to represent the event-related spectral oscillations observed within the STFT representation of the event-related data, although greater variance in the estimates was observed (see Appendix C – Model Order, Bias and Resolution).

2.4.4.2.2 Time-Varying AIC-AAR Model Validation

In order to validate the time-varying AIC-AAR model, we tested for model stability and residual whiteness following the procedure outlined in section 2.2.2. One-hundred percent of all local models were stable under the Go- and NoGo-condition. The majority of models (99.64%) were white at $\alpha = 0.01$ under the Go-condition, as was in the case for the NoGo-condition (99.62%). We computed spectral averages across trials including and excluding models with non-white residuals at different significance thresholds. There was slight variability in the spectral estimate when excluding models with non-white residuals, but this variability did not exceed the 95% confidence intervals of the spectral estimate derived when all windows (white and non-white) were included in the average.

2.4.4.2.3 Single-Trial Time-Frequency Representations: Inter-Trial Coherence (ITC)

Inter-trial coherence values were computed for each condition across all participant's data. As with event-related spectral power, ITC can be expressed as a baseline corrected time-frequency representation, where baseline correction procedures and significance testing are computed in the same manner as for spectral power.

2.4.5 EEG Results

The condition contrasts for the STFT spectral-estimator are presented in Figure 2.7. Three components that differentiate experimental conditions are identified within the figure. The topographical maps of components illustrating power and inter-trial coherence for each of the three oscillatory components are presented in Figure 2.8.

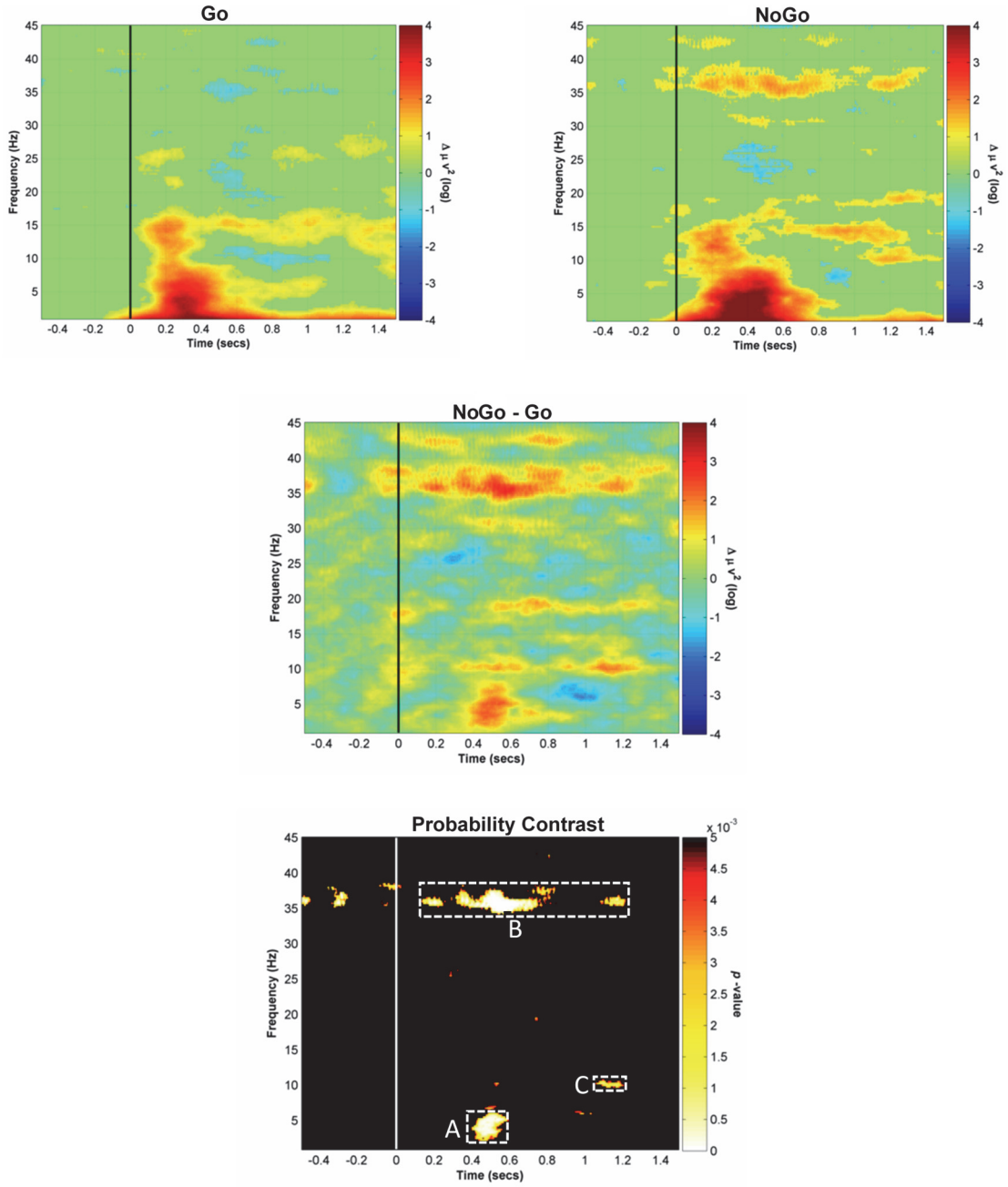

Figure 2.7: Contrasts from the experimental group's data. The top two panels in the first row are time-frequency representation: (Left) the Go-condition and (Right) the NoGo-condition taken from the Fz electrode (10/10 electrode placements). The middle panel is the contrast between conditions expressed as differences in baseline corrected log-power. The bottom-panel is the probability time-frequency contrast (FDR = 0.005). Components that differentiate conditions are highlighted in white boxes.

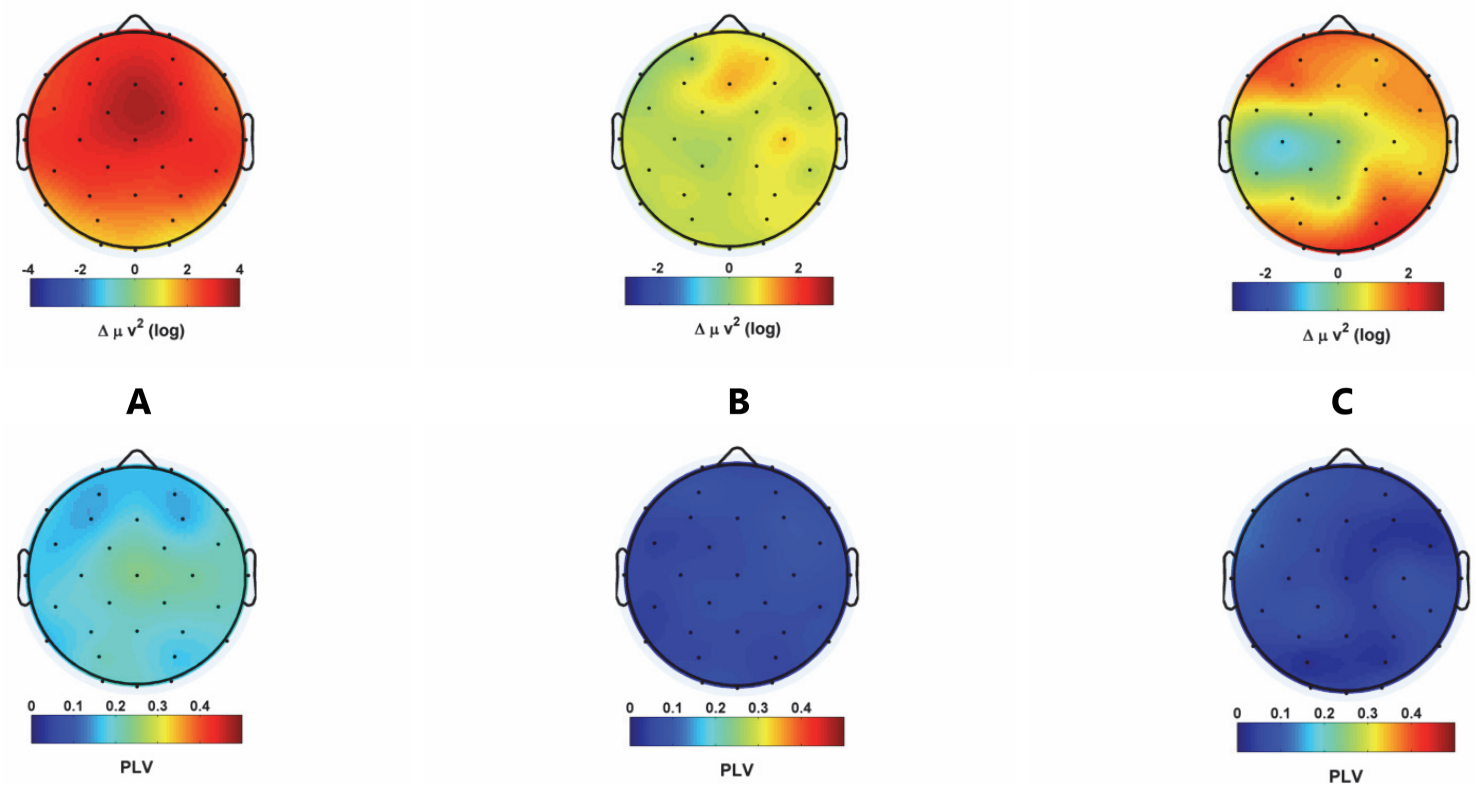

Figure 2.8: Topographical maps of each of the oscillatory components that distinguish the Go and NoGo experimental conditions; these components were identified in the previous figure, Figure 2.7. Each component arises due to the demands of response inhibition. The top row illustrates the distribution of baseline corrected power across the scalp. The bottom row illustrates ITC across trials (ITC is expressed as a phase-locking value).

The STFT approach identifies three main oscillatory components that differentiate the Go and NoGo experimental conditions:

- Evoked delta/theta oscillation (2.5Hz – 6Hz);
- Induced gamma oscillation (34Hz – 38Hz);
- Induced upper alpha oscillation (9.5Hz – 11Hz).

Component A, the evoked delta/theta oscillation, shows medium-strong levels of phase-locked activity across trials with the maximum effect focused centrally, indicating that the observed increase in spectral power within the NoGo-condition is an evoked power change. The evoked delta/theta component occurs in a 390ms – 590ms time-window and is part of the enhanced P3 ERP response that characterises the NoGo-condition within the Go/NoGo task (Burden *et al.*, 2009; Kirmizi-Alsan *et al.*, 2006). Component B, the induced gamma oscillatory component, occurs in the NoGo-condition wherein there is a prolonged increase in gamma-band oscillatory power after stimulus onset. Unlike Component A, Component B shows weakly phase locked activity across trials, indicating that the neocortical oscillation is an induced power change. Component C, an induced upper alpha oscillation, is observed later in the trial: 1000ms – 1200ms post-stimulus onset. Like Component B (induced gamma), the induced alpha shows weakly phase-locked activity across trials. The frontal ERS we observed is part of a more spatially complex cortical response wherein there is induced ERD over the left motor area (electrode C3) surrounded by the alpha band ERS. Upper alpha is known to be involved in cortical motor control with source generators located within the precentral gyrus (Pfurtscheller, Neuper, & Krausz, 2000). This induced oscillatory phenomena is known as *focal ERD/surround ERS* and is often observed during motor tasks (Pfurtscheller & Lopes da Silva, 1999; Pfurtscheller & Neuper, 1994; Pfurtscheller, Neuper, Andrew, & Edlinger, 1997). The AAR-based TFDs are presented in Figure 2.9.

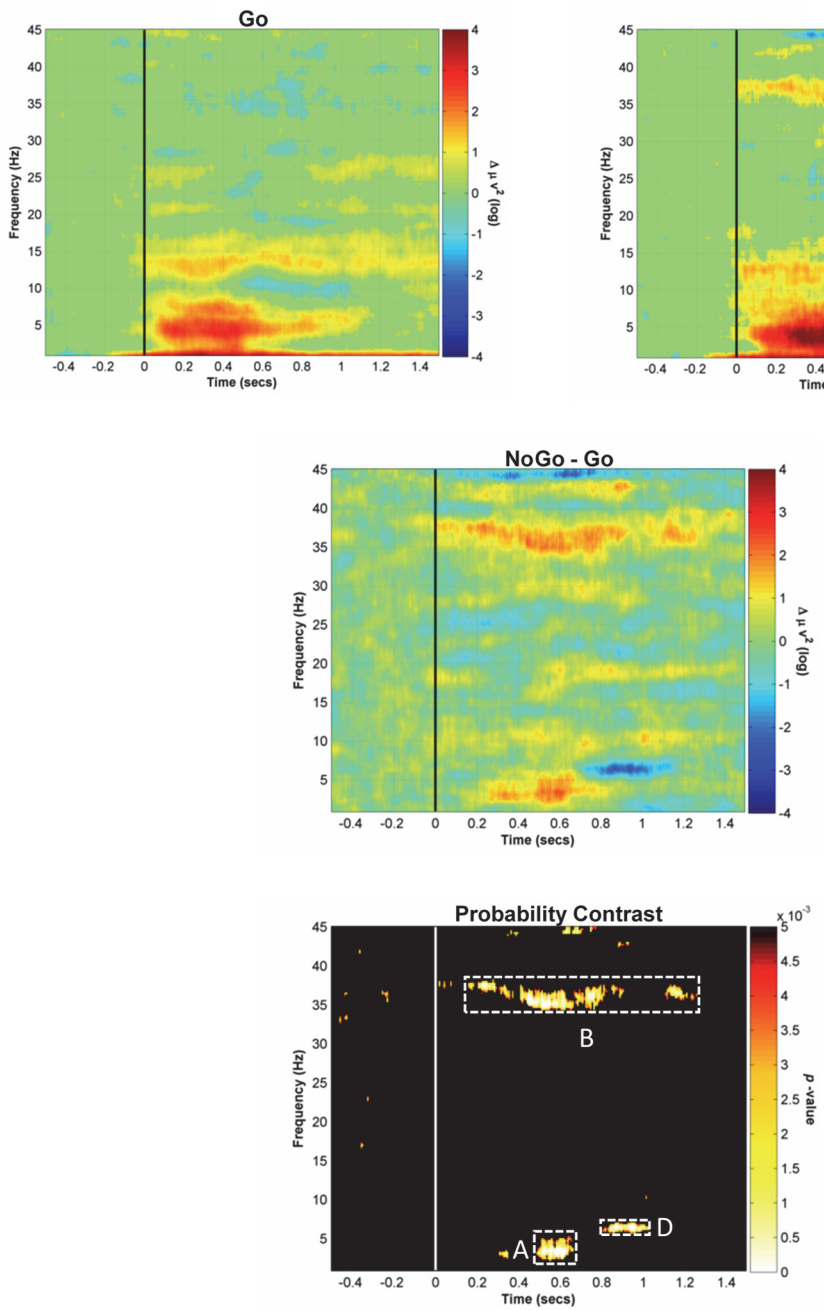

Figure 2.9: Contrasts from the experimental group's data using AAR-based representations. The top two panels in the first row are time-frequency representations from the: (Left) Go-condition and (Right) the NoGo-condition taken from the Fz electrode (10/10 electrode placements). The middle panel is the contrast between conditions expressed as differences in baseline corrected log-power. The bottom-panel is the probability time-frequency contrast (FDR = 0.005). Components that differentiate conditions are highlighted in white boxes.

The AR-based approach identifies three main oscillatory components that differentiate the Go and NoGo experimental conditions. There is overlap between the components identified using the AIC-AAR approach and STFT approach: the evoked theta oscillation (2Hz – 6Hz) and the induced gamma oscillation (34Hz – 38Hz) are identified using both methods; however, there are differences in how these components are specified in time and frequency. For example, in the STFT probability contrasts the onset and offset for Component A is 390ms – 590ms and the bandwidth is 4.2Hz, ranging from 2.2Hz – 6.4Hz; this compared to an AIC-AAR representation of Component A, with a latency of 480ms – 670ms and a 3Hz bandwidth ranging from 2.3Hz – 5.3Hz. When assessing the bandwidth of Component B in a 400ms – 600ms time-window using the STFT, the component's bandwidth is 4Hz (34Hz – 38Hz), compared to 3Hz (34Hz – 37Hz) when using AIC-AAR model. The AIC-AAR representation of the gamma-band oscillation also highlights a subtle shift in peak frequency across time that is not apparent in the STFT representation.

The two approaches emphasise different induced alpha oscillations occurring in a 800ms – 1250ms post-stimulus window. The alpha oscillation identified using an AIC-AAR approach (Component D) has a duration of 800ms – 1040ms and has a bandwidth of 1.5Hz, ranging from 5.7Hz – 7.2Hz. The scalp topography is presented in Figure 2.10. Different patterns of event-related power changes across experimental conditions were observed for Component C and Component D. The average power values and associated standard errors are present in Table 2.2.

Table 2.2: Event-related oscillatory responses in the alpha band

	Go-Condition	NoGo-Condition
Component – C (STFT)	-0.3283 (0.0160)	1.1861 (0.0158)
Component – D (AAR)	0.9843 (0.0176)	-0.6415 (0.0261)

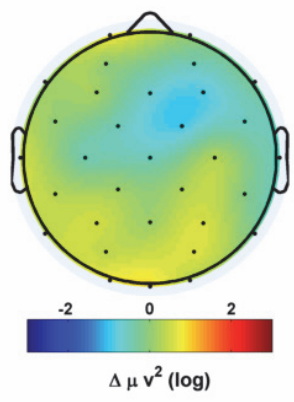

Figure 2.10: Component D identified using the AIC-AAR spectral estimator. The experimental group under the NoGo-condition shows a decrease in spectral power over the right frontal regions.

The alpha oscillation identified using the AIC-AAR method shows that in the Go-condition there is a significant increase in oscillatory power. In the NoGo-condition, a significant decrease in oscillatory power was observed. A large significant difference between conditions is apparent in the AIC-AAR-based probability contrast ($p < 0.005$). This difference is absent in the STFT probability contrast at corresponding time-frequency points when using a significance threshold of FDR = 0.005. Relaxing the probability threshold to $p = 0.01$ reveals the component in the STFT distribution, although the magnitude-of-effect within this time-frequency region is greatly affected and only a small time-frequency region is significant (see Appendix D – Significance Thresholds Empirical Data). In contrast, the alpha oscillation identified using the STFT estimator has spectral power significantly lower than baseline levels in the Go-condition; while in the NoGo-condition spectral power is significantly greater relative to baseline. The AIC-AAR probability contrast shows no significant differences between conditions at the corresponding time-frequency points, even when relaxing the statistical threshold. The differences between the two approaches with respect to the alpha oscillations are presented in Figure 2.11.

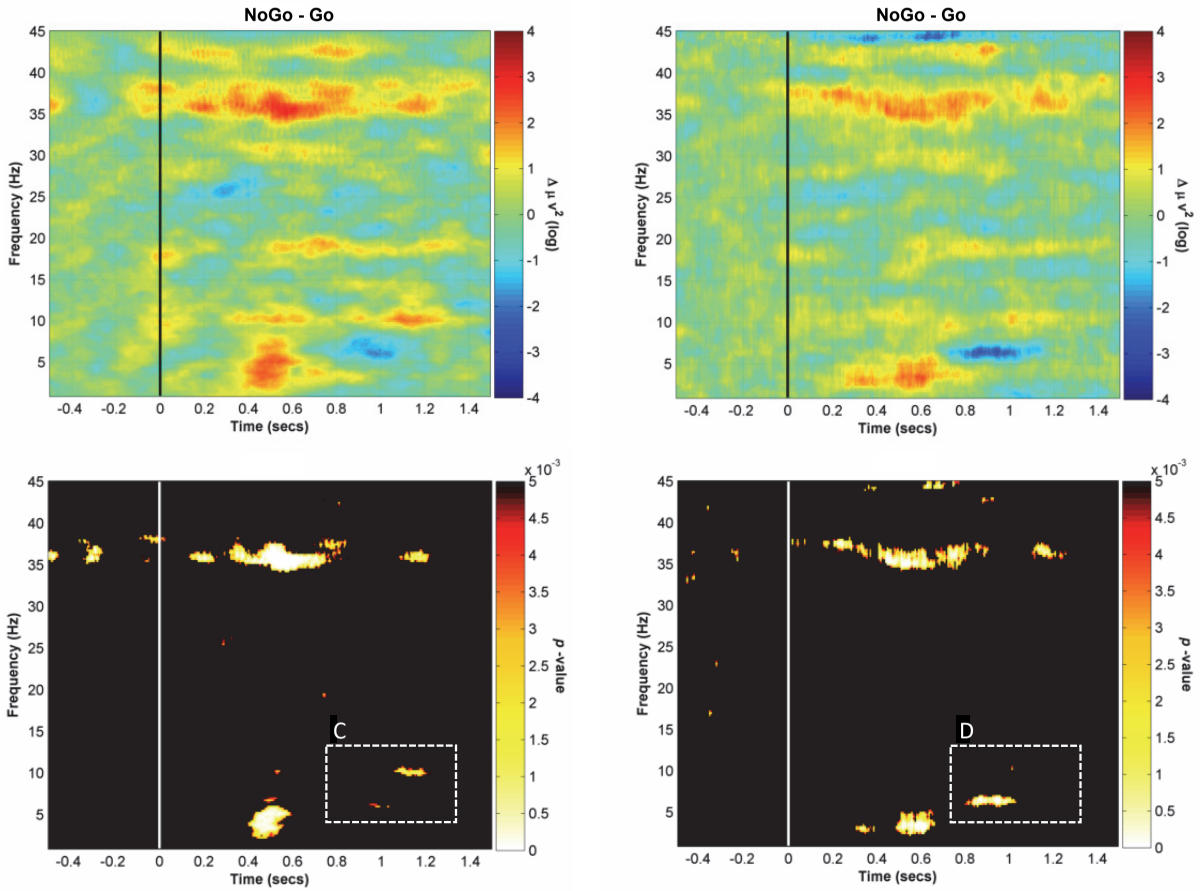

Figure 2.11: Condition contrasts computed using two different methods: (Left) STFT time-frequency representations; (Right) AAR time-frequency representations. The bottom row contains the probability contrast (FDR = 0.005). The time frequency region where the two regions differ is surrounded by a white dashed box.

2.5 Discussion - Empirical Analysis

STFT and AIC-AAR spectral estimators provide complementary and in certain instances unique information about event-related, neocortical oscillatory events. For example, our analysis shows an overlap across methods in terms of identifying a delta/theta oscillatory component that differentiates experimental conditions. The delta/theta oscillation occurs in a 350ms – 650ms time-window and constitutes the evoked power component underlying the P300 event-related potential (Andrew & Fein, 2010a). The P300 is reliably elicited with greater amplitude under the NoGo-condition within normally developing samples performing the Go/NoGo task (Davis, Bruce, Snyder, & Nelson, 2003; Johnstone, Pleffer, Barry, Clarke, & Smith, 2005; Pfefferbaum, Ford, Weller, & Kopell, 1985). We observed different bandwidths and latencies for this oscillatory event across methods. These observations can be explained based on insights gained from the simulation experiment: we demonstrated that our AIC-AAR model's time-frequency distribution provided enhanced frequency resolution, but effected a greater degree of smoothing along the temporal dimension of the distribution. The model order parameter in our AIC-AAR model provided an additional mechanism for a spectral estimation bias-variance trade-off leading to temporal smoothing. This smoothing was driven by relatively more estimation bias around regions of component onset and offset, owing to the small amount of available component sample points from which to estimate the model's parameters. Model order and window type (a rectangular window) resulted in sharper signal-components that were relatively more well-defined in frequency (reduced bias) that differentiated themselves more clearly from background noise (enhanced dynamic range).

One can understand these observations by interpreting them in light of spectral estimation theory and the uncertainty principle in signal-processing. General methodological choices such as window length, but also methodologically specific

choices that result in estimation bias-variance trade-offs, can in turn affect signal component's specification in time and frequency. In terms of AAR spectral estimation, model-order determines, over-and-above window length effects, how well-defined the distribution is in terms of its frequency dimension through its impact on the bias and variance of the estimated spectra. The observed differences, in terms of specifying the delta/theta component in time and frequency across methods are related to how the time-frequency trade-off plays out in the context of each method, and how this specification in time and frequency is further affected by other modelling/methodological choices related to statistical uncertainties.

The high-frequency gamma-band oscillation was another component identified by both methods. Gamma-band dynamics are thought to play a role in cortical-binding: a physiological mechanism by which distant regions of the cerebral cortex temporally integrate to form functional units (Roskies, 1999; Singer, 2001). These units support perceptual as well as sensorimotor function (Mima, Simpkins, Oluwatimilehin, & Hallett, 1999; Omlor, Patino, Hepp-Reymond, & Kristeva, 2007; Tallon-Baudry *et al.*, 1996). Induced gamma-band oscillations have also been observed in tasks that require a high-level of cognitive-control (Cho *et al.*, 2006; Fan *et al.*, 2007; Kieffaber & Cho, 2010). We observed that (as with the evoked delta/theta oscillation)the specification of the observed gamma component in time and frequency differs across methods. We also observed that this component is an induced oscillation, unrelated to the phase-locked evoked response, as was evidenced by weakly phase-locked activity associated with the increase in spectral power. As with the delta/theta complex, we observed partially overlapping significant time-frequency points. However, the AIC-AAR gamma-band component is more well-defined in frequency, allowing one to observe a shift in the central frequency of the oscillation early on in the NoGo trials. This shift was not observed with the STFT estimator. An observed quality of the STFT spectra is relatively increased estimation bias and reduced frequency resolution owing to the use

of a taper. Thus, the frequency shift was not observed due to reduced resolution in the instance of the spectrogram.

There were apparent differences in the components identified by both methods, specifically related to late, short-duration, narrow-band phenomena within the alpha band. In these instances, the two methods differ in their specification of late alpha-band oscillatory activity. The components identified by either method proved to be two different oscillatory events within different time-frequency regions. We demonstrated that each component had different patterns of event-related power changes across conditions as well as different scalp topographies. In the instance of the STFT estimator, we identified a late "focal-ERS/ surrounding-ERS" within the upper alpha band (10 – 12Hz) elicited in the NoGo-condition—a well-documented and understood response. This short duration, narrow-band oscillatory event is not well-represented in the AIC-AAR NoGo time-frequency distribution, and the corresponding time-frequency regions in the condition contrasts were not significant at FDR = 0.005. This is primarily because the AIC-AAR model does not concentrate the oscillatory component's energy within the same time-frequency points relative to the STFT approach; this, owing to an enhanced frequency resolution and relatively greater temporal smoothing affected by the model, which is a result of choice of window type (rectangular) as well as estimation bias-variance trade-offs related to parametrisation. The impact of this is a change in the magnitude-of-effect at each time-frequency point, in terms of difference scores in spectral power across experimental conditions. In the instance of AIC-AAR estimates, the magnitude-of-effect decreases: the temporal smoothing causes spectral energy to be more widely distributed in time, decreasing the magnitude-of-effect in the AIC-AAR model within the same time-frequency region relative to the STFT distriubution. As the late focal-ERD/surrounding-ERS within the upper alpha band is often observed in motor tasks within adult samples (Pfurtscheller & Lopes da Silva, 1999; Pfurtscheller & Neuper, 1994; Pfurtscheller *et al.*, 1997), we

view the non-significance in the AIC-AAR time-frequency analysis as a Type II statistical error owing to methodological choice.

In the AIC-AAR model, a lower alpha synchronisation within the Go-condition and a corresponding desynchronisation in the NoGo-condition differentiated the experimental conditions. A reverse pattern is represented in the STFT Go- and NoGo-condition time-frequency distributions. Within the AIC-AAR model, component energy is concentrated into a narrower band and distributed over a longer time-window. This enhances the difference across experimental conditions, leading to a significant difference in this time-frequency region. The corresponding time-frequency points are not significant in the STFT contrasts at the common significance threshold; however, relaxing the significance threshold to 0.01 (determined using EEGLAB's fdr.m function), some time-frequency points become significant. The observed significant difference, in the instance of the AIC-AAR model, is rooted in the statistical trade-offs that affect and influence time-frequency resolution: in terms of how these trade-offs lead, within the AAR model, to specific significant differences arising within the condition contrasts. Topographically this component is a focal oscillatory event that does not resemble any known neocortical dynamics elicited by motor-response/inhibition tasks. Thus, we see this significant time-frequency region as a Type I statistical error at the given threshold (FDR = 0.005).

We observe that for broader band phenomena of a longer duration, the two representations do not differ fundamentally. Minor differences arise in latency and bandwidth measures of these components. However, short-duration, narrow-band phenomena are represented very differently across estimators; differences in bias-variance trade-offs between the two approaches result in statistical errors of inference within the AIC-AAR model—the AIC-AAR model produced both Type I and Type II statistical errors at the given FDR = 0.005 threshold, but also when using other established FDR correction methods. This is owing to the enhanced frequency resolution and accompanying change in temporal resolution in time-frequency

contrasts driven by window type and the model order parameter. Importantly, the increase in frequency resolution offered by an AIC-AAR analysis suppressed features that are already well-defined in frequency within the STFT time-frequency distribution, such that the magnitude-of-effect was minimised, leading to false-negatives (Type II errors) in the probability contrasts. This was observed in the instance of the focal-ERD/surrounding-ERS alpha oscillation occurring after 1000ms post-stimulus onset in the STFT representations. Even as we relaxed the significance threshold, the component did not emerge as significant in the same time-frequency regions. The AIC-AAR methodology, with its enhanced frequency resolution, suppressed this component, despite its presence being of high neurophysiological significance (Suffczynski *et al.*, 2001).

Our study focused specifically on a comparison between a STFT distribution and an AIC-AAR distribution wherein the model is parametrised using Akaike's information criteria (AIC and AIC-C). This was done as AIC is used widely within the EEG literature to estimate model order in AR-based spectral analysis. AIC-AAR modelling, relative the tapered spectrogram, leads to divergent characteristics within the AIC-AAR TFRs, both in time and in frequency, despite both methods using a common window length. When the amount of available data from which to estimate the model is finite, AIC misrepresents the quality of the model through the underestimation of the Kullback-Lieber Index. This essentially results in an over-parametrised model. Our parametrisation in the simulation and empirical analysis provided estimates with reduced estimation bias: the components were more well-defined in frequency, closely spaced components were well resolved, and the parametrisation yielded increased dynamic range relative to the STFT distribution. The spectra were more variable; this increased variability did not lead to splitting of peaks. Such splitting was only observed when using a model order higher than that selected by AIC in the empirical data (see Appendix C – Model Order, Estimation Bias, and Resolution). Thus, there were signs of over-fit, but not to the degree that the

spectral estimates were compromised. The decreased bias offered by the higher order AIC parametrisation did affect the TFD's temporal dimension. At regions of component onset and offset within the simulation, the relationship between the amount of available component data within the analytical rectangular window and the chosen model order caused the estimates in these regions to take on more bias, misconstruing the time-points of true component onset/offset. Thus, the temporal dimension of the AIC-AAR TFD is changed over-and-above the bounds of the temporal resolution set by the window length. This was dependent upon estimation biases linked to model complexity in the context of small sample properties of the parametric spectral estimator.

Extending the research herein, our analysis could be expanded to explore comparisons across different parameterisation schemes relative to a non-parametric estimator such as the STFT, in order to understand if an optimal trade-off can be found in such an analysis. Of interest would also be comparisons between recursive parametric approaches that implement additional free parameters such as a *forgetting factor* (Haykin, 1996; Schlögl, 2006; Schlögl & Supp, 2006). A forgetting factor enables a mechanism to control the temporal smoothing effected by the interaction between model order and window length, allowing for enhanced temporal resolution in the presence of enhanced frequency resolution (Costa & Hengstler, 2011).

Future research should explore comparisons between non-parametric and parametric approaches in a multivariate context due to the growing interest in measures of directed information-flow extracted from multivariate autoregressive (MVAR) models (Astolfi *et al.*, 2007; Cheung, Riedner, Tononi, & Van Veen, 2010; Delorme *et al.*, 2011; Dentico *et al.*, 2014; Mullen, Delorme, Kothe, & Makeig, 2010; Mullen, 2014; Schlögl, 2006; Schlögl & Supp, 2006). MVAR models are attracting interest within the EEG research community, as they can provide a host of connectivity indices, such as coherence, the directed-transfer function (DTF), and various forms of partial-directed coherence (PDC) (Astolfi *et al.*, 2013; Mullen, 2014). PDC indices

provide frequency domain measures of granger causality: a frequency domain measure of causal influences between neocortical sources (Baccalá & Sameshima, 2001). Questions regarding relative performance against non-parametric alternatives and the impact of the uncertainty principle in the context of event-related EEG analysis have, to date, not been addressed in detail. When dealing with new methods it is important to understand how the method could potentially produce false positives, or not represent important narrow-band information-flow related to experimental hypotheses, specifically when two experimental conditions are present in the study. We see this as a necessity as MVAR approaches to directed information flow become more popular in EEG event-related analysis.

2.6 Conclusions

Statistical bias-variance trade-offs, time-frequency specification of components, magnitude-of-effects, and significance of oscillatory components that differentiate experimental conditions are affected by methodological choices. In our study, this was especially true for narrow-band oscillatory phenomena. A specific time-frequency analysis method, owing to its specification of components in time and frequency and method-specific choices related to the statistical properties of the estimated spectra, may enhance the magnitude-of-effect across conditions of narrow-band components, leading to significant effects that cannot be observed with a method that offers a different time-frequency specification and vice versa. In clinical neurophysiological research, an awareness of the impact of methodological choice must be expressed when identifying and interpreting oscillatory components from a given time-frequency method owing to the fact that functionally important components may be suppressed through methodological choices, while at the same time, less functionally important oscillatory events can be enhanced leading to errors in statistical inferences.

Chapter 3

The Effect of Heavy Prenatal Alcohol Exposure on Induced-Frontal Gamma-Band Oscillations in Children Performing a Visual Go/NoGo Task

Matthew M. Gerhold[1], Joseph L. Jacobson[1,2,3], Sandra W. Jacobson[1,2,3], Ernesta M. Meintjes[1], Christopher D. Molteno[3] and Colin M. Andrew[1,4]

[1]Division of Biomedical Engineering, Department of Human Biology, University of Cape Town, South Africa; [2]Department of Psychiatry and Behavioural Neurosciences, Wayne State University School of Medicine, Detroit, MI, United States; [3]Department Psychiatry and Mental Health, University of Cape Town; South Africa. [4]Essentric Technology, Cape Town, South Africa.

Abstract

Cognitive-control refers to the central nervous system's ability to dynamically reallocate cognitive resources in order to deal with a change in task demands. Response inhibition tasks as well as tasks that require participants to select against a prepotent tendency all depend heavily on such processing. In adult samples performing the Go/NoGo task, when there is a high-demand for cognitive-control in order to inhibit a prepotent motor response, an induced gamma-band event-related synchronisation (ERS) is observed over the frontal-central regions of the scalp. The gamma-band ERS is also observed when selecting an alternative motor response in the

presence of prepotency. Research in clinical populations characterised by frontal lobe dysfunction, such as in schizophrenia and schizoaffective disorders, demonstrate an absence of this oscillatory bout when experimental conditions create a high demand for cognitive-control. Fetal alcohol syndrome (FAS) shares some overlap with disorders weighted heavily towards frontal lobe function, as it is also characterised by underdeveloped regions and features in the frontal regions of the cerebral cortex as well as deficits on tasks that require cognitive flexibility. Using time-frequency approaches to study induced event-related neocortical oscillations, we tested to see if we could observe the gamma-band oscillatory bout in a normally-developing sample performing a simple visual Go/NoGo task. We also tested to see whether heavy PAE affects this scalp-measured oscillatory bout. Our results demonstrate that within the normally-developing control group a frontally-oriented, induced gamma-band ERS is observed in the NoGo-condition. This scalp-measured oscillatory bout was not observed within the Go-condition, where spectral power desynchronised relative to baseline levels. While from a behavioural perspective the heavy-exposed group achieved equivalent levels of inhibitory control, the frontal gamma-band ERS was not observed in the NoGo-condition within this group. For the heavy-exposed participants, in both experimental conditions, induced gamma-power was observed within the margins of baseline power (CI 95%). In addition, we observed significantly slower median reaction times in the HE group with relatively less errors-of-omission, suggesting that the HEs approach the task with a slower more purposive strategy. None of the observations could be attributed to confounding due to post-natal lead exposure (Pb; μg/dl), caregiver's level of education, and ADHD diagnosis. Thus, heavy PAE leads to frontal lobe dysfunction associated with less efficient cognitive-control processing, prompting more purposive performance strategies in heavy-exposed participants.

3.1 Introduction

Heavy prenatal alcohol exposure leads to a spectrum of disorders collectively known as fetal alcohol spectrum disorder (FASD) (Chudley *et al.*, 2005; Wattendorf & Muenke, 2005). It is estimated that around 119 000 children are born globally with full-blown fetal alcohol syndrome (FAS) each year, with South Africa, the United Kingdom, and Eastern Europe having the highest prevalence rates (Popova *et al.*, 2017). This spectrum of disorders is characterised by a specific symptom cluster that includes facial dysmorphologies and growth retardation, but also characteristic of FASD are a number of behavioural deficits observable during performance on experimental tasks that recruit frontal lobe executive functions (Crocker *et al.*, 2011; Fryer *et al.*, 2012; Jones & Smith, 1973; Mattson *et al.*, 1999). Facial dysmorphologies that occur in the instance of full-blown FAS, such as a flattened philtrum, flattened midface, thin upper lip, and shortened palpebral fissures have been linked to underdeveloped regions and features of the cerebral cortex (Archibald *et al.*, 2001; De Guio *et al.*, 2014; Sowell *et al.*, 2002). Diffusion tensor imaging (DTI) studies have revealed changes in the structure of cortical white-matter fibre tracts in instances of heavy PAE (Fan *et al.*, 2016). In milder cases along the spectrum, heavy alcohol exposure can lead to disordered neurophysiological function with behavioural deficits in the absence of observable dysmorphologies (Fryer *et al.*, 2012; Mattson & Riley, 1998).

The research literature indicates that heavy PAE affects executive functions. One important component of executive function is response inhibition that refers to an ability to inhibit or supress a prepotent behavioural tendency that is set in motion during an experimental task. Successful response inhibition is further dependent on cognitive-control processing, i.e. the central nervous system's ability to dynamically reallocate cognitive resources in order to deal with a change in task demands—characteristically in the service of an updated behavioural goal (Botvinick *et al.*, 2001; Brown, 2013). The requirement to inhibit a prepotent tendency increases the demand

for cognitive-control, as does the requirement to select an alternative response in the presence of prepotency (Mostofsky & Simmonds, 2008). An example of an experimental task that requires participants to select against prepotency would be the Stroop Color-Word Test, where a participant must inhibit/supress the tendency to read a word (the name of a colour) and instead name the colour of the text in which the word is written (Ridley, 1935). The preparing-to-overcome-prepotency (POP) task is another such task, wherein a participant is cued to perform a series of motor responses such as left and right button presses, but on occasion is prompted to select an opposite response to the one that is cued, i.e. press the left direction key even though the right direction key is cued or vice versa (Cho *et al.*, 2006). The Go/NoGo response inhibition task is a well-established approach used to assess response inhibition capacity. Within this task, a participant is presented with a series of stimuli: Go stimuli that cue the participant to perform a simple motor response such as a button press, and NoGo stimuli that signal that the participant should inhibit/suppress the motor response. A participant's level of performance on the task is assessed in terms of the proportion of successfully inhibited motor responses; however, the task produces a number of other useful performance metrics, such as error rates for each condition and an average reaction time for the motor responses in the Go-condition (Burden *et al.*, 2009, 2011; Gerhold *et al.*, 2017; Kodali *et al.*, 2017).

Studies that have investigated inhibiting or selecting against prepotency within the FASD population have produced mixed results. Impairment of response-selection in the presence of prepotency due to PAE has been observed on challenging measures of cognitive-control such as the Stroop Color-Word Test (Connor *et al.*, 2000; Mattson *et al.*, 1999). In studies that utilise other response inhibition tasks, such as the Go/NoGo task, deficits of inhibitory control have not been observed in FASD groups relative to normally-developing controls (Kodituwakku, 2009). A number of EEG event-related potentials (ERP) studies using the Go/NoGo task have reported equivalent levels of inhibitory control within FAS groups; however, equivalency of performance is

accompanied by significant changes in ERP waveform morphology (Burden *et al.*, 2009, 2011; Gerhold *et al.*, 2017). In a visual Go/NoGo task, Burden *et al.* (2009) reported equivalent levels of inhibitory control in the heavy-exposed group accompanied by changes in the P2-N2-P3 ERP waveform complex. Burden *et al.* (2009) also observed a late slow-wave component in the FAS group within the NoGo-condition. Gerhold *et al.* (2017), in an auditory version of the task, reported normal levels of inhibitory control in the heavy-exposed group, but demonstrated heavy-exposed participant's median reaction times were significantly slower compared to normally-developing controls. As in Burden *et al.'s* study, Gerhold *et al.* (2017) also observed significant changes on a number of ERP components.

Induced event-related oscillations are distinctly different in terms of their underlying neurophysiological generating mechanisms from those neural processes that generate an ERP waveform, and are thus of interest due to the complementary information they can offer regarding the electrical dimension of human brain function (Andrew & Fein, 2010b; Luck, 2012; Pfurtscheller & Lopes da Silva, 1999). To date, no studies exist on event-related induced oscillatory activity in heavy prenatally alcohol-exposed samples: event-related EEG studies have focused exclusively on event-related potentials (Burden *et al.*, 2009, 2011; Gerhold *et al.*, 2017; Kaneko *et al.*, 1996). Induced gamma-band oscillations and their spatial-temporal dynamics are of interest, as gamma-band oscillatory dynamics over the frontal regions of the scalp are linked to cognitive-control mechanisms involved in inhibiting and selecting against prepotency (Kieffaber & Cho, 2010; Shibata *et al.*, 1999). These studies have been conducted in healthy adult and mixed age-group samples; what clinical studies are available have focused schizophrenic and schizoaffective participants, due to an interest in understanding disordered frontal lobe function (Cho *et al.*, 2006; Minzenberg *et al.*, 2010). The published research was conducted using the Go/NoGo task and a closely related response-selection task, the POP task. The Go/NoGo and POP tasks assess prefrontal inhibitory control over the central motor system: both motor response

inhibition and selection against prepotency require prefrontal and medial frontal cognitive-control processing (Mostofsky & Simmonds, 2008). The tasks differ in that the POP task activates cognitive-control processing in order to shift away from a prepotent response tendency to an alternative motor response, compared to the Go/NoGo task, where participants shift from prepotency to an inhibited state within the central motor system.

Cho *et al.*, (2006), using a POP task within an adult sample, identified an induced gamma-band ERS in the right anterior frontal and left frontal central regions when normally-developed adults were required to switch against prepotency; this oscillatory bout was absent in the clinical group's data. Minzenberg *et al*. (2010), using the POP task in a sample of participants that ranged from adolescence to adulthood, observed an increase in frontal gamma-band oscillatory power over the left and midline frontal regions in the control group; while within the clinical group, a decrease in induced gamma-power was observed in the same regions. Using a modified POP task, wherein anticipatory cues were used to implicitly suggest the need to switch away from prepotency, Kieffaber & Cho (2010) demonstrated a frontally-oriented and a left posterior parietal induced gamma oscillation in healthy adult participants. The power of the frontal induced gamma oscillation was shown to increase when an increased need for cognitive-control was anticipated. Kieffaber & Cho's (2010) findings indicate that the observed frontal induced gamma oscillation not only reflects cognitive-control processes, but also anticipatory/preparatory prefrontal-lobe processing prior to selecting against prepotency. A study conducted by Shibata *et al.*, (1999), using a visual Go/NoGo task, reported an oscillatory bout within the gamma-band (31Hz) over the central regions of the scalp early on in the NoGo trials. However, it is unclear whether the response was an induced oscillation, as Shibata *et al.* did not subtract evoked power contributions from the oscillatory data, nor did they present an analysis of inter-trial coherence measures to distinguish between evoked and induced

power changes (Delorme & Makeig, 2004; Pfurtscheller & Lopes da Silva, 1999; Tallon-Baudry *et al.*, 1996).

The reported induced frontal gamma-band oscillations have yet to be studied in a normally-developing sample performing tasks that require inhibition of a prepotent tendency, such as in the Go/NoGo task. As an induced gamma-band ERS is observed over the frontal regions in adult and mixed age-group samples during performance of tasks that require dealing with prepotency, we should observed similar gamma-band oscillatory dynamics in a normally-developing sample when there is a need for increased cognitive-control in order to inhibit a prepotent motor response. The impact of PAE on induced gamma-band oscillations in response inhibition tasks has not been investigated to date; thus, nothing is known about how PAE may affect spatial-temporal dynamics and the magnitude of the high-frequency, scalp-measured oscillatory bout. We certainly would expect that heavy PAE is related to changes in the oscillatory feature, due to deficits seen on tasks that involve prefrontal/frontal executive functions and also due to the structural changes within the cerebral cortex and cortical white-matter.

Our aims are to: (1) elicit the cognitive-control linked induced gamma-band ERS using a simple visual Go/NoGo task within a normally-developing sample and (2) to investigate the impact of PAE on this scalp-measured oscillatory bout. Ours is the first study to extend the findings of a number of response-selection and response inhibition studies in order to explore teratogenic effects related to PAE on cognitive-control processing. We hypothesise that: (1) a frontally-oriented, induced gamma-band ERS will be elicited in an early post-stimulus time-window within a normally-developing control group in the NoGo-condition, but not within the Go-condition; (2) heavy PAE will affect the power of the frontal induced gamma-band ERS—due to lack of previous research in the FASD population, we have no expectation on the direction of this effect; (3) analysis of the phase component of the EEG event-related data will reveal that the oscillation is of an induced nature; (4) equivalent inhibitory performance will be

observed across experimental groups, although slower median reaction times will be observed for the heavy-exposed group.

3.2 Methods

3.2.1 Participants

Sixteen right-handed children and their mothers/guardians were sampled from the Cape Coloured community in Cape Town, South Africa. The Cape Coloured are descendants from a mixed ancestral lineage including European colonists, Malaysian slaves, Khoisan aboriginals, and the African Nguni ethnic group. Poor socio-economic circumstances and historical practices of compensating farm labour in part with wine have contributed to a tradition of heavy recreational weekend binge drinking in a portion of this population. This pattern of consumption persists amongst pregnant women within the population. As a result, the Cape Coloured community experiences one of the highest levels of FASD in the world (Popova *et al.*, 2017). Nine children met the diagnostic criterion for FAS or PFAS; seven children were no more than minimally exposed during pregnancy—the mothers drank less than one to two days per month and less than two standard drinks on any single occasion. Eight children were the older siblings of participants in our Cape Town Longitudinal Cohort study (Jacobson *et al.*, 2008). The remainder were identified by screening all of the 8- to 12-year-old children from an elementary school in a rural section of Cape Town where there is a very high incidence of alcohol abuse among local farm-workers (Jacobson *et al.*, 2011; Meintjes *et al.*, 2010). All mothers/guardians provided written informed consent and all children provided oral assent. Each mother received a small monetary compensation for her participation and each child was given a small gift.

3.2.2 Protocols

All protocols were approved by Wayne State University and the University of Cape Town institutional ethics review boards.

3.2.2.1 Alcohol Consumption, Diagnostic Criterion, and Psychometric Data Collection.

Each mother was interviewed in her primary language (Afrikaans or English) regarding her alcohol consumption during pregnancy using a timeline follow-back approach (Jacobson *et al.*, 2002). Volume was recorded for each type of beverage consumed on a daily basis, converted to absolute alcohol (AA) using weights that reflect AA concentrations in Cape Town (liquor—0.4, beer—0.05, wine—0.12, cider—0.06), and averaged to provide a summary measure of alcohol consumption during pregnancy (AA/day). The number of cigarettes smoked on a daily basis during pregnancy was recorded using a self-report methodology. Mothers were also interviewed regarding their education and occupational status and that of their spouse/partner; they were also scored for socio-economic status (SES) using the Hollingshead Scale (Adams & Weakliem, 2011; Hollingshead, 1975). Diagnoses of FAS or PFAS were made by two of three expert dysmorphologists (HEH, LKR, NK; see Jacobson *et al.*, 2008) based on the revised Institute of Medicine criteria (Hoyme *et al.*, 2005). Handedness was assessed with the Annett (1970) Behavioural Handedness Inventory. IQ was estimated using Sattler's (1992) formula for Short Form IQ using seven subtests from the Wechsler Intelligence Scales for Children, third edition (WISC-III): Similarities, Arithmetic, Digit Span, Symbol Search, Coding, Block Design, and Picture Completion, as well as Matrix Reasoning from WISC-IV.

3.2.2.2 EEG Data-Acquisition

EEG data were acquired using an active-electrode Biosemi ActiveTwo EEG system (BioSemi, Netherlands, Amsterdam). A Common Mode Sense (CMS) and Driven Right

Left (DRL) reference/ground scheme was used for data-acquisition, with an on-line band-pass filter set at DC-400Hz. Data were acquired at a sampling rate of 512Hz at 24-bit resolution. 34 electrodes were placed according to the 10/10 electrode placement system (Jurcak, Tsuzuki, & Dan, 2007). We placed the electrodes on the participant's head using a tight-fitting elasticised cap; a conductive gel was injected into the gel cavity of each electrode to form a conductive bridge between the scalp and measurement electrode. Measurement electrodes fitted in the cap were placed over the following regions: anterior-frontal (AF3, AF4, Fp1, Fp2), frontal (F3, F4, F7, F8, Fz), frontal-central (FC1, FC2, FC5, FC6), central (C3, C4, Cz), central-parietal (CP1, CP2, CP5, CP6), parietal (P3, P4, P7, P8, Pz), parietal-occipital (PO3, PO4), temporal (T7, T8), occipital (O1, O2, Oz), and mastoids (M1, M2). In addition, two sets of bipolar pairs were placed: (1) above and below the right eye, and (2) near the outer canthus of the left and right eye. These bipolar pairs recorded vertical and horizontal eye-movements, respectively. An additional channel was used to record participant behaviour, i.e. a button press made during the experimental task. Data was stored off-line in the *.bdf file format.

3.2.2.3 Go/No-Go Task

The experimental task was administered using E-Prime® 2.0 Professional Edition (Psychological Software Tools, Pennsylvania, USA). Each participant was instructed to press a button with the index finger of the right hand in response to a letter that appeared on the screen (the "Go" trials) with the exception of "X" (the "NoGo" trials). Inter-stimulus intervals were constant through the sessions (ISI = 5500ms), with the stimulus centered on screen for 500ms followed by a blank screen for 5000ms. Go and NoGo stimuli were alternated randomly within five consecutive blocks of 30 trials each (20 Go, ten NoGo) for a total of 150 trials. We placed a two-minute rest period between blocks. The entire task, including instructions and practice items, took approximately 20 minutes to complete.

3.2.3 EEG Data Analysis

All processing was performed within the MATLAB computing environment using an in-house toolbox and custom scripts built upon functions provided by the EEGLAB toolbox (Delorme and Makieg, 2004). EEG data were not available for three participants due to: (1) technical problems (n = 2) or (2) refusal to wear the cap (n = 1). Of the remaining 13, seven children were heavy-exposed and six children constituted the normally-developing control group.

3.2.3.1 Preprocessing

Data were imported into MATLAB, re-referenced to a linked Mastoid reference, and filtered using a band-pass filter from 0.5Hz – 45Hz. Recordings were scanned for gross-movement artefacts, and those portions of data contaminated by large movements were excluded from the dataset. The two-minute rest periods between blocks were also excluded from further analysis. Noisy channels were identified and replaced by interpolating the channel from neighbouring channels. Data were then segmented relative to stimulus onset: 750ms prior to stimulus onset and 1750ms post-stimulus onset. The epoched data were submitted to a *blind source separation* (BSS) algorithm: the *adapted infomax* algorithm within EEGLAB. Derived components were visually scanned for evidence of artefact; those components that were indicative of oculargenic and myogenic artefact were removed. Components were projected back onto the scalp to form an artefact-free dataset. Epochs were then submitted to a time domain thresh-holding algorithm: any epoch with extreme values exceeding 50μV was excluded from further analysis—this resulted in less than 5% of epochs being excluded. The epochs were then scanned for behavioural response data using custom software written within the MATLAB computing environment (The MathWorks Inc., Natick, MA, USA). The software classified and stored information associated with the following responses: correct Go, correct NoGo, incorrect Go, and incorrect NoGo. The

behavioural response data was used for further analysis of participant behaviour under the experimental conditions.

3.2.3.2 Time-Frequency Representations

Short-time Fourier transform (STFT) and adaptive-autoregressive (AIC-AAR) time-frequency representations were generated using an in-house MATLAB based toolbox that implements a number of different time-frequency estimation algorithms for the purposes of EEG event-related analysis. Prior to computing the TFRs the EEG data was down-sampled to fs = 128Hz. For the STFT and AIC-AAR approaches, 500ms windows were used with the window slid by a single sample point. When using the STFT approach, a hamming window was applied to the data. No tapering was applied to the data when using the AIC-AAR approach as the power spectral density (PSD) estimates are derived from the model coefficients and not from the data itself; thus, discontinuities at the start and end of data segments do not influence the PSD estimates as they would in an STFT approach, in terms of spectral leakage—this is due to the implicit extrapolation of the auto-covariance sequence when using autoregressive time series models (Marple, 1986).

3.2.3.3 Autoregressive Model Order Selection

We selected the model order for the AR-based approach using the Burg algorithm for coefficient estimation and AIC and AIC-C approaches for model order selection. As per the suggestion in Florian and Pfurtscheller (1995) and Mullen (2014), we utilised a subset of data segments taken across trials and across time-windows within trials, we randomly sampled 10% of trials and 3 x (500ms 0% overlapping time-windows) within each trial. Estimates using each of the information criteria—AIC and AIC-C—were computed across a range of model orders ranging from p = 1 – 30. These estimates were computed separately for each of the sampled segments and then stored for analysis. In order to derive an estimate of model order, we took the median measure for each information criterion across all data segments for which we estimated a model

order. As the distributions were skewed for these metrics, a median offered the best measure of central tendency.

AIC yielded a median estimate across segments of p = 28. AIC-C provides an estimation of model order slightly lower than that of AIC, p = 23. Optimal model orders were selected within a range defined by median AIC and median AIC-C. AIC and AIC-C parametrised representations, which utilise less hefty penalties for higher-order models, provide representations of signal components more well-defined in frequency relative to the STFT representations. As such, we expect that the two methods will estimate common oscillatory information; however, components identified by either method will have slightly different specifications in frequency and time.

3.2.3.4 Single-Trial Time-Frequency Representations: gamma power

Single-trial time-frequency representations were generated using STFT and AIC-AAR approaches. These TFRs were baseline corrected by subtracting the average baseline power (-500ms – 100ms) from each time point of the single-trial time-frequency representations. Baseline confidence intervals were then derived using bootstrap resampling procedures applied to the baseline corrected data (Efron & Tibshirani, 1986; Hastie *et al.*, 2009). Each time-frequency point in each single-trial TFR was then compared to the adjusted baseline CI = 95%, where the adjustment was made by computing an FDR significance threshold using methods presented in Durka *et al.*, (2004). This yielded baseline corrected time-frequency representations for both algorithms where in non-significant time-frequency points were set to zero.

3.2.3.5 Single-Trial Time-Frequency Representations: gamma ITC

Inter-trial coherence (ITC) is a measure of the strength of phase-alignment across trials within EEG event-related data. ITC is expressed as a phase-locking value (PLV) ranging from 0 to 1: 1 represents no difference in the phase of a signal across trials

within a time-frequency region and 0 represents consistent differences in phase across single-trials. As with event-related spectral power, ITC can be expressed as a baseline corrected time-frequency representation, where baseline correction procedures and significance testing are computed in the same manner as for spectral power. The PLV values are computed based on single-trial Fourier spectra at each time-point across multiple trials (see Delorme & Makeig, 2004; Tallon-Baudry *et al.*, 1996 for details of ITC computation). In our analysis, we use the Fourier spectra derived from windowed data segments. ITC measures are important as they have direct neurophysiological relevance. Medium-strong PLVs across trials represent evoked power, spatially wide-spread neocortical phase-reset driven by afferent-thalamocortical connections. Weak PLVs represent induced power, spatial localised neocortical oscillations, driven primarily by calcium-channel mediated low-threshold spiking in the recurrent thalamocortical relay circuits (Pfurtscheller & Lopes da Silva, 1999; Pfurtscheller, 2006; Suffczynski *et al.*, 2001). Given that the frontal beta-ERS is an induced oscillation, we expect that analysis of the phase component of the EEG across trials will reveal weakly phase-locked activity in both the Go- and NoGo-condition for both experimental groups. In addition, the ITC values and beta-power should be uncorrelated with an ERP area-measure within the same time-window (350ms – 650ms), as in the instance of an induced response, ITC and spectral-power should vary independently from ERP magnitude.

3.2.3.6 Feature Extraction

We identified a time-frequency region-of-interest (ROI) using the condition probability-contrasts within either group. We identified the target feature at the midline electrode (Fz) wherein the condition differences were significant and maximal. Preliminary analysis of the time-frequency condition contrasts highlighting the frontal gamma-band oscillation differentiating the conditions within the control group can be seen in Figure 3.1 and Figure 3.2 for STFT and AIC-AAR spectral estimates respectively (see Appendix E for the STFT group contrasts at the Fz electrode).

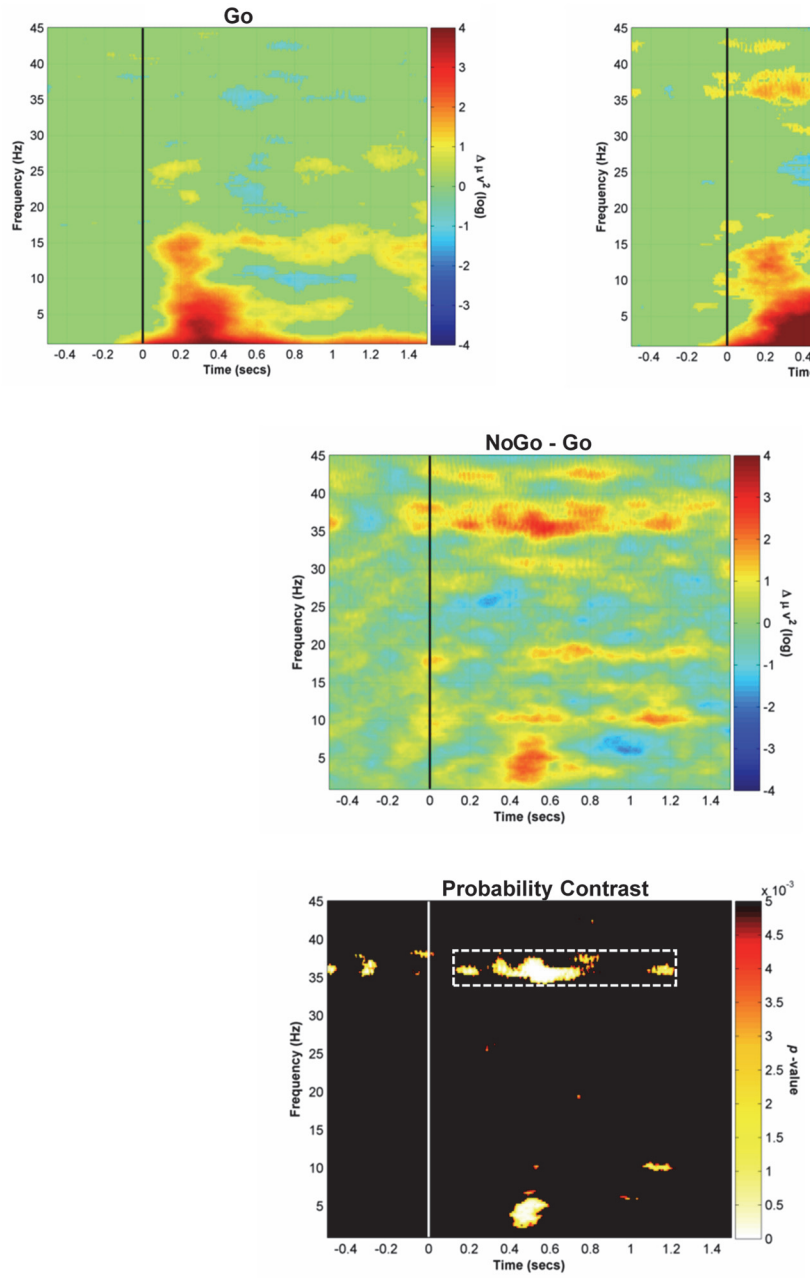

Figure 3.1: STFT condition contrasts from the control group's data. The top two panels in the first row are time-frequency representation: (Left) the Go-condition and (Right) the NoGo-condition taken from the Fz electrode (10/10 electrode placements). The middle panel is the contrast between conditions expressed as differences in baseline corrected log-power. The bottom-panel is the probability time-frequency contrast (FDR = 0.005). The gamma-band feature that differentiates conditions is highlighted by a white box.

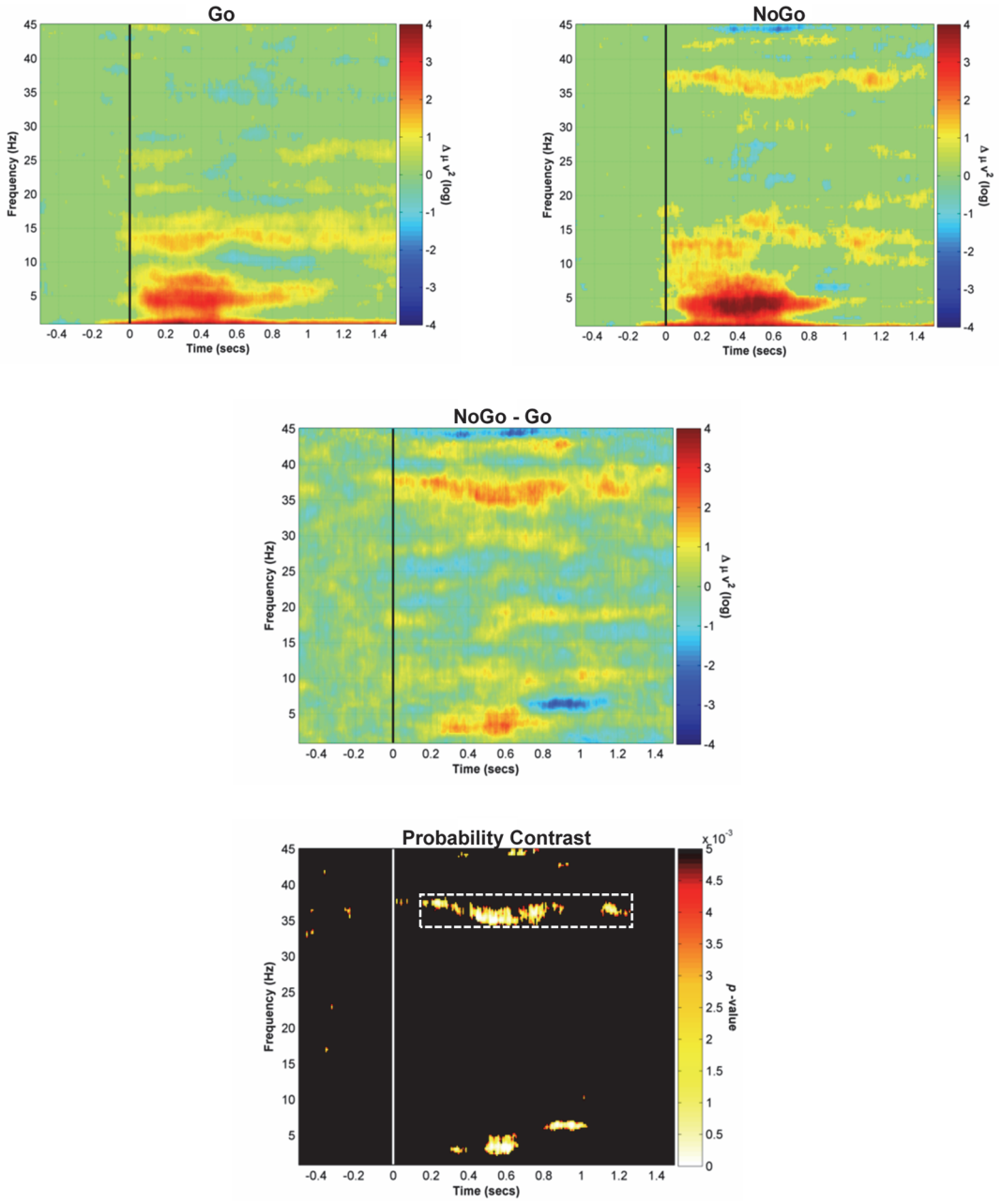

Figure 3.2: AIC-AAR condition contrasts from the control groups data using AIC-AAR-based representations. The top two panels in the first row are time-frequency representations: (Left) Go-condition and (Right) the NoGo-condition taken from the Fz electrode (10/10 electrode placements). The middle panel is the contrast between conditions expressed as differences in baseline corrected log-power. The bottom-panel is the probability time-frequency contrast (FDR = 0.005). The gamma-band feature that differentiates conditions is highlighted by a white box**.**

We further refined our frontal midline feature to a specific time-frequency region wherein maximal significant differences were observed using either spectral estimator: 450ms – 850ms, 34Hz – 38Hz. We extracted the median baseline corrected log-power measure and the inter-trial coherence (ITC) from each subject's data averaged over trials for the Go- and NoGo-conditions at the midline electrode. We chose the median as the distribution of the power and ITC values across single-trials were skewed within this time-frequency region-of-interest for all subjects; therefore, the median provided the best measure of central tendency. As high-frequency oscillations are spatially confined in comparison to lower frequency oscillations, in the instance of our frontal midline analysis, a single electrode for feature extraction was justified (Nunez & Srinivasan, 2005), this in comparison to a regional group of electrodes analysed for the lower frequency beta-band feature in Chapter Four. The frontal mid-line feature across subjects and across conditions was tabulated along with demographic and psychometric data, the socio-economic index, diagnostic classification, and alcohol consumption metrics. This table was used as the basis for a statistical analysis of the selected electrocortical feature(s).

3.2.4 Statistical Analysis

3.2.4.1 Frontal Midline Analysis

All statistical analyses were computed in SPSS 22/24 (IBM Corp, New York, United States). We used the MIXED module in SPSS to compute a fixed-effects model using group (Controls vs HE), method (STFT vs AIC-AAR), and condition (Go vs NoGo) as fixed-effects. Method and condition were defined as repeated-measures; the residual covariance matrix was estimated directly from the data. A covariance structure estimated directly from the data provided the best solution, as an initial correlation analysis and perusal of descriptive statistics on the repeated measures within the design showed unequal variances across conditions as well as different levels of

correlation between each repeated measure. The correlation structure could not be approximated by other choices for residual covariance matrix.

3.2.4.2 Parameter Estimation

Our initial set of model parameters were estimated using maximum likelihood (ML). The choice for parameter estimation (ML and an unstructured residual covariance matrix) allowed for the ML algorithm to convergence and all the conditions for a valid solution to be met. We did attempt to model the data in a number of different ways, i.e. using different covariance assumptions; however, the unstructured approach provided the best fit to the data.

3.2.4.3 Residual Analysis

We performed a check on the models residuals by assessing the normality assumption using Shapiro-Wilk's test. In all instances, this assumption was satisfied: Shapiro-Wilk's was not significant. We also checked for outliers in the residuals using the outlier labelling rule utilising a gain of G = 2.2 (Hoaglin & Iglewicz, 1987; Hoaglin, Iglewicz, & Tukey, 1986). We found two outliers, the corresponding datum points were excluded and the model was recomputed. For our final model we maintained the model parameters estimated using maximum likelihood (ML) as opposed to re-computing the model using restricted maximum likelihood (REML). Twisk (2006) argues that ML provides more accurate estimates of fixed-effects parameters, while REML provides more accurate estimates of random effects. As our model is a pure fixed-effects model, ML was the natural choice. Where interaction effects were significant, we ran a post-hoc analysis using Sidak's correction for multiple comparisons. Detrended residual plots were checked for heteroscedasticity of variance.

3.2.4.4 Covariate and Additional Fixed-Effects Analysis

In order to control for potential confounding and/or mediating effects of measured covariates and additional fixed-effects in the study, we tested nine variables for a linear

relationship between the power and ITC features. These variables included: (1) age at recording, (2) post-natal lead exposure (Pb; µg/dl), (3) WISC-IQ, (4) mother's age at delivery, (5) socio-economic status, (6) primary caregiver's education in years, (7) cigarettes smoked during pregnancy, (8) ADHD diagnosis, and (9) marital status. The first seven variables were continuous measures, while the last two were nominal-categorical and were tested as additional fixed-effects. For entry into the final model, a covariate needed to be a significant predictor of the dependent variable at trend level ($p < .10$) and provide a more parsimonious model.

3.2.4.5 Behavioural Analysis

Data tables containing performance data (reaction time data from the Go-condition and accuracy data) were used as a basis for a statistical analysis of performance under experimental conditions. We tested the reaction time data for normality and homogeneity of variance across experimental groups. All tests indicate inhomogeneity of variance and non-normal distributions, even after transforming the data (natural logarithm and BoxCox, $\lambda = .3638$) parametric assumptions were still not met. Therefore, in order to test for group differences in reaction times under the Go-condition, we computed the Mann-Whitney U test on the untransformed data. We tested to see if alcohol exposure affected error rates on a single-trial basis under the Go and the NoGo experimental conditions using Pearson's Chi-Square on cross-tabulated data. We cross-tabulated a vector with group IDs (HE vs Con) with single-trial accuracy data, where accuracy data was a vector of 0s and 1s representing incorrect and correct responses respectively. In our cross-tabulation, the null-hypothesis was that accuracy under each experimental condition was independent of alcohol exposure.

3.2.4.6 Additional Analyses

In order to add additional verification that the electrocortical oscillatory response was induced and thus varied independently from ERP magnitude, we computed a correlation analysis between ERP-area (Fz, 450ms – 850ms) versus the induced

gamma-power feature, as well as for ERP-area (Fz, 450ms – 850ms) versus the ITC feature. We utilised an ERP area-measure as opposed to measures of central tendency such as the mean or median, as an area measure is a more robust measure of magnitude due to it being less biased by noise (Luck, 2012). In order to obtain reliable confidence intervals and to generate a distribution of the test-statistic under the null hypothesis of no linear association, we adopted a resampling/permutation-based approach (Efron & Tibshirani, 1986; Hastie *et al.*, 2009). We utilised the MATLAB Parallel Computing Toolbox to generate 50 000 bootstrap resamples using resampling with replacement (The MathWorks Inc., Natick, MA, USA). In order to derive a reliable *p*-value for significance assessment, we randomly shuffled the data in either of the variables being correlated and computed the test-statistic for each iteration. This was done 50 000 times resampling with replacement. The *p*-value was calculated as the smallest proportion of the surrogate distribution that lay below/above the original sample test-statistic.

3.3 Results

3.3.1 Sample Characteristics

Table 3.1 provides participant information, mother's characteristics, and mother's alcohol consumption patterns during pregnancy. The two experimental groups did not differ on any of the measures that were used to characterise the participants or their mothers, with the exception of the alcohol consumption metrics. On average, mothers of the alcohol-exposed participants consumed 3.1 oz AA/day, which equates to 6.2 standard drinks. Scores varied over a large spread for the average daily consumption metric across the sample, ranging from 1.64 drinks/day – 19.2 drinks/day.

Table 3.1: Demographic characteristics by group.

	Alcohol Exposed (n = 7)		Controls (n = 6)		
	M (SD) or n(%)	Range	M (SD) or n(%)	Range	*F* or χ^2
Sample characteristics					
Sex (% Female)	6 (85.72)	-	5 (83.34)	-	<1
Age at recording (years)	12.39 (1.25)	10.75-14.31	12.97 (1.14)	11.84 -14.74	<1
Lead exposure (Pb; μg/dl)	6.79 (2.55)	4.00-12.00	5.93 (1.08)	3.00-11.00	<1
WISC IQ[a]	67.23 (11.50)	51.07-85.15	64.37 (11.19)	54.56-81.84	<1
ADHD (% diagnosed)[b]	2 (28.57)	-	0 (0)	-	2.026
Mothers charactersitcs					
Age at delivery (Decimal)	26.03 (4.58)	18.84-33.14	26.31 (3.86)	19.26-29.71	<1
Socio-economic status[c]	19.57 (7.03)	11.00-29.00	16.83 (7.82)	8.00-28.5	<1
Highest educational achievement	7.57 (3.46)	0.00-10.00	6.67 (0.82)	6.00-8.00	<1
Marital status (Married/Not Married)	3 (42.90)	-	2 (33.30)	-	<1
Cigarettes/day gestation period	4.71 (2.69)	0.00-8.00	3.50 (4.087)	0.00-10.00	<1
Mothers Alcohol Consumption					
AA/day (oz)	3.08 (3.27)	0.82-9.60	0.01 (0.02)	0.00-0.05	5.3*
AA/drinking day (oz)	6.44 (3.06)	2.85-10.05	0.35 (0.53)	0.00-1.06	23.17***
Frequency (% days across pregnancy)	43.17 (28.40)	29-100	1.00 (2.00)	0.00-4.00	13.39**

Note. AA refers to absolute alcohol; 1 oz AA ≈ 2 standard drinks. [a]Wechsler Intelligence Scale for Children. [b]Attention deficit/hyperactivity disorder. [c]Hollingshead (1975) Four Factor Index of Social Status Scale (Adams & Weakliem, 2011). *p <0. 05; **p < 0.01; ***p < 0.0001.

On each drinking occasion, mothers of the heavy-exposed participants consumed just under 13 standard drinks (12.9 drinks per occasion); the group's mothers varied in their consumption within a range of 5.7 drinks/occasion – 20.1 drinks/occasion. Apart from the mother of the most heavily exposed, who drank every day during pregnancy, consuming the equivalent of 19.2 standard drinks per day, the rest of the sample engaged in binge drinking spaced some days apart. Four of the mothers of the children in the control group reported abstaining entirely from alcohol during pregnancy; the other two drank less than one to two days per month and less than two standard drinks on any single occasion.

3.3.2 Behavioural Data

Results for the analysis of the behavioural data are presented in Table 3.2. The control group made proportionally more errors-of-omission ($p < .05$). The difference in omission error rates between groups was $\Delta = 2.79\%$. Both groups made proportionally the same amount of commission errors: $\Delta = 0.17\%$. Based on a non-parametric test, the control group's median reaction time was significantly faster.

Table 3.2: Behavioural data by group.

	Heavy-Exposed (% of trials/ms)	Controls (% of trials/ms)	Statistics χ^2 or U	Statistics ϕ_c or r
Error Trials				
Omission Errors	3.00%	5.79%	4.89	0.067*
Commission Errors	8.79%	8.62%	0.005	0.003
Reaction time				
Correct Go (ms)	554.69 (8.38)	513.67 (8.76)	115444	0.12**

*p <0. 05; **p < 0.01.

The data points to the fact that there is a group specific speed-accuracy trade-off within the control group. However, both groups achieved similar levels of inhibitory control—there was no group difference in terms of inhibiting a response ($p = .946$). Given the reaction time data and differences in omission error rates, heavy-exposed

participants are approaching the task with a slower more purposive strategy, enabling comparable inhibitory performance.

3.3.3 Electroencephalography

Topographical maps highlighting the frontally-oriented, event-related induced gamma-band dynamics are presented in Figure 3.3. The scalp maps of the control group under the NoGo-condition show a frontal midline increase in spectral power. The posterior regions of the scalp, specifically the right-hemisphere, show a marginal increase in gamma power. One also observes a regionally specific marginal increase in spectral power over the ipsilateral motor area. Our analysis focuses on the frontal-midline oscillation due to its connection with cognitive-control processing.

3.3.3.1 Induced Power

In our fixed-effects gamma-power model, a number of main and interaction effects were significant. There was a main effect for group, $F(1,13.033) = 6.286$, $p < 0.05$, spectral power in the control group was observed within the margins of baseline power tending towards an ERS ($M = .276$, $SE = .159$); while in the heavy-exposed group, spectral power was observed within the margins of baseline power tending towards an ERD ($M = -.260$, $SE = .143$). The main-effect for method was not significant, $F(1,12.504) = .228$, $p = .641$; however, there was a significant group x method interaction, $F(1,12.504) = 11.753$, $p < .005$, that demonstrated that different methodological choices can influence analytical outcomes. For example, group differences emerged when using a STFT spectral estimator ($p < .05$): minimally-exposed ($M = .345$, $SE = .167$) and heavy-exposed ($M = -.313$, $SE = .150$); but not when using an AIC-AAR spectral estimator ($p = .068$): minimally-exposed ($M = .206$, $SE = .155$) and heavy-exposed ($M = -.208$, $SE = .139$). The marginal means indicate that AIC-AAR spectral estimates are lesser in magnitude.

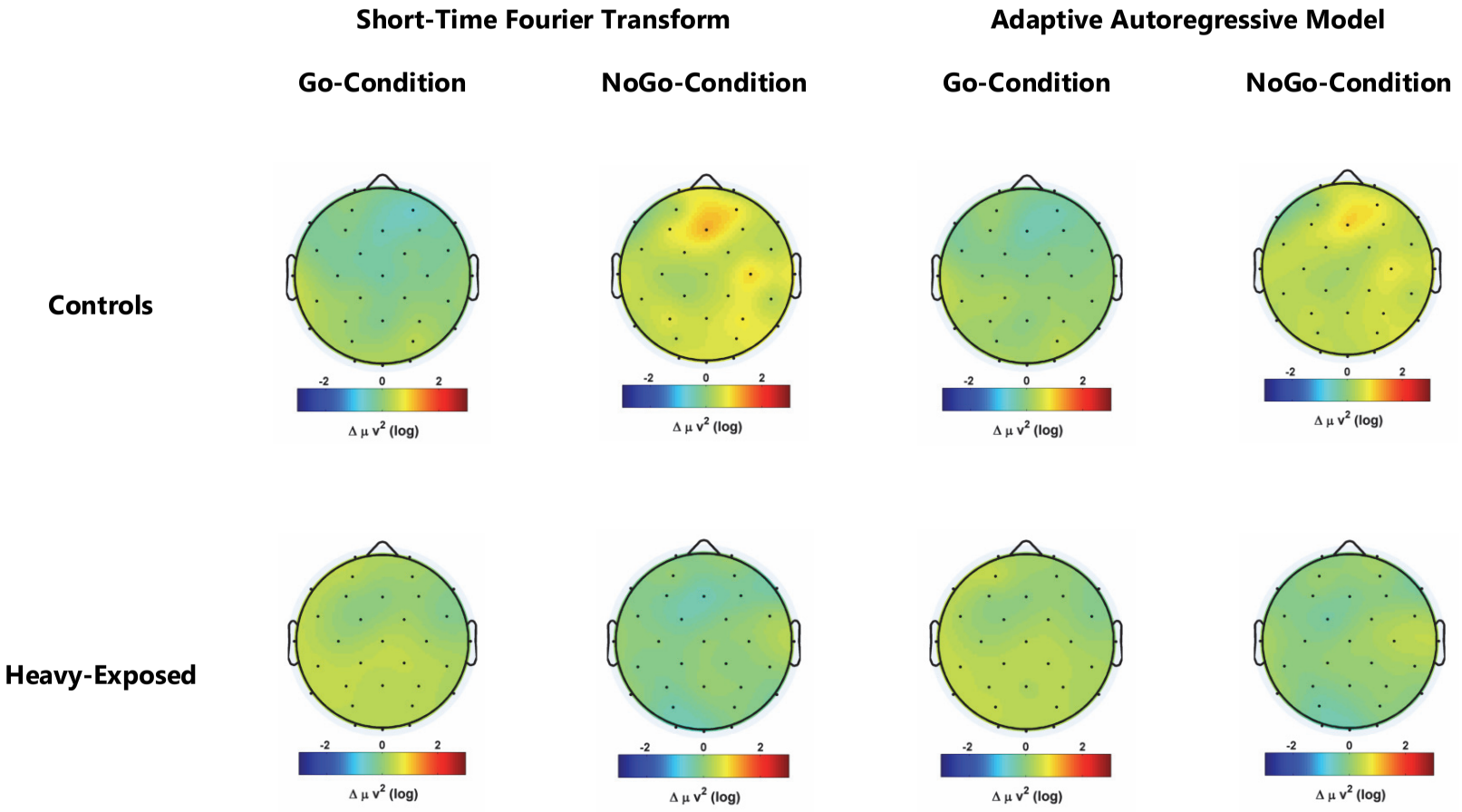

Figure 3.3: Topographical maps of the gamma-band dynamics in 34 – 38Hz band and 450ms – 850ms time-window. Map are presented by group and condition and then nested under choice of spectral estimator.

There was a significant main effect for condition, $F(1,13.033) = 15.908$, $p < 0.01$, the constraints of the NoGo-condition lead to an ERS (M = .335 SE = .160); this in comparison to the Go-condition, wherein power desynchronised relative to baseline levels within the gamma-band region of interest (M = -.320, SE = .140). However, in both instances, the levels of induced gamma-power were still observed within the margins of baseline power (CI 95%). One should interpret this effect cautiously, as the control group under the NoGo-condition is the only level within the experimental design that displays significant increases in oscillatory power relative to baseline. Thus, condition effects are influenced more by control group dynamics in the NoGo-condition than any other event-related neocortical dynamics accounted for in our experimental design. In this regard, we did find a significant group x condition effect, $F(1,13.304) = 30.191$, $p < 0.001$. This effect is illustrated in Figure 3.4.

Controls demonstrated a significant difference between the two experimental conditions, $F(1,13.751) = 39.922$, $p < 0.001$, with an ERS occurring in the NoGo-condition (M = 1.054, SE = .240) and a ERD occurring in the Go-condition (M = -.503, SE = .153). There was no significant difference between conditions for the heavily-exposed group, $F(1,12.708) = 1.298$, $p = .276$: both the Go-condition (M = -.137, SE = .141) and the NoGo-condition (M = -.384, SE = .211) were observed within the margins of baseline power. Group differences between induced gamma-power in the NoGo-condition were observed, $F(1, 12.961) = 20.262$, $p < 0.01$, with a significant increase relative to baseline occurring in the normally-developing control group (M = 1.054, SE = .240), while we observed power levels within margins of baseline power within the HE group (M = -.384, SE = .211). No group differences were observed within the Go-condition, $F(1, 13.000) = 3.096$, $p = .102$. In the control group, power desynchronised relative to baseline (M = -.503, SE = .153); while for the HE's power was observed within margins of baseline power (M = -.137, SE = .141). This interaction effect and associated post-hoc comparisons indicate that the main condition effect was driven by the control group's event-related synchronisation in the NoGo-condition. There was a

significant interaction effect for group x method x condition, $F(1, 13.440) = 4.809$, $p < 0.05$—the interaction is illustrated in Figure 3.5 and the marginal means for each level of the experimental design appear in Table 3.3.

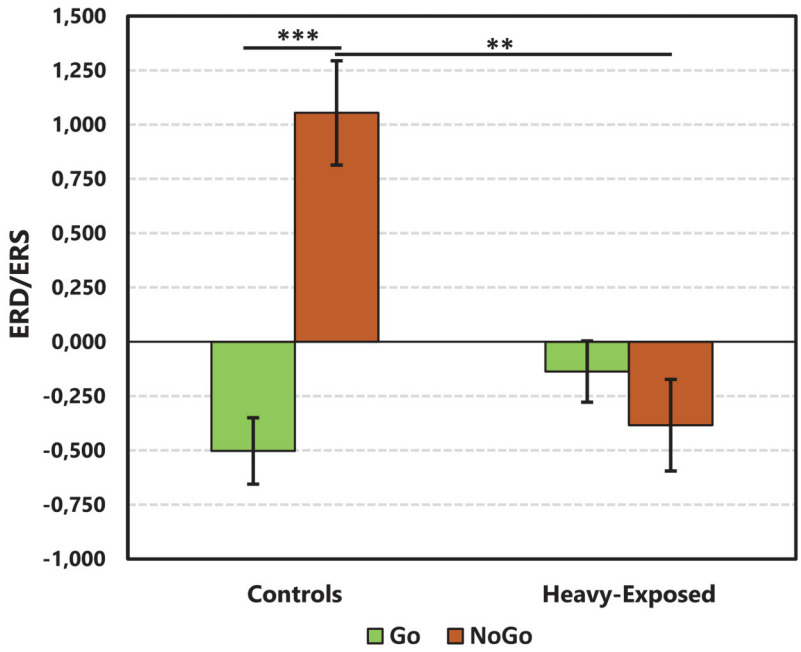

Figure 3.4: Bar graph illustrating the group x condition interaction effect. ERD/ERS represents a change in spectral power relative to pre-stimulus baseline, expressed as a difference in log power, $\Delta\mu V^2(\log)$**.** Error bars represent 2 x standard errors. ** $p < 0.01$, ***$p < 0.001$.

Table 3.3: Baseline-corrected gamma power estimates: marginal means and standard-errors.

	STFT		AIC-AAR	
	Go	NoGo	Go	NoGo
Controls	-.467 (.22)	1.157 (.25)	-.538 (.17)	.951 (.25)
Heavy-exposed	-.093 (.13)	-.532 (.21)	-.180 (.16)	-.236 (.22)

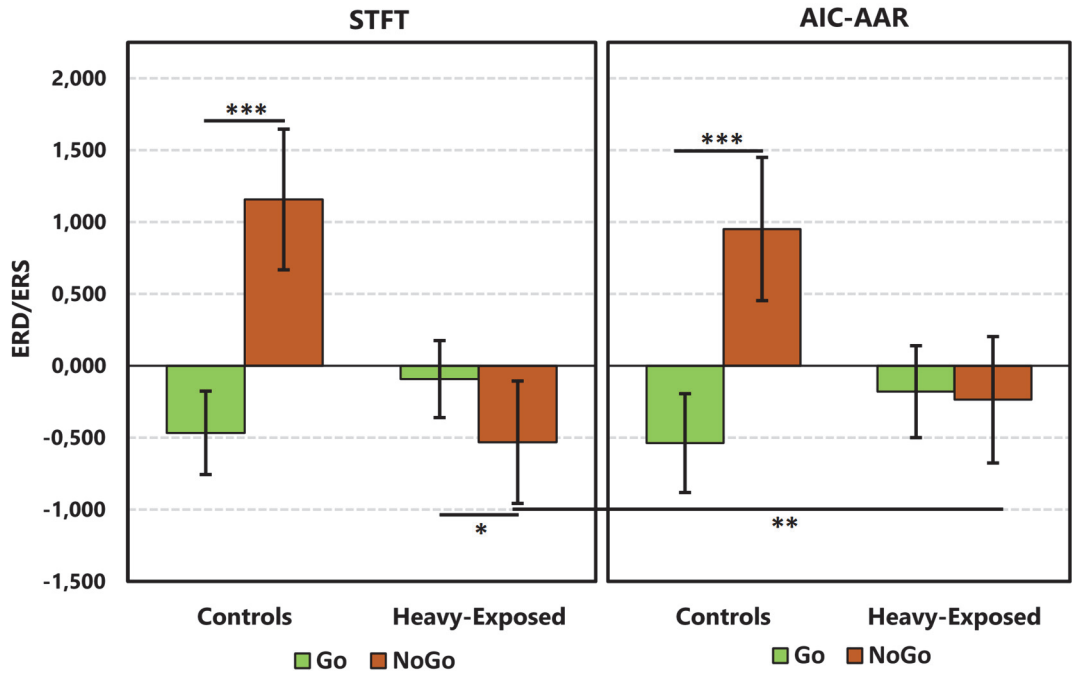

Figure 3.5: Bar graph illustrating the group x method x condition interaction. ERD/ERS represents a change in spectral power relative to pre-stimulus baseline, expressed as a difference in log power, $\Delta\mu V^2$(log). Error bars represent 2 x standard errors. *p < 0.05, **p < 0.01, ***p < 0.001.

Irrespective of methodological choice, the control group showed significant differences between conditions: using a STFT spectral estimator, there was a large difference between Go- and the NoGo-conditions in the control group, $F(1,12.861) = 53.372$, $p < 0.001$; when using an AIC-AAR spectral estimator, this difference was also observed $F(1,13.926) = 25.383$, $p < 0.001$, although the effect was not as large. A significant difference between conditions was observed in the heavy-exposed group when using a STFT spectral estimator, $F(1,12.329) = 5.278$, $p < 0.05$; however, spectral power was observed at baseline levels with a tendency towards ERD under the NoGo-condition within this group, in contrast to observed ERS within the control group. AIC-AAR spectral estimates did not yield the condition difference in the heavily-exposed group, $F(1,12.877) = 0.044$, $p = 0.837$.

Estimates from the two spectral estimators did not differ significantly across the control group's data in the Go-condition, $F(1,13.000) = .607$, $p = .450$, and neither for the NoGo-condition, $F(1,13.082) = 3.296$, $p = .092$. The spectral estimates from either spectral estimator did not differ significantly within the HE group's data within the Go-condition, $F(1,13.000) = 1.058$, $p = .322$. However, they did differ for the NoGo-condition, $F(1,12.420) = 9.161$, $p < 0.010$, with the both STFT estimates ($M = -.532$; $SE = .213$) and AIC-AAR estimates ($M = -.235$; $SE = .220$) showing spectral power within the margins of baseline power tending towards an ERD—more so for the STFT estimates.

3.3.3.1.1 Covariates and Additional Fixed Effects

The unstandardised parameter estimates (slope coefficients), standard errors, and significance for seven continuous covariates and two nominal categorical predictors entered separately into the model are presented in Table 3.4.

Table 3.4: Covariate parameter estimates and standard errors: gamma power.

Covariate	Beta	SE
Age at EEG recording	-0.530	0.086
Postnatal lead exposure	-0.108	0.027**
WISC IQ	0.001	0.009
Mother's Age (at delivery)	-0.009	0.024
Socio-economic status	0.007	0.014
Caregiver's education (in years)	-0.077	0.036
Cigarettes/day	0.063	0.028*
ADHD†	0.210	0.284
Marital status†	-0.018	0.200

† - nominal categorical variable; *$p < 0.05$, **$p < 0.01$ & ***$p < 0.001$.

Post-natal lead exposure (Pb; µg/dl) shared a linear association with the dependent variable ($p < 0.01$): higher lead body-burdens were associated with reduced gamma-power. Cigarettes smoked per day during pregnancy also shared a linear association

with gamma-power: more cigarettes smoked were associated with higher levels of induced power. Caregiver's education in years shared a weak-moderate association (p = 0.051). Neither of the nominal categorical predictors shared an association with induced gamma-power.

We entered post-natal lead exposure into the model; the resultant model provided a significantly better fit to the data as assessed by the likelihood-ratio test, $\chi^2(1)$ = 21.328, p < 0.001—AIC and BIC indicated a more parsimonious model. We then entered mother's cigarette-smoking into the model, the additional variable did not provide a better explanation of the data, as assessed by the likelihood-ratio test, $\chi^2(1)$ = 0.59, p = 0.387—AIC and BIC indicated an overly complex model. Maintaining post-natal lead exposure, we included caregiver's education which provided a better explanation of the variance of gamma-power within the time-frequency ROI, $\chi^2(1)$ = 11.392, p < 0.001—AIC and BIC indicated a more parsimonious model. Thus, of the continuous covariates, we maintained post-natal lead exposure and caregiver's education (in years) in our final model. We retested the categorical nominal predictors in the presence of the two additional continuous covariates: the addition of ADHD, but not mother's marital status, provided a better explanation of the data, $\chi^2(1)$ = 10.088, p < 0.001—AIC and BIC indicated a more parsimonious fit.

Our final model controlled for potential confounding due to the following covariates and additional fixed effects: post-natal lead exposure, $F(1,13.226)$ = 13.223, p < 0.001, B = -.128, 95% CI [-.167 -.089]; caregiver education, $F(1,9.766)$ = 9.766, p < 0.01, B = -.067, 95% CI [-.104 -.030] and ADHD, $F(1,9.999)$ = 8.912, p < 0.05, B = .368, 95% CI [.094 .641]. All the significant fixed-effects discussed in the previous section were still significant after the additional predictor variables were added: group, $F(1,12.534)$ = 11.756, p < 0.01; group x method, $F(1,12.513)$ = 12.003, p < 0.01; group x condition, $F(1,12.101)$ = 23.794, p < 0.001, and group x method x condition, $F(1,13.419)$ = 4.893, p < 0.001. The main method effect did not reach significance, $F(1,12.513)$ = .263, p = .617, neither did the method x condition interaction, $F(1,13.419)$ = 1.063, p = 321.

3.3.3.2 Inter-Trial Coherence

The main effect for group was not significant, $F(1,13) = 1.057$, $p = .323$. The main condition effect was significant, $F(1,13) = 27.797$, $p < 0.001$, there was greater phase-locking across trials in the NoGo-condition ($M = .166$, $SE = .016$) compared to the Go-condition ($M = .102$, $SE = .006$). The group x condition interaction did not reach significance, $F(1,13) = .242$, $p = .631$. Marginal means for inter-trail coherence are presented in Table 3.5.

Table 3.5: Estimated marginal means and standard-errors: gamma ITC.

	Go-Condition	NoGo-Condition
Controls	0.094 (.009)	0.152 (.024)
Heavy-exposed	0.110 (.009)	0.180 (.022)

ITC scalp maps displaying PLV values are presented in Figure 3.6. Strong phase-locked activity was not observed across trials in either group under any of the experimental conditions. Weak consistency of phase relative to baseline values is observed on all levels of the experimental design, indicating that the gamma component is an induced oscillatory response, as opposed to being part of the evoked, phase-locked cortical response—research in our laboratory indicates that ITC = .25-.30 was related to the P300 event-related potential.

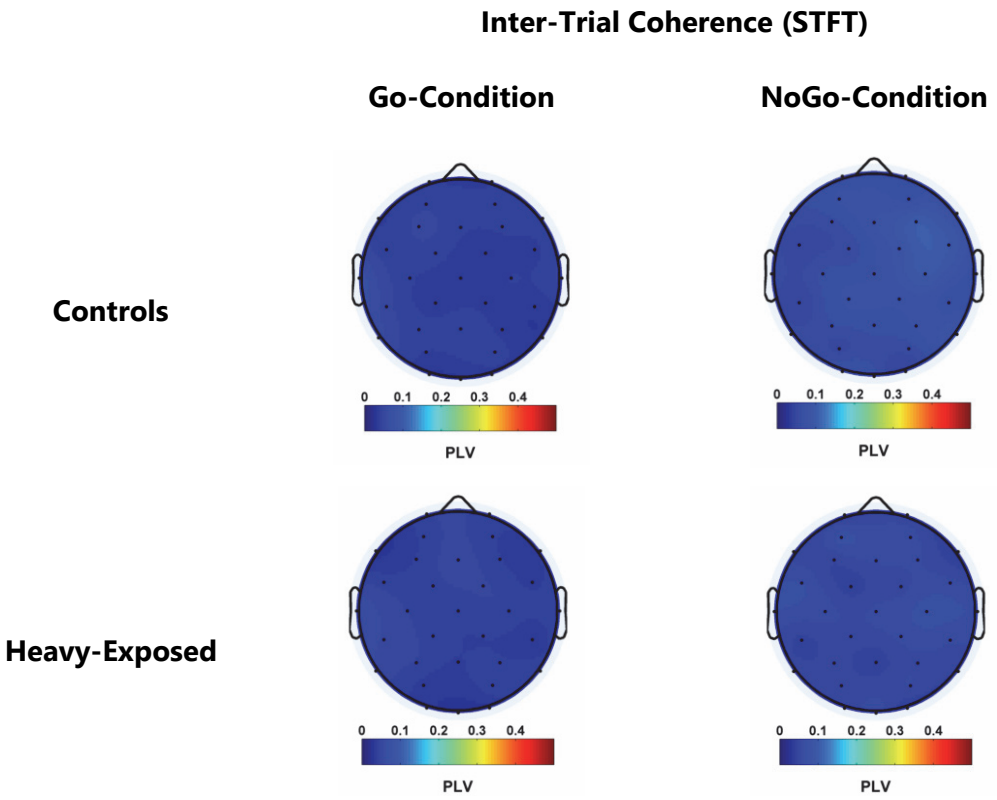

Figure 3.6: Topographical maps of the ITC feature distributed across the scalp in 34 –38Hz band and 450ms – 850ms time-window. Map are presented by group and condition. As all values were above baseline levels, the scalp maps are scaled with 0 as the minimum value.

In order to further verify that the observed oscillation with in the gamma ROI is induced, we conducted a correlation analysis between the ITC feature and the ERP time-domain area-measure within the same time-window (450ms – 850ms). As stated, the power feature is an induced oscillation, it logically follows that the power measures should not share a linear association with the ERP magnitudes: induced power varies independently from the ERP, which is comprised of evoked power contributions (Andrew & Fein, 2010a; Luck, 2012; Pfurtscheller & Lopes da Silva, 1999). The results of this analysis are presented in Table 3.6 below.

Table 3.6: Gamma-band (34Hz - 38Hz) power and ITC measures versus ERP area.

Feature-Condition	ρ	95% lower	95% upper	p
Phase (ITC)				
Go	-0.088	-0.683	0.643	0.380
NoGo	-0.165	-0.703	0.464	0.289
Power (STFT)				
Go	0.022	-0.599	0.592	0.476
NoGo	-0.104	-0.7151	0.6169	0.361
Power (AIC-AAR)				
Go	0.006	-0.594	0.619	0.493
NoGo	-0.247	-0.732	0.392	0.205

Note. *p*-values are computed via a monte-carlo simulation; 95% Confidence intervals were derived using bootstrap resampling.

The ITC feature does not covary with ERP magnitude, neither in the Go-condition or the NoGo-condition. For the power features, no significant covariance is observed for the STFT features, nor for the AIC-AAR spectral-power features under either experimental condition. The results of the correlation analysis indicate that the power and ITC measures do not covary with ERP magnitude, confirming the induced nature of the oscillations.

3.3.3.2.1 Covariates and Additional Fixed Effects

The unstandardised parameter estimates (slope coefficients), standard errors, and significance for seven continuous covariates and two nominal categorical predictors entered into the model separately are presented in Table 3.7

Table 3.7: Covariate parameter estimates and standard errors: gamma ITC.

Covariate	Beta	SE
Age at EEG recording	-0.001	0.005
Postnatal lead exposure	-0.000	0.002
WISC IQ	0.001	0.000*
Mother's age (Delivery)	-0.004	0.001**
Socio-economic Status	0.001	0.001
Caregiver Education (in years)	0.006	0.002**
Cigarettes/Day	-0.000	0.002
ADHD†	0.007	0.020
Marital Status†	-0.009	0.011

† - nominal categorical variable; *$p < 0.05$, **$p < 0.01$ & ***$p < 0.001$.

Intellectual abilities as assessed by WISC-IQ shared a linear association with gamma ITC levels ($p < 0.05$): increased intellectual capacity was associated with higher levels of ITC within the gamma-ROI. Mother's age at delivery was associated with ITC ($p < 0.01$), where increasing age was associated with lower levels of ITC across trials. Caregiver's education shared a linear association with ITC levels ($p < 0.01$). Increases in years-of-education was associated with higher levels of ITC. Neither ADHD nor marital status were associated with the induced gamma-power, $p = .685$ and $p = .415$ respectively.

We entered mother's age at delivery into the model and the resultant model provided a significantly better fit to the data, as assessed by the likelihood-ratio test, $\chi^2(1) = 20.352$, $p < 0.001$—AIC and BIC indicated a more parsimonious model. We then entered caregiver education into the model, in the presence of mother's age at delivery the resultant model provided a significantly better fit to the data, as assessed by the likelihood-ratio test, $\chi^2(1) = 4.714$, $p < 0.05$—only AIC indicated a more parsimonious

model, BIC indicated an overly complex model. Caregiver education was no longer a significant predictor of induced gamma-power (p = .132). Using the resampling-correlation approach on the covariates, we observed that there was significant covariance between mother's age at delivery and caregiver education (ρ = -.70, p < 0.01), suggesting that the two variables account for common variability in the DV. We further tested additional two variable combinations: (1) IQ with mother's age at delivery and (2) IQ with caregiver's education. Of all two covariate combinations, IQ with caregiver's education provided the best fit to the data relative to the model where no were covariates included, $\chi^2(1) = 25.746$, $p < 0.01$—both AIC and BIC indicated a more parsimonious model. In addition, both the covariates entered into the model were significant predictors of gamma-ITC at $p < 0.05$: caregiver's education ($p < 0.01$) and IQ ($p < 0.05$). A combination of all three continuous, individually-significant covariates produced an overly complex model relative to when two covariates, were included. ADHD, in addition to the two chosen continuous covariates did not produce a more parsimonious model; however, marital status did, $\chi^2(1) = 6.77$, $p < 0.01$—both AIC and BIC indicated a more parsimonious model. With the inclusion of marital status, all of the additional predictors were significant at trend-level ($p < 0.10$), with the exception of IQ which was highly significant ($p < 0.01$).

Our final model controlled for confounding effects of the following covariates and the fixed-effect: caregiver education, $F(1,13.000) = 4.269$, p = .059, B = 0.003, 95% CI [-.000 .006]; IQ, $F(1,13.0000) = 11.470$, $p < 0.01$, B = .001, 95% CI [.000 .002], and marital status, $F(1,13.0000) = 3.889$, p = 0.07, B = -.016, 95% CI [-.033 .002]. After including the covariates and fixed-effects into the model, the condition main effect was still significant, $F(1,13) = 27.797$, $p < 0.001$. The group main effect did not reach significance, $F(1,13.206) = 1.437$, p = .252, neither did the group x condition interaction, $F(1,13)$ = .242, p = .631.

3.4 Discussion

Our aims in this study were: (1) to elicit the frontally-oriented, cognitive-control linked, induced gamma-band event-related synchronisation (ERS) within a normally-developing sample using a simple visual Go/NoGo task, and (2) to investigate the impact of PAE on this scalp-measured oscillatory bout. In-line with our first hypothesis, within the control group we observed a significant increase in induced gamma-band power relative to baseline levels at the frontal midline electrode when participants were required to inhibit a motor response in the NoGo-condition. We also observed that NoGo induced gamma-power was significantly greater relative to the Go-condition within this group—induced gamma-power within the Go-condition did not synchronise, rather it was observed desynchronised relative to baseline levels. In our study, the gamma-band ERS shows maximum power at the frontal midline electrode with an approximate symmetric scalp distribution. Increases in induced gamma-band power over the frontal and central regions of the scalp have been observed during performance on the Go/NoGo and POP tasks when there is an increased demand for cognitive-control in order to inhibit or select against prepotency (Cho *et al.*, 2006; Kieffaber & Cho, 2010; Minzenberg *et al.*, 2010; Shibata *et al.*, 1999).

In terms of our second hypothesis, which relates to our second main aim, we expected to observe significant differences in oscillatory power within the NoGo-condition between the normally-developing controls and the heavy-exposed group. Due to the lack of previous research within the FASD population, we left the direction of this effect unspecified. Our findings were in-line with the hypothesis: in the HE group within the NoGo-condition we observed induced gamma-power within the margins of baseline power in the group x condition interaction-effect post-hoc analysis. This compared to the significant ERS we observed in the control group. In the post-hoc analysis of the group x method x condition interaction, when using a STFT estimator, an ERD was observed in the NoGo-condition for the HEs. This was not the case with the AIC-AAR gamma power estimates which were observed at baseline

power levels. Regardless of estimator specific analytic outcomes, greater induced power was consistently observed in the NoGo-condition for the control group. In addition, for the HEs, gamma-band power in the NoGo-condition did not differ significantly from the Go-condition, in contrast to the control group where significant differences were observed—the exception to this pattern of results was with the STFT estimates in the group x method x condition interaction, where significant differences were observed in the HE group, gamma-power within the margins of baseline power in the Go-condition and an ERD observed in the NoGo-condition. The pattern of results indicate that heavy PAE affects the power of the gamma-band ERS in conditions where increased cognitive-control is required in order to select against prepotency: the induced gamma-band ERS is not elicited in the heavy exposed participants.

Studies in clinical groups characterised by deficits of frontal lobe function and disordered cognitive-control, such as in schizophrenia and schizoaffective disorders, demonstrate an absence of an observable induced gamma-band ERS on the scalp during performance on the POP task (Cho *et al.*, 2006; Minzenberg *et al.*, 2010). The absence of a scalp-measured induced gamma-band ERS within these patients is attributed to microstructural changes within frontal cortical-deepbrain connections; specifically, structural abnormalities in the frontal thalamocortical relay (TCR) circuitry. Within the FASD population, the volumetric study of Sowell *et al.*, (2002) pin-pointed hypoplasias on the orbital frontal cortical surfaces of FAS patients. In addition, diffusion tensor imaging studies and structural magnetic resonance imaging (MRI) studies have demonstrated changes in cortical white-matter as well as underdeveloped regions and features of the cerebral cortex in the instance of an FASD (Archibald *et al.*, 2001; De Guio *et al.*, 2014; Fan *et al.*, 2016). Cognitive-behavioural research in FAS patients has consistently demonstrated deficits in tasks that utilise executive control mechanisms, such as the Tower of Hanoi, the Wisconsin Card Sorting Task, and cognitive inhibition tasks such as the Stroop Task (Burden *et al.*, 2005;

Kodituwakku, 2009; Mattson *et al.*, 1999; Mattson & Riley, 1998). Thus, the frontal circuitry involving cerebral cortex and thalamus is also highly likely to be dysfunctional in the instance of heavy PAE, manifesting in the reported cognitive and behavioural deficits, as well as changes in electrical dimensions of human brain function noted in this study and by others (Burden *et al.*, 2009, 2011; Gerhold *et al.*, 2017; Kaneko *et al.*, 1996).

We observed that post-natal lead exposure, caregiver education, and ADHD diagnosis accounted for a significant amount of variability in induced gamma-power. More specifically, increased lead body burdens were associated with a reduction in frontal induced gamma-power. This is in-line with the findings that demonstrate teratogenic effects related to early childhood lead exposure, with a measurable impact on prefrontal and frontal lobe cortical structures as well as regional hemodynamic responses (Cecil *et al.*, 2008; Yuan *et al.*, 2006)—clinical groups generally show decreases in gamma-power due to frontal lobe dysfunction but, as our findings shows, also due to teratogenic effects associated with childhood lead exposure. Caregiver education shared a negative association with induced gamma-power, possibly related to socio-economic circumstances within our sample where there was a trend for higher status mothers to smoke more cigarettes on a daily basis during pregnancy ($\rho = 0.43$, $p = 0.07$). ADHD shared a positive linear association with the induced gamma-power, this is in-line with observations from a modified auditory Go/NoGo study of Karch *et al.*, (2012) that demonstrated selecting against prepotency was linked to increases in gamma-band power in an adult ADHD sample relative to normally-developed controls—Karch *et al.*'s Go/NoGo task included a third condition, wherein participants could freely choose between responses in the context of an established prepotency. After accounting for the variability owing to these effects, the stated main and interaction effects attributable to alcohol exposure were still significant. Demonstrating that the observed variability in induced gamma-power owing to PAE could not be alternatively explained by other teratogens and/or comorbidity.

In our third hypothesis, we expected to observe weak/minimally phase-locked activity in the NoGo-condition indicating that the gamma-band oscillation was an induced power change. Across experimental conditions, the phase-locked activity was significantly greater in the NoGo-condition compared to the Go-condition, as is evidence by a significant main condition effect in the ITC analysis. However, if the observed changes in power were evoked, we would observe a significant increase in ITC across trials within the NoGo-condition compared to the Go-condition within the control group, but not within the HE group, this was not the case: the group x condition interaction effect for ITC did not reach significance. We only observed weakly phase-locked activity in both conditions. We did observed that caregiver education, intellectual abilities as assessed by WISC-IQ, and mother's marital status shared a linear association with gamma-band ITC. Accounting for the variability in frontal induced gamma ITC owing to these effects did not provide an alternative explanation for the observed significant effects owing to condition. As the data was analysed in a reference derivation, it is likely that current source contributions from neighbouring regions that are phase-locked to stimulus onset within the NoGo-condition could conduct up to the frontal mid-line electrode, contributing to an increase in ITC within that condition. Research in our laboratory indicates that an ITC = .25 - .30, was related to the P300 event-related potential, thus the observed levels within our study are too low to indicate a regional evoked power response. Using a permutation-based correlation analysis, we also observed that the magnitude of the induced frontal gamma-ERS did not covary with the ERP area-measure, which is what we would expect if the increase in gamma-power was evoked as opposed to induced, as the ERP is composed of evoked power contributions (Andrew & Fein, 2010a; Luck, 2012; Pfurtscheller & Lopes da Silva, 1999). In addition, ITC did not covary with the ERP-area measure, which is also what is expected for an evoked response. Therefore, the power changes were due to induced oscillatory activity: increased power owing to changes in oscillatory control parameters within the TCR circuitry.

From a behavioural perspective, we expected to see similar error rates for either group across conditions, but slower median reaction times within the HE group. Our data showed that while equivalent inhibitory performance was achieved across groups, the groups differed on median reaction times and errors-of-omission. Given the reaction time data, normally-developing participants process the task demands more efficiently and respond more rapidly; however, with reduced accuracy in the Go-condition. Heavy-exposed participants performed the task with a slower, more purposive strategy. Slower processing speeds are a known feature of FASD thought to be partially mediated by changes in the microstructure of cortical white-matter (Burden *et al.*, 2005; Fan *et al.*, 2016)—observed changes in cortical white-matter suggest less densely packed fibre bundles and decreased myelination.

In order to understand the task performance observations, we can consider the relationship between performance and arousal as well as the connection between arousal and motivation (Broadbent, 1965; Mendl, 1999; Yerkes & Dodson, 1908). Performance on a given task is dependent on arousal: low levels as well as extreme levels of arousal are associated with poor task performance, while optimal performance is achieved with medium levels of arousal. Seen in light of Yerkes and Dodson's law—also known as the inverted-U function or the inverted-U hypothesis—we may then consider that the two groups may not have found the task equally as challenging, and that group-specific levels of arousal and motivation were important factors driving task performance. For the controls, the task may have been trivial, while the HEs may have been more challenged and thus engaged in more purposive strategies, leading to less errors-of-omission and equivalent levels of inhibitory control. The differences in task difficulty experienced by either of the groups would also have had an impact on metabolite utilisation in neural tissue, as studies point to the fact that different patterns of regional blood flow arise due to different levels of task-related difficulty (Mostofsky & Simmonds, 2008).

In terms of comparing analytical outcomes when using STFT vs AIC-AAR spectral estimates, there was no significant main effect for method, but there was a significant group x method interaction effect: STFT spectral estimates lead to a significant group difference, but not AIC-AAR estimates. The divergence between the two estimators, seen in these cited effects and the post-hoc analysis of group x method x condition interactions, despite using the same window length for the sliding window, is attributable to a number of factors. Within finite samples AIC has a tendency to over-parametrise—select an overly complex model (De Waele, 2003). This over parametrisation brings into effect different estimation bias-variance trade-offs relative to those of the STFT estimates, consequently yielding divergent spectral estimates in the time-frequency domain. The small sample properties of either estimator also affect estimation bias-variance trade-offs: on a single-trial basis, the STFT estimates are inconsistent, while the AR estimate is consistent but biased—reduction in variance of the STFT estimate can be achieved by averaging over trials. These estimator dependent statistical bias-variance trade-offs lead to different specifications of components in time and frequency, due to the relationship between estimation bias and resolution (Oppenheim & Schafer, 2009). Over-and-above these points, the use of Gaussian tapering in the STFT and rectangular windowing in the AAR approach lead to further differences in signal component representations in time and frequency, primarily due to weighting on the leading and trailing edges of the analytical window that in turn affects overall datum-points available for the spectral estimates within the sliding analytical window. Due to these differences, we observe that spectral power estimates differ enough to affect analytical outcomes; the scalp maps derived using either estimator also provided different power measures across the scalp due to the estimation bias-variance trade-offs specific to each method—AIC-AAR estimates appear attenuated relative to the STFT estimates.

A limitation of the study is its sample size: we were only able to potentially detect large magnitude effects within our analyses. Despite this limitation, in our gamma-band power analysis the main effects for group and condition were significant, group x condition and group x method interaction effects reached significance as well as the group x method x condition interaction effect. We were also able to detect covariance between the induced gamma-band ERS and post-natal lead body burdens, caregiver education as well as ADHD. The same was true for main effects, interaction effects, and potential confounding effects within our ITC analysis. These observations point to the fact that the induced gamma-band ERS is a large magnitude effect, detectable within smaller samples when using the Go/NoGo task. This is supported by the observation that Shibata *et al.*, (1999) only used a sample of eight participants and was able to observe significant response inhibition linked changes in gamma-power when participants were required to inhibit against prepotency within the Go/NoGo task. We can certainly confirm that the ERS was observed for all of the normally-developing controls within the NoGo-condition, while an ERD was observed in the Go-condition. For each individual HE participant, induced gamma-power desynchornised or was within the margins of baseline power for both conditions. These observations point to the fact that the cognitive-control linked gamma-band ERS is a large magnitude effect detectable with in smaller samples and observable within normally-developing, individual participant's EEG data. Thus, in order to investigate the effects of interest related to the main aims of our research, our experimental design provided adequate power.

We strongly believe that future research should focus on manipulating task parameters in the Go/NoGo task in order to progressively make the task more challenging. This could be done by manipulating task parameters such as inter-stimulus intervals (ISI) and the relative number of inhibition cues within the task—our task only used a single cue, the letter "X". Alternatively, the time for an allowable response could be manipulated (Benikos, Johnstone, & Roodenrys, 2013). Sympathetic

nervous system measures should be included within the experimental design: measures such as galvanic skin response, heart-rate variability, and pupillary dilation provide indices of participant's arousal levels, allowing for a more detailed understanding of the arousal/motivation dimension of task performance. A clear way forward in terms of EEG analysis is to either decompose the data into independent components or to apply other classes of spatial filters (Delorme & Makeig, 2004; Gross *et al.*, 2001; Van Veen, van Drongelen, Yuchtman, & Suzuki, 1997). Time-frequency analysis of estimated cortical current sources as well as an analysis of how different independent sources project to scalp electrodes will allow us to assess hypotheses related to the source generators of the cognitive-control linked induced gamma ERS. Source level data would also allow for the application of multivariate adaptive autoregressive models and access to connectivity measures that index the direction of information flow between cortical current-source generators (Brunner, Billinger, Seeber, Mullen, & Makeig, 2016; Mullen, 2014).

3.5 Conclusions

Our electrophysiological data provides support for alcohol-linked changes within the frontal TCR circuitry involved in cognitive-control processing in response selection/inhibition tasks. Heavy-exposed participants do not demonstrate the characteristic scalp-measured induced gamma-band ERS observed in young and adult controls. Our results suggest a change in frontal lobe function due to heavy PAE, specifically related to processes and circuitry involved in shifting away from a prepotent motor response to an inhibited state. Changes in the experience of task difficulty due to alcohol-related effects lead to more purposive performance that allows for equivalent inhibitory control relative to normally-developing controls.

Chapter 4

The Effect of Heavy Prenatal Alcohol Exposure on Induced-Frontal Beta-Band Oscillations in Children Performing a Visual Go/NoGo Task

Matthew M. Gerhold[1], Joseph L. Jacobson[1,2,3], Sandra W. Jacobson[1,2,3], Ernesta M. Meintjes[1], Christopher D. Molteno[3] and Colin M. Andrew[1,4]

[1]Division of Biomedical Engineering, Department of Human Biology, University of Cape Town, South Africa; [2]Department of Psychiatry and Behavioural Neurosciences, Wayne State University School of Medicine, Detroit, MI, United States; [3]Department Psychiatry and Mental Health, University of Cape Town; South Africa. [4]Essentric Technology, Cape Town, South Africa.

Abstract

Previous studies conducted within adult samples using the Go/NoGo task have demonstrated the presence of a frontal, induced beta-band event-related synchronisation (ERS) believed to be linked to decision-making processes. To date this oscillatory bout has not been elicited in a normally-developing sample, nor is anything known about the impact of heavy prenatal alcohol exposure on the neural mechanisms involved in its generation. In our study, a frontal, induced beta-band oscillation was elicited shortly following presentation of both Go and No Go cues within the control group, with a frontal central scalp distribution. The frontal-central beta-ERS was not

elicited in the heavy-exposed group, rather a hemispheric asymmetry was observed over the frontal regions, with left-hemisphere power-measures observed at baseline levels while right-hemisphere power was desynchronised relative to baseline levels. Comparable inhibitory control was observed across groups; however, other differences in performance were apparent. Normally-developing controls had significantly faster median reaction times and made more errors-of-omission compared to the heavy-exposed group. As the induced beta-ERS is linked to decision-making, we expected performance accuracy to be predictive of oscillatory power within the beta band. We did not observe this in the control group; however, in the heavy-exposed group, performance accuracy predicted oscillatory power: errors occurred when frontal regional power desynchronised relative to baseline levels. Our findings demonstrate that the beta-ERS is elicited in normally-developing children performing a simple visual Go/NoGo task and that heavy prenatal alcohol exposure is linked to changes in this oscillatory feature. Our observations lead us to believe that the beta-ERS may not be directly linked to decision-making, as performance accuracy was not predictive of beta-power within the control group. It is more likely that the ERS is associated with a parallel process such as self-reflexive awareness of decision-making, which appears to be affected by heavy PAE, leading to erroneous decision-making during task performance.

4.1 Introduction

Fetal alcohol spectrum disorders (FASDs) are a spectrum of disorders that arise from heavy prenatal alcohol consumption (Chudley *et al.*, 2005; Hoyme *et al.*, 2005). It is estimated that around 119 000 children are born globally with full-blown fetal alcohol symdrome (FAS) each year, with South Africa, the United Kingdom, and Eastern Europe having the highest prevalence rates (Popova *et al.*, 2017). Common symptoms of FAS include facial dysmorphologies, microencephaly, and other forms of growth retardation (Jones & Smith, 1973). Facial dysmorphologies such as a flattened philtrum, flattened midface, thin upper lip, and shortened palpebral fissures are associated with changes in the structure of the cerebral cortex (Archibald *et al.*, 2001; Sowell *et al.*, 2002). Diffusion tensor imaging (DTI) studies have revealed changes in the structure of cortical white-matter fibre tracts in instances of heavy PAE (Fan *et al.*, 2016). In milder cases along the spectrum, the facial dysmorphologies do not present themselves, but cognitive-behavioural deficits occur in the context of altered/compensatory neurophysiological function (Fryer *et al.*, 2012; Mattson & Riley, 1998).

Response inhibition is an important component of executive function (Lezak, 2004). In the most general sense, response inhibition refers to the ability to inhibit/suppress a dominant behavioural tendency that is set in motion during an experimental task. The Go/NoGo response inhibition task is one of a number of approaches used to assess response inhibition capacity. Within this task, a participant is presented with a series of stimuli: "Go" stimuli that cue the participant to perform a simple motor response, such as a button press, and "NoGo" stimuli that signal that the participant should inhibit/suppress the motor response. The relative probabilities of each condition (Go vs NoGo) are often manipulated to yield equiprobable occurrence of either condition, or more commonly, relatively less inhibitory cues. A participant's level of performance on the task is assessed in terms of the proportion of successfully inhibited motor

responses; however, the task produces a number of other useful performance metrics, such as error rates for each condition and an average reaction time for the motor responses in the Go-condition (Burden *et al.*, 2009, 2011; Gerhold *et al.*, 2017; Kodali *et al.*, 2017).

Previous research on response inhibition within the developing heavy alcohol-exposed population has produced mixed results. A study by Kodituwakku *et al.* (1995) demonstrated that high-functioning children with FAS can perform as well as controls on simple versions of the Go/NoGo task; however, other studies have linked PAE to impairment of response inhibition on more challenging measures of inhibitory control, such as the Stroop Color-Word Test (Connor *et al.*, 2000; Mattson *et al.*, 1999). A study by Burden *et al.* (2009), using a visual Go/NoGo task, demonstrated comparable inhibitory control between the FAS and control groups; although within the FAS group, significant amplitude and latency differences in a number of ERP components were observed. Gerhold *et al.* (2017), in a simple auditory version of the Go/NoGo task, reported that a heavy alcohol-exposed group achieved comparable levels of inhibitory control relative to a normally-developing sample; however, the median reaction times within the Go-condition were significantly longer for the heavy-exposed group compared to the controls—slower processing speeds during performance of cognitive tasks are characteristic of the FASD population (Burden *et al.*, 2005). As in Burden *et al.*'s study, Gerhold *et al.* also observed altered neurophysiological function within the FAS group, as indicated by changes in amplitude and latency of ERP components.

Induced event-related oscillations are distinctly different in terms of their underlying neurophysiological generating mechanisms from those neural processes that generate an ERP waveform complex, and are thus of interest due to the complementary information they can offer regarding the electrical dimension of human brain function (Luck, 2012; Pfurtscheller & Lopes da Silva, 1999). To date, no

studies exist on event-related induced oscillatory activity in heavy, prenatally alcohol-exposed samples: event-related EEG studies have focused exclusively on event-related potentials (Burden *et al.*, 2009, 2011; Gerhold *et al.*, 2017; Kaneko *et al.,* 1996). Induced classes of neocortical oscillations, specifically in the beta-band, are important biomarkers for sensorimotor function (Pfurtscheller, 1981; Pfurtscheller *et al.,* 1997; Pfurtscheller *et al.,* 1996). Lesser known are the properties of induced beta oscillations occurring in regions other than the sensorimotor areas. Furthermore, nothing is currently known about how heavy PAE alters the neurophysiological mechanisms involved in generating these cognitive-related beta oscillations. In a very general sense, such oscillations are currently thought to be related to top-down cognitive-control components involved in task performance (Engel & Fries, 2010). These oscillations have been elicited in a variety of tasks, including visual search paradigms and movement tasks such as the Go/NoGo response inhibition task, although different scalp distributions of spectral power are observed across the different tasks (Alegre *et al.*, 2004; Alegre *et al.*, 2006a; Alegre *et al.*, 2006b; Okazaki, Kaneko, Yumoto, & Arima, 2008).

In a motor response inhibition study, Alegre *et al.* (2004) used a modified auditory version of the Go/NoGo task, wherein two paired-stimuli were used in each trial instead of a single Go/NoGo stimulus. The first stimulus in the pair provided information on whether movement or inhibition was required (a decision cue), while the second stimulus signalled to the participant to execute the cued response (a movement-inhibition cue). An equal number of trials were used for the Go- (50%) and NoGo- (50%) conditions. Alegre *et al.*, in addition to the known sensorimotor beta oscillations, reported a frontally-oriented, induced beta-ERS in both the Go- and NoGo-conditions that was elicited after the onset of the first stimulus (the decision cue). The focal frontal oscillation was observed early on in the trials within the region of 15H – 23Hz, and was temporally overlapping, but spatially distinct from the well-known sensorimotor movement-related dynamics. Due to the latency at which this

oscillatory bout occurred—prior to any initiated/inhibited motor response—the researchers linked it to decision-making processes. There is some evidence to support this proposed association. For example, Liddle, Kiehl, & Smith (2001) in an fMRI study, demonstrated the involvement of the bilateral dorsal anterior cingulate in decision-making during performance of the Go/NoGo task. Ikeda *et al.*, (1996) using subdural electrode recordings, demonstrated the bilateral involvement of the mesial prefrontal regions in task performance and indicated that the observed early transient potentials are likely to be involved in decision-making. In addition, the Go/NoGo task is intentionally designed to have a heavy decision-making component early on within each trial (Eagle *et al.*, 2008).

Alegre *et al.* (2006a) in a follow-up study used the decision-move, stimulus-pair auditory Go/NoGo task. This version of the task was augmented to allow for additional Go-conditions by delaying the second stimulus within the pair by an increasing inter-stimulus interval (1.5, 3, and 4.5 seconds). In addition, the researchers manipulated the probabilities of each condition: 84% of trials were Go and 16% were NoGo. The reported results aligned with those of the previous study: in both the Go- and NoGo-conditions a frontal beta-ERS, skewed towards the left-hemisphere, was observed shortly after the onset of the first stimulus within the stimulus-pair; the oscillatory bout was observed regardless of the inter-stimulus interval between the first and second stimuli within the stimulus-pair. As with numerous movement related EEG studies, the authors observed the central-parietal beta-ERD/ERS oscillatory complex after the onset of the second stimulus, the movement-inhibition cue.

The reported frontal beta-ERS elicited in the studies of Alegre *et al.* has not, to date, been elicited in a normally-developing sample, nor using a visual version of the task. Given the proposal that the ERS is related to generic decision-making processes engaged during task performance, this oscillatory complex should be observed in auditory and visual versions of the task, as well as in other simpler (single stimulus

per trial) forms of the task. The impact of heavy PAE on cognitive-related induced frontal beta-band oscillatory dynamics has, to date, not been studied; certainly, no studies exist on induced oscillatory dynamics elicited in the FASD population using motor response inhibition tasks such as the Go/NoGo task in the auditory or visual domain. Thus, little if anything at all is currently known about the impact of heavy PAE on induced beta oscillatory activity, and how such changes, if they do indeed occur, lead to changes in observed scalp-measured event-related oscillatory activity. We have conducted the first study to extend the findings of Alegre *et al.* into a developing sample and to explore the impact of PAE on the frontal induced beta-ERS using a simple, single stimulus per trial, visual-based task. Based on previous studies and existing explanations for the induced beta-ERS, we hypothesise that: (1) an early induced beta-band ERS will be elicited within the control group in both the Go- and NoGo-conditions; (2) the scalp topography of the induced frontal ERS within the control group will be observed skewing towards the left hemisphere; (3) heavy PAE will affect the power of the frontal induced ERS irrespective of experimental condition: we expect a significant group difference, but not a group x condition interaction effect; (4) equivalent inhibitory performance will be observed across experimental groups, although slower median reaction times will be observed for the heavy-exposed group; (5) single-trial frontal beta-power measures should correlate with task performance parameters linked to decision-making, such as performance accuracy.

4.2 Methods

4.2.1 Participants

Sixteen right-handed children and their mothers/guardians were sampled from the Cape Coloured community in Cape Town, South Africa. The Cape Coloured are descendants from a mixed ancestral lineage including European colonists, Malaysian slaves, Khoisan aboriginals, and the African Nguni ethnic group. Poor socio-economic circumstances and historical practices of compensating farm labour in part with wine have contributed to a tradition of heavy recreational weekend binge drinking in a portion of this population. This pattern of consumption persists amongst pregnant women within the population. As a result, the Cape Coloured community experiences one of the highest levels of FAS in the world (Popova *et al.*, 2017). Nine children met the diagnostic criterion for FAS or partial PFAS; seven children were no more than minimally exposed during pregnancy: the mothers drank less than one to two days per month and less than two standard drinks on any single occasion. Eight children were the older siblings of participants in our Cape Town Longitudinal Cohort study (Jacobson *et al.*, 2008). The remainder were identified by screening all of the 8- to 12-year-old children from an elementary school in a rural section of Cape Town where there is a very high incidence of alcohol abuse among local farm workers (Jacobson *et al.*, 2011; Meintjes *et al.*, 2010). All mothers/guardians provided written informed consent and all children provided oral assent. Each mother received a small monetary compensation for her participation and each child was given a small gift.

4.2.2 Protocols

All protocols were approved by Wayne State University and the University of Cape Town institutional ethics review boards.

4.2.2.1 Alcohol Consumption, Diagnostic Criterion, and Psychometric Data Collection

Each mother was interviewed in her primary language (Afrikaans or English) regarding her alcohol consumption during pregnancy using a timeline follow-back approach (Jacobson *et al.*, 2002). Volume was recorded for each type of beverage consumed on a daily basis, converted to absolute alcohol (AA) using weights that reflect AA concentrations in Cape Town (liquor—0.4, beer—0.05, wine—0.12, cider—0.06), and averaged to provide a summary measure of alcohol consumption during pregnancy (AA/day). The number of cigarettes smoked on a daily basis during pregnancy was recorded using self-report methodology. Mothers were also interviewed regarding their education and occupational status and that of their spouse/partner, they were also scored for socio-economic status (SES) using the Hollingshead Scale (Adams & Weakliem, 2011; Hollingshead, 1975). Diagnoses of FAS or PFAS were made by two of three expert dysmorphologists (HEH, LKR, NK; see Jacobson *et al.*, 2008) based on the revised Institute of Medicine criteria (Hoyme *et al.*, 2005). Handedness was assessed with the Annett (1970) Behavioural Handedness Inventory. IQ was estimated using Sattler's (1992) formula for Short Form IQ using seven subtests from the Wechsler Intelligence Scales for Children, third edition (WISC-III): Similarities, Arithmetic, Digit Span, Symbol Search, Coding, Block Design, and Picture Completion, as well as Matrix Reasoning from WISC-IV.

4.2.2.2 EEG Data-Acquisition

EEG data were acquired using an active-electrode Biosemi ActiveTwo EEG system (BioSemi, Netherlands, Amsterdam). A Common Mode Sense (CMS) and Driven Right Left (DRL) reference/ground scheme was used for data-acquisition, with an on-line band-pass filter set at DC-400Hz. Data were acquired at a sampling rate of 512Hz at 24-bit resolution. 34 Electrodes were placed according to the 10/10 electrode placement system (Jurcak, Tsuzuki, & Dan, 2007). We placed the electrodes on the

participant's head using a tight-fitting elasticised cap; a conductive gel was injected into the gel cavity of each electrode to form a conductive bridge between the scalp and measurement electrode. Measurement electrodes fitted in the cap were placed over the following regions: anterior-frontal (AF3, AF4, Fp1, Fp2), frontal (F3, F4, F7, F8, Fz), frontal-central (FC1, FC2, FC5, FC6), central (C3, C4, Cz), central-parietal (CP1, CP2, CP5, CP6), parietal (P3, P4, P7, P8, Pz), parietal-occipital (PO3, PO4), temporal (T7, T8), occipital (O1, O2, Oz), and mastoids (M1, M2). In addition, two sets of bipolar pairs were placed: (1) above and below the right eye, and (2) near the outer canthus of the left and right eye. These bipolar pairs recorded vertical and horizontal eye-movements, respectively. An additional channel was used to record participant behaviour, i.e. a button press made during the experimental task. Data was stored off-line in the *.bdf file format.

4.2.2.3 Go/NoGo Task

The experimental task was administered using E-Prime® 2.0 Professional Edition (Psychological Software Tools, Pennsylvania, USA). Each participant was instructed to press a button with the index finger of the right hand in response to a letter that appeared on the screen (the "Go" trials) with the exception of "X" (the "NoGo" trials). Inter-stimulus intervals were constant through the sessions (ISI = 5500ms), with the stimulus centered on screen for 500ms followed by a blank screen for 5000ms. Go and NoGo stimuli were alternated randomly within five consecutive blocks of 30 trials each (20 Go, ten NoGo) for a total of 150 trials. We placed a two-minute rest period between blocks. The entire task, including instructions and practice items, took approximately 20 minutes to complete.

4.2.3 EEG Data Analysis

All processing was performed within the MATLAB computing environment using an in-house toolbox, and custom scripts built upon functions provided by the EEGLAB toolbox (Delorme and Makieg, 2004). EEG data were not available for three

participants due to: (1) technical problems (n = 2) or (2) refusal to wear the cap (n = 1). Of the remaining 13, seven children were heavy-exposed and six children constituted the normally-developing control group.

4.2.3.1 Preprocessing

Data were imported into MATLAB, re-referenced to a linked Mastoid reference, and filtered using a band-pass filter from 0.5Hz – 45Hz. Recordings were scanned for gross-movement artefacts, and those portions of data contaminated by large movements were excluded from the dataset. The two-minute rest periods between blocks were also excluded from further analysis. Noisy channels were identified and replaced by interpolating the channel from neighbouring channels. Data were then segmented relative to stimulus onset: 750ms prior to stimulus onset and 1750ms post-stimulus onset. The epoched data were submitted to a *blind source separation* (BSS) algorithm: the *adapted infomax* algorithm within EEGLAB. Derived components were visually scanned for evidence of artefact; those components that were indicative of oculargenic and myogenic artefact were removed. Components were projected back onto the scalp to form an artefact-free dataset. Epochs were then submitted to a time domain thresh-holding algorithm: any epoch with extreme values exceeding 50μV was excluded from further analysis—this resulted in less than 5% of epochs being excluded. The epochs were then scanned for behavioural response data using custom software written within the MATLAB computing environment (The MathWorks Inc., Natick, MA, USA). The software classified and stored information associated with the following responses: correct Go, correct NoGo, incorrect Go, and incorrect NoGo. The behavioural response data was used for further analysis of participant behaviour under the experimental conditions.

4.2.3.2 Time-Frequency Representations

Short-time Fourier transform (STFT) and adaptive-autoregressive (AAR) time-frequency representations were generated using an in-house MATLAB based toolbox

that implements a number of different time-frequency estimation algorithms for the purposes of EEG event-related analysis. Prior to computing the TFRs, the EEG data was down-sampled to fs = 128Hz. For the STFT and AAR approaches, 500ms windows were used with the window slid by a single sample point. When using the STFT approach, a hamming window was applied to the data. No tapering was applied to the data when using the AIC-AAR approach, as the power spectral density (PSD) estimates are derived from the model coefficients and not from the data itself. Thus discontinuities at the start and end of data segments do not influence the PSD estimates as they would in an STFT approach—in terms of spectral leakage. This is due to the implicit extrapolation of the auto-covariance sequence when using autoregressive time series models (Marple, 1986).

4.2.3.2.1 Autoregressive Model Order Selection

We selected the model order for the AR-based approach using the Burg algorithm for coefficient estimation and AIC and AIC-C approaches for model order selection. As per the suggestion in Florian and Pfurtscheller (1995) and Mullen (2014), we utilised a subset of data segments taken across trials and across time-windows within trials, we randomly sampled 10% of trials and 3 x 500ms 0% overlapping time-windows within each trial. Estimates using each of the information criteria—AIC and AIC-C—were computed across a range of model orders ranging from 1 – 30. These estimates were computed separately for each of the sampled segments and then stored for analysis. In order to derive an estimate of model order, we took the median measure for each information criterion across all data segments for which we estimated a model order. As the distributions were skewed for these metrics, a median offered the best measure of central tendency.

AIC yielded a median estimate across segments of p = 28. AIC-C provides an estimation of model order slightly lower than that of AIC, p = 23. Optimal model orders were selected within a range defined by median AIC and median AIC-C. AIC

and AIC-C parametrised representations, which utilise less hefty penalties for higher-order models, provide representations of signal components more well-defined in frequency relative to the STFT representations. As such, we expect that the two methods will estimate common oscillatory information; however, components identified by either method will have slightly different specifications in frequency and time.

4.2.3.2.2 Single-Trial Time-Frequency Estimates: Spectral Power

Single-trial time-frequency representations were generated using STFT and AIC-AAR approaches (Burg algorithm) and log transformed. These TFRs were baseline corrected by subtracting the average baseline power (-500ms -100ms) from each time point of the single-trial time-frequency representations. Baseline confidence intervals were then derived using bootstrap resampling procedures applied to the baseline corrected data (Efron & Tibshirani, 1986; Hastie *et al.*, 2009). Each time-frequency point in each single-trial TFR was then compared to the adjusted baseline CI=95%, where the adjustment was made by computing an FDR significance threshold using methods presented in Durka *et al.* (2004). This yielded baseline corrected time-frequency representations for both algorithms where in non-significant time-frequency points were set to zero.

4.2.3.2.3 Single-Trial Time-Frequency Representations: Inter-Trial Coherence

Inter-trial coherence (ITC) is a measure of the strength of phase-alignment across trials within EEG event-related data. ITC is expressed as a phase-locking value (PLV) ranging from 0 to 1: 1 represents no difference in the phase of the signal across trials within a time-frequency region and 0 represents consistent differences in phase across single-trials. As with event-related spectral power, ITC can be expressed as a baseline corrected time-frequency representation, where baseline correction procedures and significance testing are computed in the same manner as for spectral power. The PLV values are computed based on single-trial Fourier spectra at each time-point across

multiple trials (see Delorme & Makeig, 2004; Tallon-Baudry *et al.*, 1996 for details of ITC computation). In our analysis, we use the Fourier spectra derived from windowed data segments. ITC measures are important as they have direct neurophysiological relevance. Medium-strong PLVs across trials represent evoked power, spatially wide-spread neocortical phase-reset driven by afferent-thalamocortical connections. Weak PLVs represent induced power, spatial localised neocortical oscillations driven primarily by calcium-channel mediated low-threshold spiking in the recurrent thalamocortical relay circuits (Pfurtscheller & Lopes da Silva, 1999; Pfurtscheller, 2006; Suffczynski *et al.*, 2001). Given that the frontal beta-ERS is an induced oscillation, we expect that analysis of the phase component of the EEG across trials will reveal weakly phase-locked activity in both the Go- and NoGo-condition for both experimental groups. In addition, the ITC values and beta-power should be uncorrelated with an ERP area-measure within the same time-window (350ms – 650ms), as in the instance of an induced response, ITC and spectral-power should vary independently from ERP magnitude.

4.2.3.2.4 Feature Extraction

We identified a time-frequency region-of-interest (ROI) using the group probability-contrasts from the Go- and NoGo-conditions wherein the group differences where maximal: 350ms – 650ms, 13.5Hz – 16.5Hz over the frontal region. The frontal beta-band oscillatory dynamics were distributed across the frontal electrodes: Fp1, AF3, F3, Fz, F4, AF4 and Fp2. Due to the spatial dynamics observed over the frontal regions, we were interested in the frontal regional dynamics as a whole as well as the frontal hemispheric spatial pattern of the electrocortical response (see Appendix E for the STFT group contrasts at the Fz electrode). We extracted the median baseline-corrected log-power measure and the inter-trial coherence (ITC) from each subject's data averaged across trials for the Go- and NoGo-conditions at the seven frontal electrodes. We chose the median as the distribution of the power and ITC values across single-trials were skewed within this time-frequency region-of-interest for all subjects;

therefore, the median provided the best measure of central tendency. As high-frequency oscillations are spatially confined in comparison to lower frequency oscillations, in the instance of our frontal beta analysis a group of electrodes within a given scalp region (frontal) was justified (Nunez & Srinivasan, 2005). This in comparison to the single electrode analysis used for the gamma-band (see Chapter 3). The regional and hemispheric features across subjects and across conditions were tabulated along with demographic, psychometric data, socio-economic index, diagnostic classification, and alcohol consumption metrics. This table was used as the basis for a statistical analysis of the selected electrocortical feature(s).

4.2.4 Statistical Analysis

All statistical analyses were computed in SPSS 23/24 (IBM Corp, New York, United States). We used the MIXED module in SPSS to compute a series of fixed-effects models using the features extracted within the beta ROI; these analyses were applied to power and ITC features—ITC data were BoxCox transformed due to significant skewing in the data, λ= -.3009. Generally speaking, the analyses focused on frontal regional comparisons including all seven electrodes and hemispheric comparisons that included the more laterally situated electrodes within the frontal region-of-interest: Left (Fp1, AF3 and F3) and Right (F4, AF4 and Fp2).

4.2.4.1 Regional Analyses

The frontal analysis contained the factors: group (controls vs HEs), method (STFT vs AIC-AAR), and condition (Go vs NoGo), with condition represented by all seven individual electrodes within the frontal region. Method and condition were defined as repeated-measures; initially, the residual covariance matrix was estimated directly from the data. The initial fit did converge, however, the Hessian matrix was not positive-definite even after fitting the model with updated fitting parameters as suggested by IBM SPSS ("IBM Technote", 2016). This suggested that a simpler residual covariance structure was more suitable to describe the correlations within the repeated

measures of the model. In these instances, a Toeplitz structure provided the best fitting models relative to other available covariance structures provided in SPSS, for both the power and ITC analyses. This was confirmed by the observation that the chosen residual covariance matrix significantly minimised the -2 log likelihood criterion relative to all other covariance structures tested. This observation was mirrored in the information criteria indices that showed the chosen residual covariance structure provided the most parsimonious fit to the data.

We conducted follow-up analyses to assess for the presence of asymmetric power distributions across the frontal regions in either group and to see if hemispheric asymmetries developed as a result of movement-inhibition demands. In these analyses, we introduce a two-level hemispheric factor: hemisphere (Left vs Right), with each hemisphere represented by three electrodes: Left (Fp1, A3 and F3); Right (F4, A4, and Fp2). We computed these follow-up analyses using the STFT and AIC-AAR estimates separately—we omitted the two-level method factor to provide simpler models that were more readily interpretable. Due to the use of the common electrodes from the regional analysis, the same residual covariance structure (Toeplitz) provided the best fitting models, as assessed by the -2 log likelihood criterion.

4.2.4.2 Parameter Estimation

For all the above-mentioned analyses, our initial set of model parameters were estimated using maximum likelihood (ML). The choice for parameter estimation (ML and a Toeplitz residual covariance matrix) allowed for the ML algorithm to converge and all the conditions for a valid solution to be met. This is due to the large covariance in the power and ITC measures over the frontal electrodes: as they share a common pattern of covariance, a sparse set of parameters adequately describes residual covariance.

4.2.4.3 Residual Analysis

We performed a check on the models residuals by assessing the normality assumption using Shapiro-Wilk's test. In all instances, this assumption was satisfied: Shapiro-Wilk's was not significant. We also checked for outliers in the residuals using the outlier labelling rule utilising a gain of G = 2.2 (Hoaglin & Iglewicz, 1987; Hoaglin, Iglewicz, & Tukey, 1986); outliers were excluded when the labelling rule indicated. Detrended residual plots were checked for heteroscedasticity of variance. For our final model we maintained the model parameters estimated using maximum likelihood (ML) as opposed to recomputing the model using restricted maximum likelihood (REML). Twisk (2006) argues that ML provides more accurate estimates of fixed-effects parameters, while REML provides more accurate estimates of random effects. As our model is a pure fixed-effects model, ML was the natural choice. Where interaction effects were significant, we ran a post-hoc analysis using Sidak's correction for multiple comparisons.

4.2.4.4 Covariate Analysis and Additional Fixed Effects

In order to control for potential confounding effects of measured covariates in the study, we tested nine covariates for a linear relationship between the power and ITC features used in each of the two mixed-factorial ANOVAs—frontal and hemispheric. These covariates included: (1) age at recording, (2) post-natal lead exposure (Pb; μg/dl), (3) WISC-IQ, (4) mother's age at delivery, (5) socio-economic status, (6) primary caregiver's education in years, (7) cigarettes smoked during pregnancy, (8) ADHD diagnosis and (9) marital status. The first seven variables were continuous measures, while the last two were nominal-categorical and were tested as additional fixed-effects to see if they could explain a significant amount of variance in the dependant variable. For entry into the final model, the covariate needed to be a significant predictor of the dependent variable.

4.2.4.5 Behavioural Analysis

Data tables containing performance data (reaction time data from the Go-condition and accuracy data in terms of correctly responding) were used as a basis for a statistical analysis of performance under experimental conditions. We tested the reaction time data for normality and homogeneity of variance across experimental groups. All tests indicate inhomogeneity of variance and non-normal distributions. Even after transforming the data (natural logarithm and BoxCox, $\lambda = .3638$) parametric assumptions were still not met; therefore, we computed the Mann-Whitney U test on the untransformed data to test for group differences in reaction times under to Go-condition. We tested to see if alcohol exposure affected error rates on a single-trial basis under the Go and the NoGo experimental conditions using Pearson's Chi-Square on cross-tabulated data. We cross-tabulated a vector with group IDs (HE vs Con) with single-trial accuracy data, where accuracy data was a vector of 0s and 1s representing incorrect and correct responses respectively. In our cross-tabulation, the null-hypothesis was that accuracy under each experimental condition was independent of alcohol exposure.

4.2.4.6 Behavioural and Regional Power Measures

We computed a linear mixed-effects model with beta-band power as the dependent variable and accuracy as a nominal-categorical predictor. We coded accuracy as a dummy variable 0-error and 1-accurate response. We computed separate models for the control and alcohol-exposed group using the spectral estimates from the nonparametric spectral estimator—the short-time Fourier transform. Our model included a random intercept for each participant in order to model between participant variance. We also attempted to see if the addition of random slopes provided more explanatory power to the model, over-and-above the addition of random intercepts. The addition of random slope terms into the model did not provide a more parsimonious model. Owing to the inclusion of a random-effect, we opted for

REML parameter estimates. Our interest lay in observing the linear association between the behavioural response (accuracy) and the oscillatory feature; thus, we considered the estimated beta-coefficients as the most important statistical quantity. Our diagnostic checks were as before and all assumptions were satisfied.

4.2.4.7 Additional Analyses

In order to add additional verification that the electrocortical oscillatory response was induced and thus varied independently from ERP magnitude (the evoked power response), we computed a correlation analysis between ERP-area (Fz, 450ms - 850ms) versus the induced gamma-power feature, as well as for ERP-area (Fz, 450ms - 850ms) versus the ITC feature. We utilised an ERP area-measure as opposed to measures of central tendency such as the mean or median, as an area measure is a more robust measure of magnitude due to it being less biased by noise (Luck, 2012). In order to obtain reliable confidence intervals and to generate a distribution of the test-statistic under the null hypothesis of no linear association, we adopted a resampling/permutation-based approach (Efron & Tibshirani, 1986; Hastie *et al.*, 2009). We utilised the MATLAB Parallel Computing Toolbox to generate 50 000 bootstrap resamples using resampling with replacement (The MathWorks Inc., Natick, MA, USA). In order to derive a reliable *p*-value for significance assessment, we randomly shuffled the data in either of the variables being correlated and computed the test-statistic for each iteration. This was done 50 000 times resampling with replacement. The *p*-value was calculated as the smallest proportion of the surrogate distribution that they lay below/above the original sample test-statistic.

4.3 Results

4.3.1 Sample characteristics

Table 4.1 provides participant information, mother's characteristics and mother's alcohol consumption patterns during pregnancy. The two experimental groups did not differ on any of the measures that were used to characterise the participants or their mothers with the exception of the alcohol consumption metrics. On average, mothers of the alcohol-exposed participants consumed 3.08 oz AA/day, which equates to 6.16 standard drinks. Scores varied over a large spread for the average daily consumption metric across the sample, ranging from 1.64 drinks/day to 19.2 drinks/day. On each drinking occasion, mothers consumed just under 13 standard drinks (12.88 drinks per occasion); the alcohol-exposed group varied within a range of 5.7 drinks to 20.1 drinks per occasion. Apart from the mother of the most heavily exposed, who drank every day during pregnancy, consuming the equivalent of 19.2 standard drinks per day, the rest of the sample engaged in binge drinking spaced some days apart. Four of the mothers of the children in the control group reported abstaining entirely from alcohol during pregnancy; the other two drank less than one to two days per month and less than two standard drinks on any single occasion.

4.3.2 Behavioural Data

Results for the analysis of the behavioural data are presented in Table 4.2. The control group made proportionally more errors-of-omission ($p < .05$); the difference in omission error rates between groups was $\Delta = 2.79\%$. Both groups made proportionally the same amount of commission errors: $\Delta = 0.17\%$. Based on a non-parametric test, the control group's median reaction time was significantly faster.

Table 4.1: Demographic characteristics by group.

	Alcohol Exposed (n = 7)		Controls (n = 6)		
	M (SD) or n(%)	Range	M (SD) or n(%)	Range	*F* or χ^2
Sample characteristics					
Sex (% Female)	6 (85.72)	-	5 (83.34)	-	<1
Age at recording (years)	12.39 (1.25)	10.75-14.31	12.97 (1.14)	11.84 -14.74	<1
Lead Exposure (Pb; μg/dl)	6.79 (2.55)	4.00-12.00	5.93 (1.08)	3.00-11.00	<1
WISC IQ[a]	67.23 (11.50)	51.07-85.15	64.37 (11.19)	54.56-81.84	<1
ADHD (% Diagnosed)[b]	2 (28.57)	-	0 (0)	-	2.026
Mothers charactersitcs					
Age at delivery (Decimal)	26.03 (4.58)	18.84-33.14	26.31 (3.86)	19.26-29.71	<1
Socioeconomic status[c]	19.57 (7.03)	11.00-29.00	16.83 (7.82)	8.00-28.5	<1
Highest educational achievement	7.57 (3.46)	0.00-10.00	6.67 (0.82)	6.00-8.00	<1
Marital status (Married/Not Married)	3 (42.90)	-	2 (33.30)	-	<1
Cigarettes/day gestation period	4.71 (2.69)	0.00-8.00	3.50 (4.087)	0.00-10.00	<1
Mothers Alcohol Consumption					
AA/day (oz)	3.08 (3.27)	0.82-9.60	0.01 (0.02)	0.00-0.05	5.3*
AA/drinking day (oz)	6.44 (3.06)	2.85-10.05	0.35 (0.53)	0.00-1.06	23.17***
Frequency (% days across pregnancy)	43.17 (28.40)	29-100	1.00 (2.00)	0.00-4.00	13.39**

Note. AA refers to absolute alcohol; 1 oz AA ≈ 2 standard drinks. [a]Wechsler Intelligence Scale for Children. [b]Attention deficit/hyperactivity disorder. [c]Hollingshead (1975) Four Factor Index of Social Status Scale (Adams & Weakliem, 2011). *p <0. 05; **p < 0.01; ***p < 0.0001.

Table 4.2: Behavioural data by group.

	Heavy-Exposed (% of trials/ms)	Controls (% of trials/ms)	Statistics	
			χ^2 or U	ϕ_c or r
Error Trials				
Omission Errors	3.00%	5.79%	4.89	0.067*
Commission Errors	8.79%	8.62%	0.005	0.003
Reaction time				
Correct Go (ms) a	554.69 (8.38)	513.67 (8.76)	115444	0.12**

*p <0. 05; **p < 0.01.

The data points to the fact that there is a group-specific speed-accuracy trade-off within the control group. However, both groups achieved similar levels of inhibitory control—there was no group difference in terms of inhibiting a response (p = .946). Given the reaction time data and differences in omission error rates, alcohol-exposed participants are approaching the task with a slower more purposive strategy, enabling comparable inhibitory performance.

4.3.3 Electroencephalography

Topographical maps highlighting the frontally-oriented, event-related beta-band dynamics are presented in Figure 4.1. The scalp maps for the control group's data show a frontally-oriented ERS under both experimental conditions. The control group's scalp maps also show an ERD over the posterior regions of the scalp with a central/parietal topography. The ERD and ERS are observed when using either the STFT or AIC-AAR spectral estimates. The ERS observed in the control group is only just discernible in the heavy-exposed group's data, the induced oscillatory feature appears skewed towards the left frontal hemisphere and is more prominent in the AIC-AAR spectral estimates. Within the HE group, there is a large magnitude ERD over the occipital/parietal regions that appears to be skewed to the right-hemisphere. This oscillatory pattern extends into the central and frontal-central regions within the right hemisphere.

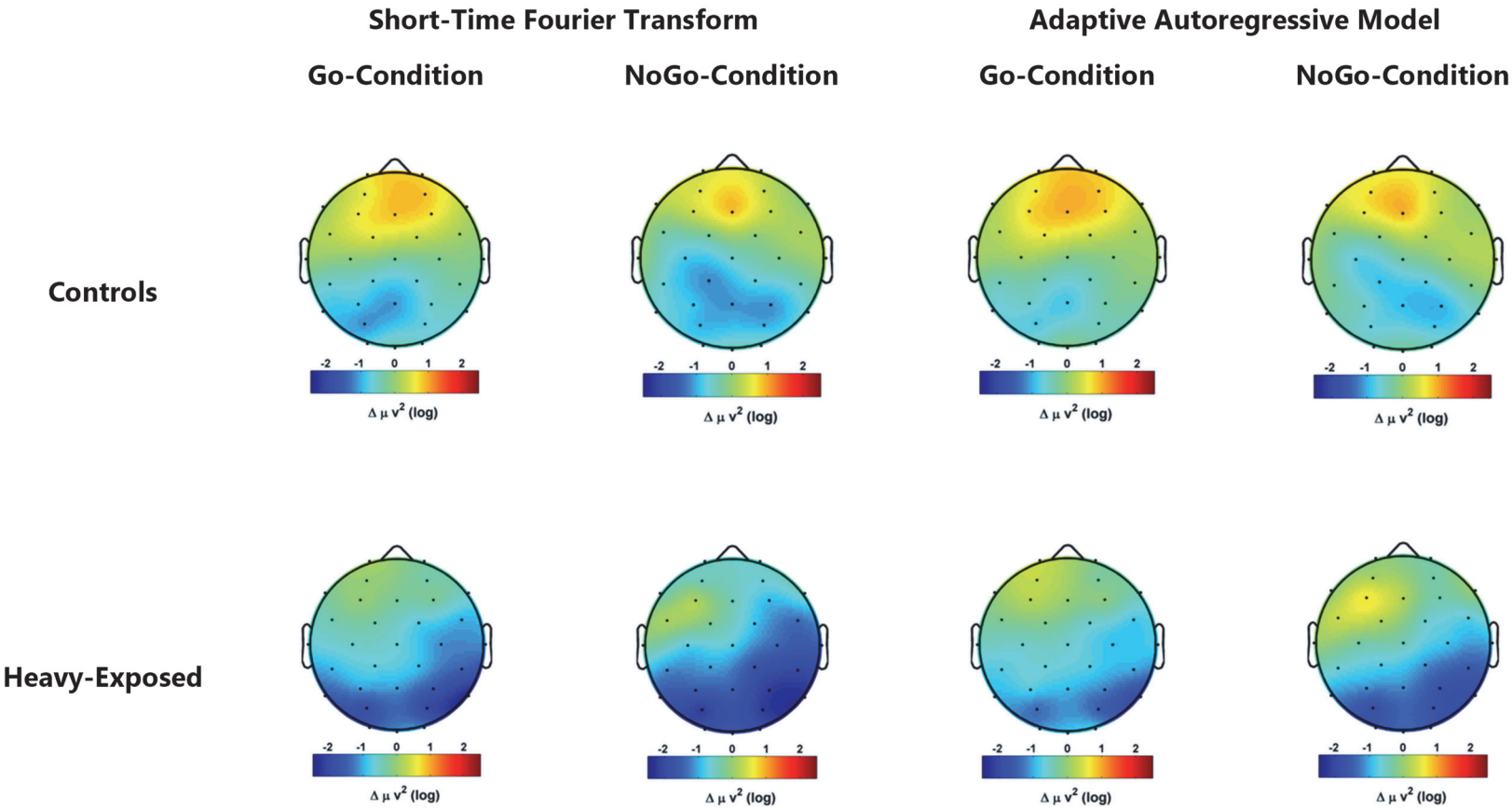

Figure 4.1: Topographical maps of the beta-band dynamics in 13.5 – 16.5Hz band and 350ms – 650ms time window. Map are presented by group and condition and then nested under choice of spectral estimator.

4.3.3.1 Induced Power

In our fixed-effects model, wherein frontal regional spectral power was the dependent variable, we observed a number of significant main and interaction effects. There was a main effect for group, $F(1,13.534) = 8.251$, $p < 0.05$: within the control group, spectral power synchronised relative to baseline levels ($M = .682$, $SE = .212$); while in the heavy-exposed group, spectral power was observed within the margins of baseline levels of spectral power ($M = -.148$, $SE = .196$). A follow-up analysis, wherein the 2-level hemispheric factor was added, indicated a significant group x hemispheric effect when using the STFT estimator $F(1,36.866) = 7.800$, $p < 0.01$, and when using the AIC-AAR estimator $F(1,15.190) = 9.763$, $p < 0.01$. Both estimators showed a significant hemispheric asymmetry in the HE group, wherein spectral power was greater within the left frontal hemispheric region compared to the right: STFT-Left-HE ($M = -.115$, $SE = .246$) and STFT-Right-HE ($M = -.578$, $SE = .246$); AAR-Left-HE ($M = .450$, $SE = .197$) and AAR-Right-HE ($M = -.214$, $SE = .197$). Within the control group, spectral power did not differ significantly across frontal hemispheric regions when using either spectral estimator: STFT $p = .214$) and AIC-AAR $p = .823$). When addressing group differences within either hemisphere, there was no significant differences in spectral power within the left frontal hemispheric region when using either of the spectral estimators: STFT ($p = .126$) and AIC-AAR ($p = .533$). However, group differences were observed within the right frontal hemispheric region with both estimators, STFT ($p < 0.01$) and AIC-AAR ($p < 0.01$): STFT-Right-Con ($M = .702$, $SE = .266$) and STFT-Right-HE ($M = -.578$, $SE = .246$); AAR-Right-Con ($M = .672$, $SE = .212$) and AAR-Right-HE ($M = -.214$, $SE = .197$). Thus, irrespective of experimental condition, the results indicate synchronised oscillatory activity within the control group, wherein no significant hemispheric asymmetry was observed. Within the HE group, regional spectral power remained within the margins of baseline power; however, in the HE group we did observe a significant hemispheric asymmetry with spectral power desynchronised within the right hemispheric regions, while spectral power was observed within

baseline-margins of spectral power within the left frontal region. These results were robust regardless of the spectral estimator used, although we observed different levels of power when using either of the spectral estimation methods.

Within the frontal regional power analysis, there was a significant main effect for method, $F(1,13.779) = 25.769$, $p < 0.001$, where overall spectral power was greater when using the AIC-AAR spectral estimates ($M = .392$, $SE = .146$) compared to the STFT estimates ($M = .142$, $SE = .146$). The group x method interaction effect was significant, $F(1,13.779) = 11.324$, $p < 0.01$. In the instance of an STFT estimator, significant differences in frontal regional oscillatory power were observed ($p < 0.01$): an ERS was observed in the control group ($M = .640$, $SE = .215$), while spectral power remained within baseline level margins within the HE group ($M = -.355$, $SE = .199$). These significant differences were also observed when using the AIC-AAR estimator ($p < 0.05$): ERS was observed in the control group ($M = .724$, $SE = .215$), while spectral power remained within baseline level ranges in the HE group ($M = .060$, $SE = .199$). However, when we compared spectral estimation methods within each group, the control groups spectral estimates (STFT vs AIC-AAR) did not differ ($p = .263$), while the spectral estimates within the HE group did ($p < 0.001$): STFT ($M = -.355$, $SE = .199$) vs AIC-AAR ($M = .060$, $SE = .199$). Thus, demonstrating that the choice of spectral estimator and associated parametrisation can affect analytical outcomes. Generally speaking, this occurs due to bias-variance trade-offs in the spectral estimates and how differences in estimation-bias can lead to significant differences in downstream comparisons across estimators.

The main effect for condition did not reach significance, $F(1,84.078) = 1.708$, $p = 0.195$, neither did the group x condition interaction effect, $F(1,84.097) = .369$, $p = 0.545$, indicating that the frontal beta-ERS was not associated with response inhibition or movement, results that are consistent with previous research in adult samples (Alegre *et al.*, 2004; Alegre, *et al.*, 2006a; Alegre, *et al.*, 2006b). In a follow-up analysis the 2-level hemispheric factor was used to assess if any hemispheric asymmetry effects arose due

to differences in experimental condition. When using the STFT estimator, the group x condition x hemisphere interaction effect did not reach significance, $F(1,22.094) = 1.008$, $p = 0.326$; neither when using the AIC-AAR estimator, $F(1,31.594) = .607$, $p = 0.442$, indicating that, within the two groups, a hemispheric frontal asymmetry was not induced nor suppressed by the necessity for inhibitory control. The method x condition interaction effect reached significance, $F(1,23.900) = 17.995$, $p < 0.001$: within each condition, the STFT and AIC-AAR spectral estimates differed significantly ($p < 0.01$). In the Go-condition, the AIC-AAR estimate (M = .438, SE = .163) was greater than the STFT estimate ($M = .279$, $SE = .163$), and in the NoGo-condition we observed the same pattern of results ($p < 0.001$): AIC-AAR ($M = .345$, $SE = .163$) vs STFT ($M = .006$, $SE = .163$). The condition differences (Go vs NoGo) did not reach significance when using the STFT estimator ($p = .057$); neither for the AIC-AAR spectral estimates ($p = .513$). These results further indicate that analytical outcomes are dependent upon the underlying type of estimator.

There was a significant interaction effect for group x method x condition, $F(1,23.900) = 14.121$, $p < 0.01$. The interaction is illustrated in Figure 4.2 and the marginal means for each level of the experimental design appear in Table 4.3.

Table 4.3: Baseline-corrected beta power estimates: medians and standard errors.

	STFT		AIC-AAR	
	Go	NoGo	Go	NoGo
Controls	.779 (.24)	.501 (.24)	.853 (.24)	.595 (.24)
Heavy-exposed	-.221 (.22)	-.489 (.22)	.024 (.22)	.096 (.22)

Note. Median power estimates were extracted from a beta-band (13.5Hz-16.5Hz) region-of-interest (ROI) within a 350ms-650ms time window.

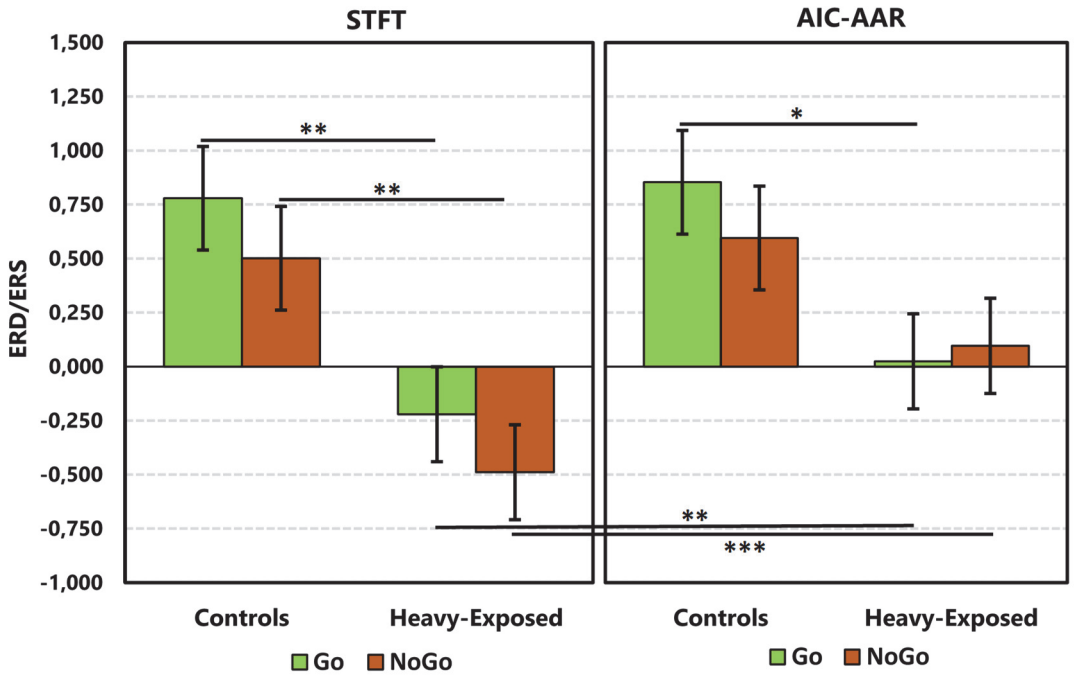

Figure 4.2: Bar graph illustrating the group x method x condition interaction effect. ERD/ERS represents a change in spectral power relative to pre-stimulus baseline, expressed as a difference in log power, $\Delta\mu V^2(\log)$. Error bars represent 2 x standard errors. *$p < 0.05$, **$p < 0.01$, ***$p < 0.001$.

Regardless of the choice of spectral estimator, we did not observe significant differences across conditions within either of the experimental groups. When using a STFT estimator, within the control group there was no difference between conditions (p = .184). This was also true when using the AIC-AAR spectral estimator (p = .218). The same observations were made within the HE group when using the STFT estimator (p = .168). This was also true when using the AIC-AAR estimator (p = .711). The lack of any significant condition differences within either of the experimental groups when using either of the spectral estimators further indicates that the beta-ERS is not associated with response inhibition.

Despite there being no significant condition differences within either of the groups, we did observe a number of significant group differences within either of the experimental conditions when using different spectral estimators. When using the STFT estimator, within the Go-condition we observed a significant group difference (p < 0.01): Controls (M = .779, SE = .239) vs HEs (M= -.221, SE = .221); we also observed a group difference in the NoGo-condition (p < 0.01): Controls (M = .501, SE = .239) vs HEs (M = -.489, SE = .221). When using the AIC-AAR estimator, we observed a group difference in the Go-condition (p < 0.05): Controls (M = .853, SE = .239) vs HEs (M = .024, SE = .221); however, we did not observe a group difference within the NoGo-condition (p = .139).

In terms of further addressing the impact of AIC parametrisation on the AAR spectral-estimates relative to STFT estimates, we unpacked estimator comparisons within each condition for either experimental group. Within the control group under the Go-condition, the STFT spectral estimates and AIC-AAR spectral estimates did not differ significantly (p = .360); neither did they differ under the NoGo-condition (p = .245). While in the HE group, under the Go-condition, the STFT spectral estimates (M = -.221, SE = .221) and the AIC-AAR estimates (M = .024, SE = .221) did differ (p < 0.01); for the HE group, this was also true under the NoGo-condition (p < 0.001): the STFT estimates (M = -.489, SE = .221) differed from the AIC-AAR estimates (M = .096, SE = .221).

4.3.3.1.1 Covariates and Additional Fixed Effects

The unstandardised parameter estimates (slope coefficients), standard errors, and significance for seven continuous covariates and two nominal categorical predictors are presented in Table 4.4.

Table 4.4: Covariate parameter estimates and standard errors: beta power analysis.

Covariate	Beta	SE
Age at EEG recording	0.198	0.116
Postnatal lead exposure	0.041	0.057
WISC IQ	-0.019	0.013
Mother's age (at delivery)	0.040	0.034
Socio-economic status	-0.046	0.017*
Caregiver education	-0.102	0.052
Cigarettes/Day	-0.082	0.039
ADHD†	-0.707	0.381
Marital status†	-0.079	0.293

† - nominal categorical variable.; *$p < 0.05$, **$p < 0.01$ & ***$p < 0.001$.

Of the seven continuous covariates tested for inclusion into the frontal power model, socio-economic status—as measured by the Hollingshead scale—was the only covariate that shared a significant linear association with the frontal power measure ($p < 0.05$). Mother's cigarette-smoking and caregiver education shared a moderate association with the frontal power measure, although they were not significant ($p = .056$ and $p = 0.07$, respectively). We entered socio-economic status into the model, and assessed the model fit using the likelihood-ratio test, the entry of this covariate provided a better explanation of the experimental data, $\chi^2(1) = 11.664$, $p < 0.001$—AIC indicated a more parsimonious fit; however, BIC indicated that the inclusion of the variable was not necessary. Neither of the categorical predictors (ADHD diagnosis and marital status) were significant after entry into the model, although ADHD shared a moderate association with the regional power measure ($p = 0.086$).

We observed that SES, mother's cigarette-smoking, and maternal education covaried within the sample. For example, SES and cigarettes smoked per day during pregnancy shared a moderate correlation, $\rho = .43$, $p = 0.07$—mothers from a higher socio-economic status tended to smoke more. SES and caregiver education shared a

significant correlation, ρ = .56, p = 0.03; as one would expect, higher status mother's had relatively more education than lower status mothers. Mother's education in years was not correlated/anti-correlated with cigarette smoking. As SES, mother's cigarette-smoking, and maternal education shared a common explanation of the covariance in the dependent variable, inclusion of a single covariate amongst them was justified (Hastie *et al.*, 2009). SES explained a larger proportion of the variability in the dependent variable and provided a unifying explanation for the patterns of covariance within the sample. After entering SES as a covariate, the addition of the other covariates did not offer any additional explanatory power.

All the significant fixed-effects discussed were still significant after controlling for potential confounding due to socio-economic status. Thus, none of the effects stated in the main frontal regional analysis or the follow-up hemispheric analyses could be alternatively explained by socio-economic status and other characteristics generally associated with higher status mothers. Fixed-effects that did not reach significance such as condition and the group x condition interaction, as well as certain hemispheric post-hoc comparisons: the spectral power across the two hemispheres within the control group, the group difference in the left frontal regions, and condition induced group hemispheric effects were, as before, non-significant.

4.3.3.2 Inter-Trial Coherence

The main effect for group was not significant, $F(1,11.770) = 1.368$, $p = .265$. The main condition-effect was significant, $F(1,77.322) = 30.127$, $p < 0.001$, there was greater phase-locking across trials in the NoGo-condition (M = .140, SE = .012) compared to the Go-condition (M = .100, SE = .008). The group x condition interaction did not reach significance, $F(1,77.322) = 1.618$, $p = .207$. Marginal means and standard errors for inter-trail coherence are presented in Table 4.5.

Table 4.5: Estimated marginal means and standard errors for inter-trial coherence (back-transformed, λ= -.3009).

	Go-Condition	NoGo-Condition
Controls	0.096 (.011)	0.124 (.015)
Heavy-exposed	0.105 (.011)	0.160 (.019)

ITC scalp maps displaying phase-locking values are presented in Figure 4.3. Strong phase-locked activity was not observed across trials in either group under any of the experimental conditions. Weak consistency of phase relative to baseline values is observed on all levels of the experiment, indicating that the beta component is an induced oscillatory response, as opposed to being part of the evoked, phase-locked cortical response; such a response would elicit medium-strong PLV values: .25 - .30 (cf. Figure 2.8 A vs Figure 2.8 B).

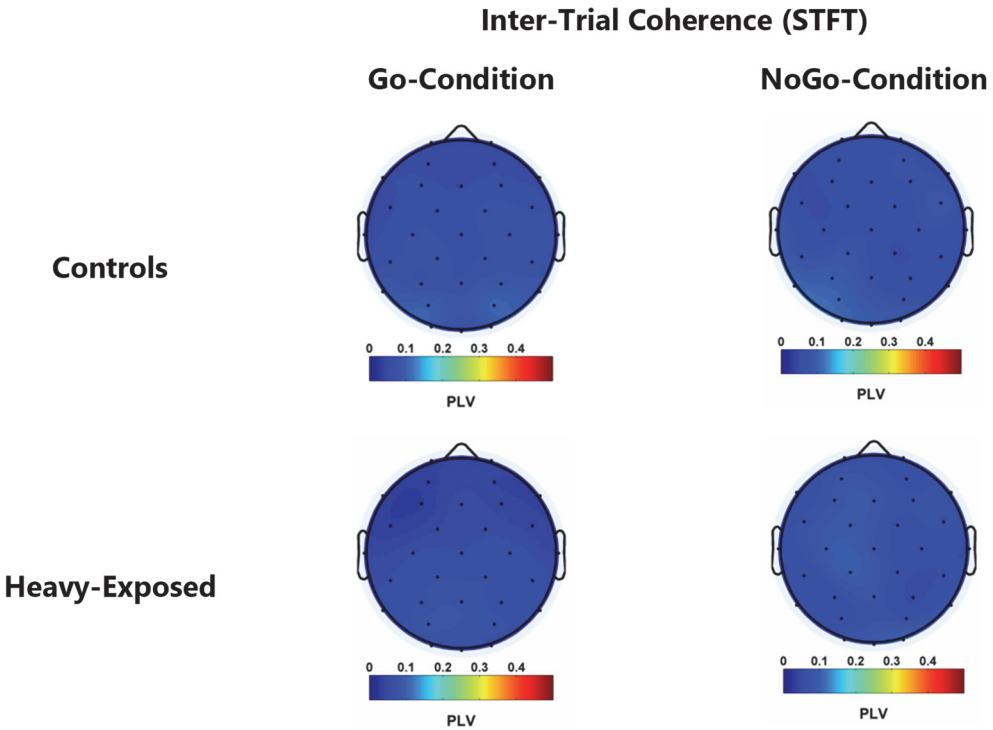

Figure 4.3: Topographical maps of the ITC feature distributed across the scalp in 13.5 – 16.5Hz band and 350ms – 650ms time-window. Maps are presented by group and condition.

Table 4.6: Beta-band (13.5Hz – 16.5Hz) power and ITC measures vs ERP area.

Feature-Condition	ρ	95% lower	95% upper	p
Phase (ITC)				
Go	-0.088	-0.683	0.643	0.380
NoGo	-0.165	-0.703	0.464	0.289
Power (STFT)				
Go	0.022	-0.599	0.592	0.476
NoGo	-0.104	-0.7151	0.6169	0.361
Power (AIC-AAR)				
Go	0.006	-0.594	0.619	0.493
NoGo	-0.247	-0.732	0.392	0.205

Note. p-values are computed via a monte-carlo simulation; 95% Confidence intervals were derived using bootstrap resampling.

The ITC feature does not covary with ERP magnitude, neither in the Go-condition or the NoGo-condition. For the power features, no significant covariance is observed for the STFT features or the AIC-AAR spectral-power features under either experimental condition. The results of the correlation analysis indicate that the power and ITC measures do not covary with ERP magnitude, confirming the induced nature of the oscillations.

4.3.3.2.1 Covariates and Additional Fixed Effects

The unstandardised parameter estimates (slope coefficients), standard errors, and significance for seven continuous covariates and two nominal categorical predictors are presented in Table 4.7.

Table 4.7: Covariate parameter estimates and standard errors: beta ITC.

Covariate	Beta	SE
Age at EEG recording	0.303	0.082**
Post Natal Lead Exposure	-0.079	0.050
WISC IQ	-0.007	0.012
Mother's Age (Delivery)	-0.020	0.033
Socioeconomic Status	-0.017	0.019
Caregiver Education	0.010	0.055
Cigarettes/Day	-0.041	0.041
ADHD†	-0.425	0.380
Marital Status†	-0.364	0.252

† - nominal categorical variable.; *$p < 0.05$, **$p < 0.01$ & ***$p < 0.001$.

Age at EEG recording was the only covariate tested for entry into the model that was significantly associated with regional ITC, indicating that, within our sample, the ITC phase feature was sensitive to neural maturation effects: higher levels of ITC were observed for the older participants within the sample. After entry into the model, the likelihood-ratio test indicated a significant improvement to model fit, χ^2 (1) = 18.536, $p < 0.001$; all information criteria (AIC and BIC) indicated a more parsimonious model. After controlling for potential confounding the group main effect reached significance, $F(1,11.411) = 6.818$, $p < 0.05$: Controls ($M = .104$, $SE = 0.007$) vs HEs ($M = .135$, $SE = .010$). The condition main effect was still significant, $F(1,75.588) = 30.175$, $p < 0.001$. The group x condition interaction remained non-significant, $F(1,75.88) = 1.683$, $p = .198$.

4.3.3.2.2 Behavioural and Regional Power Measures

In the normally-developing control group, our single-trial linear-mixed effects model on performance accuracy showed that spectral power varied independently of task performance, $F(1,807.243) = 0.000$, $p = .987$; however, in the HE group, spectral power

shared a significant linear association with task performance, $B = 1.341$, $F(1,817.915) = 5.115$, $p < .05$, 95% CI [0.177, 2.505]. Our model shows that within the HE group, on the single-trial level of the design, inaccurate responses were associated with desynchronised beta-power, while accurate responses were observed at baseline levels of spectral power or occasional synchronised activity. In the control group, beta-power remained synchronised relative to baseline levels throughout the task and varied independently of task performance (accuracy).

4.4 Discussion

Our aims in this study were twofold: (1) to elicit the decision-making linked beta-band ERS within a normally-developing sample using a single-stimulus per trial visual version of the Go/NoGo task and (2) to understand if there is an association between heavy prenatal alcohol consumption and changes in the induced, frontal beta-band ERS. Hypothesis 1 and 2 were related to our first aim, wherein we sought to elicit the beta-ERS across conditions within a normally-developing sample. We also expected to see a left-skewed scalp topography as was observed in the 2006a study of Alegre *et al.* In-line with our first experimental hypothesis, our study replicated and extended the findings of Alegre *et al.* in a normally-developing sample: we observed the early decision-making linked beta-ERS in both the Go and NoGo experimental conditions within the control group. Despite differences in modality (our task was a visual task and Alegre *et al*'s were auditory) we still identified the frontal beta oscillation, indicating the ERS is generic across modalities. The fact that the implementations differ across studies (single stimulus/trials vs paired-stimuli) and that we were still able to elicit the oscillatory bout, supports the argument that the beta-band ERS must be related to demands of the Go/NoGo task in general, rather than due to the manner in which the stimuli are presented to the participant. Most importantly, our findings provide evidence for the existence of the early frontal beta-band ERS at preadolescent and adolescent stages of human development.

Our second hypothesis stated that we expected to observed a left-skewed ERS within the control group; however, the early beta-band ERS was observed over the frontal regions without a skewed scalp topography. The control group's scalp maps appear to show a frontal central scalp distribution of spectral power and what appears to be a more midline response in the NoGo-condition relative to the Go-condition, very similar to the observations of Alegre *et al.* (2004), but different from the left-skewed response of Alegre *et al.* (2006a). The fact that no significant hemispheric differences were observed within our normally-developing sample is attributable to two main factors: the number of electrodes used in the 2006a study were larger (58 channels), thus higher spatial sampling may have given a better spatial specification of the oscillation in comparison to the 19 channels used in the 2004 study, and the 32 channels used in our study. Our data is analysed in reference derivation (linked mastoids), while Alegre *et al.* opted for reference free derivations—Hjorth laplacian and current source densities (CSDs)—meaning that the oscillations were observed at different spatial scales, as Hjorth and CSD derivations are instances of spatially filtered data. Despite these differences, our scalp maps are still very similar to those of Alegre *et al.* (2004) wherein a Hjorth laplacian was used.

Our third hypothesis was related to the effect of heavy PAE on the frontal beta oscillations, in that we expected the heavy-exposed group to differ from the controls in frontal beta-band spectral power measures, although we left unspecified the direction of this effect due to the lack of previous research findings. There was a significant main effect for group, as post-stimulus oscillatory power within the ROI for the heavy-exposed group remained at baseline levels in both the Go and NoGo conditions, as opposed to the significant ERS observed in both conditions within the control group The group x condition interaction effect was not significant, indicating that the beta-ERS was not associated with movement or inhibition demands specific to each condition, but was part of generic task-related neural processing taking place at early stages of each condition prior to movement or inhibition. A follow-up

hemispheric analysis indicated a significant group x hemisphere interaction effect. This was the case when using either of the spectral estimators. We did not observe any differences across hemispheres for the controls; however, in the heavy-exposed group a frontal asymmetry was present, with post-stimulus beta spectral power desynchronised relative to baseline levels in the right hemisphere, but remaining at baseline levels in the left. The group x hemisphere interaction effect showed a large significant difference between groups over the right hemisphere; this was due to the asymmetric scalp distribution in the heavy-exposed group. The group x condition x hemisphere interaction effect was not significant when using either of the spectral estimators, indicating the distribution of power across the left and right frontal regions was independent of movement/inhibition-related processing.

Socio-economic status was shown to be a significant predictor of the induced frontal beta-band ERS. In relation to this finding, we observed that SES was correlated with mother's cigarette smoking and SES correlated with mother's education; however, we observed that education was not associated with cigarette smoking. Thus, a proportion of the variance in beta-band power could be explained by the smoking habits of higher SES mothers, demonstrating that frontal beta is sensitive to prenatal teratogen-exposure linked to cigarette-smoke. This impact was significant, but did not offer an alternative explanation of experimental outcomes: the group main effect and group x hemisphere interaction effect were still significant after controlling for socio-economic circumstances; the non-significant three-way group x condition x hemisphere interaction-effect remained non-significant. Intellectual abilities, as measured by a subset of scales from WISC, were not related to beta-band power dynamics across the frontal-regions. This is of interest, if the frontal beta-ERS is linked to decision-making then we would expect intellectual abilities to be linked to the oscillatory bout which was not the case. These observations cast some doubt on Alegre *et al.*'s proposal of a decision-making link to the induced oscillation.

Our analysis of the ITC measure indicated weakly phase-locked activity across groups and across experimental conditions; however, we did observe significant main effects in our frontal ITC model for group and condition after controlling for neural maturation—age at which the EEG recording took place. Since the participants age-range was spread across preadolescence and adolescence, changes in oscillatory parameters such as ITC with age are likely to be observed in such a sample. The significant effects showed greater ITC in the heavy-exposed group and greater levels of ITC in the NoGo-condition with no interaction effect. As the data was analysed in a reference derivation, it is likely that current source contributions from neighbouring regions that are phase-locked to stimulus onset could conduct up to frontal electrodes. Even though this is likely to have occurred, the observed ITC levels are still low. Research in our laboratory indicates that an ITC = .25 to .30, was related to the P300 event-related potential, thus the observed levels are too low to indicate a regional evoked power response. We also observed that the magnitude of the induced frontal beta-ERS did not covary with the ERP area-measure, which is what we would expect if the increase in beta-power was evoked as opposed to induced—the ERP is composed of evoked power. In addition, the ITC did not covary with the ERP-area measure, which is also expected for an evoked response. Thus, we can confidently conclude that all evidence points to the fact that the beta-ERS is induced and that the impact of PAE affects the control parameters that regulate induced neocortical oscillatory activity.

In terms of our fourth hypothesis, we expected to see equivalent inhibitory performance with differences in median reaction times within the Go-condition. Our results showed that while equivalent inhibitory performance was observed across groups, the groups differed on: (1) median reaction times and (2) errors-of-omission. Given the reaction-time data and differences in omission error rates, normally-developing participants process the task demands more efficiently and respond more rapidly; however, with reduced accuracy in the Go-condition. Heavy-exposed participants performed the task with a slower more purposive strategy—slower

processing speeds are a known feature of FASD (Burden *et al.*, 2005). In order to understand these observations, we can consider the relationship between performance and arousal as well as the connection between arousal and motivation (Yerkes & Dodson, 1908). Performance on a given task is dependent on physiological arousal: low levels as well as extreme levels of arousal are associated with poor task performance, while optimal performance is achieved at medium levels of arousal (Broadbent, 1965; Mendl, 1999). Seen in light of Yerkes and Dodson's law, also known as the inverted-U function, the performance metrics point to the fact that the controls were not as challenged and were perhaps casual in their approach, while the heavy-exposed group were somewhat more challenged and achieved better performance levels leading to less errors-of-omission and equivalent inhibitory control. The differences in task difficulty experienced by either groups would also have had an impact on metabolite utilisation in neural tissue, as studies point to the fact that different patterns of regional blood flow arise due to different levels of task-related difficulty (Mostofsky & Simmonds, 2008).

Although there was evidence to support the presence of a speed-accuracy trade-off within the control group, it was also of interest to see if accuracy on a single-trial basis was related to the decision-making linked frontal beta-ERS. As the ERS is proposed to be an electrophysiological biomarker for decision-making, significant changes in levels of spectral power (increases or decreases) should be related to faulty decision-making during task performance. Based on our fifth experimental hypothesis, we expected to see a significant association within both groups between performance accuracy and beta-band oscillatory power. In the control group, we observed that beta-power was not associated with performance accuracy; however, within the heavy-exposed group, we observed that inaccurate responses were associated with desynchronised beta-band oscillatory activity, while accurate responses were observed around baseline levels or during occasional event-related synchronisation. Thus, the association of frontal oscillatory power measures and performance parameters associated with

erroneous decision-making within each group are very different: speed accuracy trade-offs for the controls in the context of synchronised beta activity, while for the HEs, slower purposeful performance wherein faulty decision-making is linked to desynchronised beta-power.

As we did not observe the expected relationship between beta-band power and performance accuracy in both groups and beta-power also did not covary with intellectual abilities as assessed by the Wechsler Intelligence Scale for Children, alternative explanations regarding the functional significance of the oscillatory bout are justified. Based on our findings, the beta-ERS is not directly associated with decision-making. A likely alternative explanation to that offered by Alegre *et al*, would propose that the induced beta-ERS is linked to self-reflexive awareness of the decision-making process. If the heavy-exposed group were impaired in terms of their metacognitive awareness (inwardly directed attention), it may make it more challenging for them to adapt during task performance, producing slower more purposive performance with higher levels of task-related arousal.

In terms of comparing analytical outcomes when using STFT vs AIC-AAR spectral estimates, we found that there was a significant main effect for the method: overall spectral power was greater when using the AIC-AAR spectral estimates compared to the STFT estimates. In addition, the group x method interaction was also significant: we observed that AIC-AAR estimates were biased relative to STFT estimates. The divergence between the two estimators, despite using the same window length for the sliding window, is related to a number of factors. Within finite samples, AIC has a tendency to over-parametrise—select an overly complex model (De Waele, 2003). This over parametrisation brings into effect different estimation bias-variance trade-offs relative to those of the STFT estimates, consequently yielding divergent spectral estimates in the time-frequency domain. In addition, the small sample properties of either estimator also affect estimation bias-variance trade-offs: on a single-trial basis, the STFT estimates are inconsistent, while the AR estimate is consistent but biased.

These estimator dependent statistical bias-variance trade-offs lead to different specifications of components in time and frequency. Over-and-above these points, the use of Gaussian tapering in the STFT and rectangular windowing in the AAR approach lead to further differences in signal component representations in time and frequency: primarily due to weighting on the leading and trailing edges of the analytical window that in turn affects overall datum-points available for the spectral estimates within the sliding analytical window. Due to these differences, we observe that spectral power estimates differ enough to affect analytical outcomes. The scalp maps derived using either estimator also provide slightly different spatial representations across the scalp due to the estimation bias-variance trade-offs specific to each method.

A limitation of the study would be its sample size: only large effects could potentially be detected within the design. Given the aims of the study, that in part sought to replicate Alegre *et al*'s findings within a developing sample using a simple single-stimulus visual version of the Go/NoGo task, our sample was adequate—bearing in mind that Alegre *et al.* (2004, 2006a and 2006b) observed the beta-ERS using samples of seven to ten participants. Thus Alegre *et al.*'s and our findings collectively speak to the fact that the ERS is a large effect that is detectable even within smaller samples. At the level of power within the design, we were also able to observe significant group main effects related to spectral power over the frontal regions, we were also able to observe significant group x hemisphere interaction effects when using either spectral estimator. The heavy-exposed sample was larger than the controls, so there is a higher likelihood of observing the beta-ERS if it in fact is elicited within the heavy-exposed group, which it was not.

A clear way forward in terms of further analysis is to decompose the data into independent components and to source-localise these components. Time-frequency analysis as well as an analysis of how different independent sources project to scalp electrodes will allow us to assess hypotheses related to the source generators of the induced beta oscillation. We have strong evidence for the foundations of a hypothesis

wherein we would expect electrical dipolar sources to be localised to the mesial prefrontal regions and the dorsal anterior cingulate cortex (Ikeda *et al.*, 1996; Liddle *et al.*, 2001). Source level analysis will allow us to assess such localisation hypotheses. Source level data would also allow for the application of multivariate adaptive autoregressive models, and access to connectivity measures that index the direction of information flow between cortical source generators (Brunner *et al.*, 2016; Mullen, 2014). The explicit link between electrical and organic within the spectrum of PAE disorders has yet to be made in a single empirical endeavour. It will provide important clinical understanding of the disorder and a more detailed understanding of frontal lobe function in the context of motor response inhibition.

4.5 Conclusions

Our findings indicate that the induced frontal beta-ERS elicited in the studies of Alegre *et al.* are present at earlier stages of development and can be elicited using a single-stimulus visual version of the Go/NoGo task. The oscillatory bout is not observed on the scalp of heavy-exposed participants, suggesting that heavy PAE is associated with a change in the underlying neural circuitry that generates the frontal beta-band ERS. Normally developing controls are less challenged by the task and approach performance based on a speed accuracy trade-off. Our observations based on single-trial analysis lead us to believe that the beta-ERS may not be directly linked to decision-making, but is more likely associated with parallel metacognitive processes related to inwardly directed attention towards the decision-making process. Reduced metacognitive awareness associated with PAE is a key factor that makes the task more challenging and leads to erroneous decision-making for heavy-exposed participants.

Chapter 5

An ERP Study of Response Inhibition in the Auditory Domain in Children with Fetal Alcohol Spectrum Disorders

Matthew M. Gerhold[1], Sandra W. Jacobson[1,2,3], Joseph L. Jacobson[1,2,3], Christopher D. Molteno[3], Ernesta M. Meintjes[1,2], and Colin M. Andrew[1,4]

[1]Division of Biomedical Engineering, Department of Human Biology, University of Cape Town, South Africa; [2]Department of Psychiatry and Behavioural Neurosciences, Wayne State University School of Medicine, Detroit, MI, United States; [3]Department Psychiatry and Mental Health, University of Cape Town; South Africa. [4]Essentric Technology, Cape Town, South Africa.

Abstract

Previous event-related potentials (ERPs) studies of response inhibition in children with fetal alcohol spectrum disorders (FASD) have used a visual Go/NoGo task to study the impact of prenatal alcohol exposure on response inhibition. No studies exist using auditory versions of the task; thus, it is unclear how the deficits observed in visual tasks translate into the auditory domain. This study examined ERPs using an auditory Go/NoGo paradigm in a sample of 35 school-age children—18 with heavy PAE and 17 normally-developing controls. Alcohol-exposed children performed as well as controls in terms of inhibiting their responses; however, their reaction times were significantly slower under the Go-condition. As in the ERP visual Go/NoGo task

previously administered to these children, group differences were seen in early perceptual processing, specifically related to stimulus discrimination, with a decrease in P2 amplitude in the alcohol-exposed group. The control group exhibited greater N2 amplitude in the NoGo compared to the Go-condition while the alcohol-exposed group did not, suggesting a group difference in the neural substrates underlying conflict monitoring. The alcohol-exposed group demonstrated longer latency P3 with reduced amplitude, suggesting poorer allocation of attention. The alcohol-exposed group also exhibited a late positive component (LPC) similar to the one observed in the previous visual ERP study. This LPC may indicate compensatory neurophysiological function related to resetting of attentional control networks in preparation for the next trial. None of the ERP outcomes in this study were related to potential confounders which included cognitive and socio-economic measures as well as ADHD diagnosis. The observed ERP group differences point to elements of perceptual and attentional processing likely to be involved in the performance-deficits often observed in children with FASD. We also observed changes in ERPs related to conflict-monitoring/response-inhibition, highlighting fetal alcohol-related effects on how the brain responds when there is need to identify and respond to environmental cues by switching away from a prepotent motor response to an inhibited state.

5.1 Introduction

Fetal alcohol spectrum disorder (FASD) is an umbrella term used to describe the range of disorders that have been linked to maternal alcohol consumption during pregnancy (Chudley *et al.*, 2005; Hoyme *et al.*, 2005). Symptoms include, but are not limited to facial dysmorphologies, pre- and postnatal growth retardation as well as cognitive and behavioural deficits (Fryer *et al.*, 2012; Jones and Smith, 1973). Heavy alcohol exposure during pregnancy, with or without overt craniofacial dysmorphologies, is also associated with a wide range of neuropsychological deficits (Mattson and Riley, 1998).

Response inhibition, which is often assessed using a Go/NoGo paradigm, refers to the ability to inhibit/suppress a prepotent motor response: a motor response (button press) is cued during a large proportion of the trials (Go-condition) interspersed with a limited number of cues to withhold the response (NoGo-condition). Behavioural performance is assessed in terms of the proportion of correctly withheld responses. Although high-functioning children with fetal alcohol syndrome (FAS) performed as well as controls on a simple Go/NoGo task (Kodituwakku *et al.*, 1995), previous research has linked PAE to impairment of response inhibition on more challenging measures of inhibitory control, such as the *Stroop Color-Word Test* (Connor *et al.*, 2000; Mattson *et al.*, 1999). Prenatal alcohol-related changes in patterns of regional brain activation have also been found during a *response inhibition n-back task* using functional magnetic resonance imaging (Diwadkar *et al.*, 2013).

An event-related potential (ERP) involves a spatially widespread phase reset of the on-going neocortical activity, which is time-locked to stimulus onset (Luck, 2012). The phase reset is driven by afferent fibers projecting from the *thalamus* up to primary sensory areas within the *cerebral cortex* (primary visual, auditory, and tactile areas). By averaging repeated trials, the phase locked oscillatory activity is enhanced, while the on-going "noise" is attenuated. The resultant waveform/feature is known as an *evoked-potential* (EP) or an event-related potential (Pfurtscheller and Lopes da Silva, 1999;

Pfurtscheller, 2006). EPs and ERPs are useful indices used to assess neurophysiological function in healthy and clinical populations.

Two ERP components elicited under the Go/NoGo experimental paradigm are the N2 and P3. The N2 is linked to response inhibition and conflict monitoring; the P3, to attention and working memory processes. The P3 has been shown to be a sensitive biomarker for alcoholism (Bauer, 2001). When the Go/NoGo paradigm is administered to normally developing samples, the amplitude of the N2 is larger for the NoGo compared to the Go-condition, and greater amplitude is observed for the P3 in the NoGo compared to the Go-condition (Davis *et al.*, 2003; Johnstone *et al.*, 2005). Kaneko *et al.* (1996), using an auditory oddball-plus-noise task, reported that decreased P3 amplitude discriminated participants with developmental disorders (FAS and Down syndrome) from each other: the FAS group showed decreased amplitude over the frontal regions. The FAS group also differentiated itself from controls in that they showed longer P3 latencies over the parietal regions—this task is similar in terms of stimulus presentation to our auditory Go/NoGo task.

Burden *et al.* (2009) conducted the only previous study to examine ERPs using a Go/NoGo paradigm in children with heavy PAE. This study, conducted in Cape Town, South Africa, used a simple visual Go/NoGo task. Despite similar behavioural performance during the task, several differences were found in the ERPs. When participants were required to inhibit a response, the control group showed an increased amplitude N2 within the NoGo compared with the Go-condition, a response that is observed in normally developing samples across both the visual and auditory stimulus modalities (Davis *et al.*, 2003; Johnstone *et al.*, 2005). By contrast, the alcohol-exposed group exhibited a reduction in N2 amplitude, which has been shown to be indicative impairment in conflict monitoring processes.

In the Burden *et al.* (2009) visual ERP study, under the Go-condition, the controls exhibited a larger P2 component than in the NoGo-condition, an amplitude difference that was not observed within the alcohol-exposed group. In addition, the alcohol-

exposed group exhibited longer P2 latencies in both conditions. Using the same paradigm, these P2 latency effects were seen in a less heavily alcohol-exposed group of Inuit children in Arctic Quebec (Burden *et al.*, 2011). Based on the limited data available using the Go/NoGo task within normally developing samples, the P2 amplitude effects seen within the control group on the visual task (larger P2 in the Go compared to the NoGo-conditions) are also seen in an auditory version of the task (Johnstone *et al.*, 2005). Thus, the increase in amplitude of the P2 in the Go-condition within normally developing samples occurs independent of stimulus modality. The P2 component has been linked to early perceptual processes involving initial interactions between bottom-up perceptual and top-down executive control driven processes.

In Burden *et al.* (2009), a late positive component (LPC) was observed under the NoGo-condition within the alcohol-exposed group. This response was attributed to "increased cognitive effort", but is more likely to signify resetting of frontal-parietal attentional networks in preparation for the next trial; namely, regions of the *anterior cingulate cortex*, the *dorsolateral prefrontal cortex* and the *parietal lobules* that need to be integrated to implement attentional control (Wang *et al.*, 2010).

We conducted the first study to examine effects of PAE on response inhibition during a Go/NoGo task in the auditory domain. The aim of this study was to examine the degree to which the ERP waveforms, elicited during aurally-cued response inhibition, resemble those elicited in Burden *et al.*'s (2009) visual ERP study. Based on previous studies in normally developing and alcohol-exposed samples, we hypothesised that: (1) increased P2 amplitude would be observed in the Go compared to the NoGo-condition within the control group, but not the alcohol-exposed group; (2) slower P2 latency would be observed in the alcohol-exposed compared to the control group across both conditions; (3) the NoGo-condition would elicit greater N2 amplitude when compared with the Go-condition for the control group, but not in the alcohol-exposed group; (4) increased P3 amplitude would be observed in the NoGo-

compared to the Go- condition within the control group but not in the alcohol-exposure group; (5) an LPC would be manifest in the NoGo-condition only for the alcohol-exposed group.

5.2 Methods

5.2.1 Participants

Thirty-five Cape Coloured children from our Cape Town FASD cohort (Jacobson *et al.*, 2011) took part in this study. Fourteen of these children had previously participated in the Burden *et al.* (2009) visual ERP study. The Cape Coloured are descendants from a mixed ancestral lineage including European colonists, Malaysian slaves, Khoisan aboriginals, and the African Nguni ethnic group. Poor socio-economic circumstances and historical practices of compensating farm labour in part with wine have contributed to a tradition of heavy recreational weekend binge drinking in a portion of this population. This pattern of consumption persists amongst pregnant women within the population. As a result, the Cape Coloured community experience one of the highest levels of FASD in the world (May *et al.*, 2007, 2013). Twenty-three children participating in this study were the older siblings of participants in our Cape Town Longitudinal Cohort study (Jacobson *et al.*, 2008). The others were identified by screening all of the 8-12-year-old children from an elementary school in a rural section of Cape Town where there is a very high incidence of alcohol abuse among local farm workers (Jacobson *et al.*, 2011; Meintjes *et al.*, 2010). All of the children were right-handed as they were originally recruited to participate in an FASD neuroimaging study (Dodge *et al.*, 2009; Meintjes *et al.*, 2010).

Each mother was interviewed in her primary language (Afrikaans or English) regarding her alcohol consumption during pregnancy using a timeline follow-back approach (Jacobson *et al.*, 2002). Volume was recorded for each type of beverage consumed on a daily basis, converted to absolute alcohol (AA) using multipliers

proposed by Bowman *et al.* (1975), and averaged to provide a summary measure of alcohol consumption during pregnancy (AA/day). Two groups were recruited: (1) heavy drinkers who consumed at least 14 standard drinks per week (1.0 oz AA/day) or engaged in binge drinking (5 or more drinks/occasion); (2) controls who abstained or drank no more than minimally during pregnancy. Number of cigarettes smoked on a daily basis during pregnancy was also recorded, as was use of illicit drugs. Mothers were also interviewed regarding their education and occupational status and that of their spouse/partner; these data were used to assess socio-economic status (SES) on the *Hollingshead Four Factor Index of Social Status* (Hollingshead, 2011).

5.2.2 IQ, FASD and ADHD Diagnoses

5.2.2.1 IQ Assessment

The children were administered seven of the ten subtests from the Wechsler Intelligence Scale for Children, 3rd edition (WISC-III)—Similarities, Arithmetic, Digit Span, Symbol Search, Coding, Block Design, and Picture Completion—and Matrix Reasoning from the WISC-IV at the first 11-year visit. IQ was estimated from these subtests using Sattler's (1992) formula for computing Short Form IQ; validity coefficients for Sattler Short Form IQ based on five or more subtests consistently exceed $r = 0.90$. The cognitive and Go/NoGo assessments were administered by an advanced graduate research assistant (MP) who was blind regarding FASD diagnosis and prenatal alcohol history.

5.2.2.2 FASD Diagnosis

The children were independently examined by two U.S. expert dysmorphologists (H.E. Hoyme, M.D., and, L.K. Robinson, M.D.) using a standard protocol based on the IOM-revised criteria (Hoyme *et al.* 2005) at a dysmorphology clinic held in 2005 (Jacobson *et al.*, 2011). Children who could not attend the clinic were examined by a South African expert FASD dysmorphologist (N Khaole, M.D.), whose assessments of

key anomalies were highly correlated with those provided by HEH and LKR (Jacobson *et al.* 2011) and whose diagnoses were all confirmed by examinations conducted in follow-up clinics we held with the same dysmorphologists in 2009 and with HEH in 2013. HEH, LKR, SWJ, JLJ, and CDM subsequently conducted case conferences to reach consensus regarding which chldren met criteria for FAS or PFAS diagnoses.

5.2.2.3 ADHD Diagnosis

CDM administered the Schedule for Affective Disorders and Schizophrenia for School Aged Children (K-SADS) to each mother to assess ADHD, and each child's classroom teacher completed the Disruptive Behavior Disorders (DBD) Scale (Pelham *et al.* 1992). Participants were assigned a DSM-IV ADHD diagnosis following criteria developed in consultation with Joel Nigg, Ph.D., an expert in ADHD research. An ADHD classification was assigned if (a) at least 6 of the 9 inattention and/or six of the nine hyperactivity /impulsivity symptoms were endorsed ("pretty much" or "very much true") by one or more informants, and (b) some impairment was reported by seven years of age and in two or more settings.

In addition to the above-mentioned scales, blood samples were obtained from the children at 10.4 years (SD=1.2) and checked for lead concentrations (pb; ug/dl).

5.2.3 Procedure

All protocols were approved by Wayne State University and the University of Cape Town institutional review boards. The mothers provided written informed consent, and the children provided oral assent. The mothers and children were given breakfast, a snack, and lunch and at the end of the visit, each mother received a small monetary compensation for her participation; each child was given a small gift.

The children were seated in-front of the computer screen in a dimly lit room approximately 70 cm away from the monitor and were fitted with a 128-channel Electrical Geodesics net (Electrial Geodesics Inc., Eugene, OR), which had been soaked

in an electrolytic solution. The net was adjusted to fit the participant, and an impedance check was conducted. The testing took approximately 20 minutes. The presentation of the Go/NoGo task was controlled by E-Prime 2.0 software (Psychology Software Tools, Pittsburgh, PA).

5.2.3.1 Data Acquisition

EEG signals were acquired using NetStation 4, a Netamps amplifier, and a high-resolution 128-channel Geodesic net (EGI System 200 Technical Manual). Impedance was kept below 50kΩ according to the manufacturers specifications. Data were recorded using a sampling rate of 250Hz and a 0.1Hz – 80Hz on-line band-pass filter. A vertex reference (central midline) was used during data acquisition. Data were stored and analysed off-line.

5.2.3.2 Go/NoGo Task

In the Go/NoGo task, the Go-condition was represented by a 1000Hz tone; the NoGo, by a 2000Hz tone. In the Go-condition the child was instructed to press a button with his/her right index finger, whereas in the NoGo-condition s/he was told to inhibit the motor response. The inter-trial stimulus interval (ISI) was constant throughout the experiment. In each trial the auditory stimulus was presented for 500ms, followed by 4000ms of silence. The Go- and NoGo- conditions were randomised with the only constraint being that there were 35 Go-trials and 15 NoGo-trials equating to 50 trials per block. Seven 50-trial blocks were presented to each participant. Each block was interleaved with a 1-minute rest period. Subjects were instructed to execute a response as quickly and accurately as possible.

5.2.4 ERP Analysis

All processing was performed within the MATLAB computing environment using custom scripts built upon functions provided by the EEGLAB toolbox (Delorme and Makieg, 2004). Data were imported into MATLAB and filtered using a band-pass filter

from 0.5Hz – 30Hz. Recordings were scanned for gross-movement artefacts, and those portions of data were excluded from the data set. The 1-minute rest periods between blocks were also excluded from further analysis. Noisy channels were identified, removed, and replaced by an average of surrounding electrodes. In addition, the perimeter ring of electrodes was removed from further analysis due to gross-movement artefact. Data were then segmented relative to stimulus onset: 200ms prior to stimulus onset and 1500ms post-stimulus onset. Segments had their mean baseline amplitude removed from the entire segment to yield a set of baseline corrected trials. The segments were then scanned for behavioural response data using custom software written within the MATLAB computing environment. The software classified and stored information associated with the following responses: correct Go, correct NoGo, incorrect Go, and incorrect NoGo. The response time data were used for further analysis of participant behaviour under the experimental conditions. The data tables containing the behavioural response data formed the basis for automated segment rejection whereby error-trials (incorrect Go's and incorrect NoGo's) were removed from further analysis—we did not look at error-related ERPs as the number of incorrect trials in this relatively simple task was too few to perform a meaningful analysis.

The segmented, error response-free-data were submitted to a *blind source separation* (BSS) algorithm in order to identify and remove unwanted artefacts from the data: eye-movement, eye-blinks, and electrical activity arising from muscles of the jaw and face (Delorme and Makieg, 2004). Artefact free data were then re-referenced to the average of all electrodes (an average reference). Any segment with extreme values exceeding 50μV was excluded from further analysis as such extreme values are not cortical in origin and introduce bias into the ERP waveforms. The remaining segments were averaged by condition for each participant as well as for each group. Automated peak/trough detection within predefined latency windows was used to identify peaks/troughs in the average ERP waveforms for each participant. We were interested

in the P2, N2, P3, and LPC as these were the ERP features that were analysed in the visual study—"P" indicating a maximal amplitude peak in the waveform, while "N" is a minimal amplitude trough; a series of these peaks/troughs constitute and ERP waveform. The algorithm searched for maximal-peaks and minimal-troughs across all recording sites within each participant's data using the following latency windows: P2 (150-300 ms); N2 (175-300 ms); P3 (350-500 ms); and LPC (500-1050 ms). The data segments were then visually checked to ensure that the algorithm identified ERP peaks and troughs, rather than boundary markers at the start and end of each latency window. Initially, we used latency windows defined in the visual study as a guideline, adjusting these incrementally to accommodate all observed peaks and troughs within the artefact free segments.

To calculate the averages of amplitude and latency measures for the ERP waveform features, the identified recording site (electrode) with the maximal-peak/minimal-trough as well as the corresponding peak/trough from adjacent surroundings electrodes were included in the averages; these averages were computed for each participant within the sample. For each peak or trough within the ERP waveform, maximal amplitude and latency effects were consistently observed within the same scalp region across participants; for example, the N2 was maximal over the frontal regions for all participants and thus the amplitude and latency averages were formed by taking into account a subset of electrodes from within the frontal region (F7-FC5-F3-AF3-FC1-Fz-FC2-AF4-F4-FC6-F8). This was true for each of the ERP features we analysed in terms of the respective regional origins. Amplitude and latency averages were stored for statistical analysis. For the LPC, an average was taken in a predefined latency window since clear peaks were not well-defined.

5.2.5 Behavioural Analysis

Response times were checked for outliers using an iterative Grubbs algorithm—*extreme studentized deviate method* (Snedecor and Cochran, 1989). In its simplest form, the Grubbs test is calculated as the difference between the sample mean and the most extreme value in the data divided by the sample standard deviation (z-test). The resultant statistic is then assessed for significance, and if significant, the data point is excluded from analysis. Extreme outliers in the current experiment appear to represent trials in which there were lapses in attention leading to extreme response times; their exclusion resulted in normally distributed variables which otherwise deviated from normality. The corresponding EEG data segments were excluded from further analysis, this resulted in 5% of trials being rejected.

5.2.6 Statistical Analysis

Statistical analyses were conducted in MATLAB using the Statistics toolbox and customised scripts. Independent samples t-tests were used to compare response times in the Go-condition between the alcohol-exposed and control groups. For the ERP data, separate repeated measures ANOVAs were used to test for significant differences in amplitude and latency for each ERP component (P2, N2, P3 and LPC), with two experimental groups (alcohol-exposed vs controls) under two experimental conditions (Go vs NoGo).

Nine covariates were collected and are listed in Table 5.1. Eight of the nine were considered as potential confounders of any observed effects of PAE on the ERP component amplitudes and latencies: (1) child's sex, (2) age at EEG recording, (3) postnatal lead exposure, (4) ADHD, (5) mother's age at delivery, (6) socioeconomic status, (7) maternal education, and (8) cigarettes smoked per day during pregnancy. Because none of the covariates were even weakly related to any of the ERP components (all p's>0.20), there was no need to adjust statistically for potential confounders in any of the analyses. We also examined the relation of IQ to each of the ERP component

amplitues and latencies. Although child IQ was related to PAE, it was not related to any of these ERP outcomes (all *p*'s > 0.15) and, therefore, cannot be a mediator of any observed effects of alcohol exposure.

5.3 Results

5.3.1 Exclusions and Sample Characteristics

Accuracy and reaction time on the Go trials were used to identify subjects with performance that did not align with the rest of the sample. Reaction time paradigms characteristically will include some data validation processes and filtering of results prior to final analyses as reaction times are affected by lapses in attention, compulsive responding, or simply button pressing unrelated to the goal of the task. Thus, it was important to address this to avoid a single outlying subject biasing the results. Ten children (four exposed and six controls) had accuracy scores < 80% and/or reaction times < 420ms or > 750 ms; their EEG data were also contaminated with heavy movement-related artifact. These children's data were, therefore, excluded from further analysis, leaving a sample of 25 subjects: 13 alcohol-exposed and twelve controls. We compared the excluded participants with those retained in the sample to see if they were more likely to have low IQ scores or meet criteria for ADHD. There were no IQ differences, $t(33)=0.13$, ns, and the excluded group did not have a higher proportion of children with ADHD: two of ten (20.0%) of the excluded children compared to four of the 25 (16%) retained were diagnosed with ADHD, $\chi^2(1)= 0.08$, ns. In addition, there was no bias created by excluding participants from either of the groups in our analysis, $\chi^2(1)= 0.412$, ns—proportionally a similar number of participants were excluded from both groups.

Table 5.1: Sample characteristics.

	Alcohol-Exposed (n = 13) *M (SE)*	Controls (n = 12) *M (SE)*	F or χ^2
Sample characteristics			
Sex (% Female)	6 (46.2)	5 (41.7)	<1
Age at testing (years)	11.8 (1.2)	12.1 (1.1)	<1
Lead exposure (pb; ug/dl)	5.2 (2.3)	7.2 (3.4)	4.43*
WISC IQ[a]	66.5 (11.7)	77.8 (11.6)	5.85*
ADHD (yes/no)[b]	3 / 10	1 / 11	1.01
Mothers characteristics			
Age at delivery (years)	25.3 (5.2)	26.7 (6.5)	1.28
Socio-economic status[c]	17.4 (6.7)	19.3 (9.0)	<1
Education (years)	7. 6(2.8)	8.2 (1.5)	<1
Cigarettes/day gestation period	10.8 (8.5)	9.7 (6.0)	<1
Maternal alcohol consumption			
AA/day (oz)	2.9 (2.7)	0.1 (0.02)	6.40*
AA/drinking day (oz)	6.3 (2.8)	0.3 (0.5)	32.73***
Frequency (days/week)	2.8 (2.1)	0.07 (0.14)	16.39**

Note. AA refers to absolute alcohol; 1 oz AA ≈ 2 standard drinks. [a]Wechsler Intelligence Scale for Children. [b]Attention deficit/hyperactivity disorder. [c]Hollingshead (1975) Four Factor Index of Social Status Scale (Adams & Weakliem, 2011). *p <0. 05; **p < 0.01; ***p < 0.0001.

Table 5.1 provides background information from the children whose data were included in the analysis. As planned, the mothers of the children in the alcohol-exposed group drank substantially higher quantities of alcohol during pregnancy, averaging twelve drinks per occasion. Ten (83.3%) of the control mothers abstained during pregnancy; the other two drank minimal amounts: one reported drinking two drinks on one occasion, and the other, two drinks/occasion monthly. The control children had slightly higher lead body burdens (pb; ug/dl) than the alcohol-exposed group in this sample. Among the 13 children in the exposed group, three (23.1%) met criteria for fetal alcohol syndrome (FAS) and two (15.4%) for PFAS; eight (61.5%) were heavily exposed but nonsyndromal (HE). As expected, children in the alcohol-exposed group had lower IQ scores than the nonexposed. By contrast, ADHD diagnosis did not differ between the groups.

5.3.2 Behavioural Go/NoGo Data

Overall, subjects were more accurate when executing a Go response than a NoGo response $F(1, 23) = 7.89$, $p < 0.01$. No group differences were seen in terms of accuracy of Go and NoGo responses (Table 5.2); both groups performed well on the task. Response times were significantly longer in the alcohol-exposed group.

Table 5.2: Behavioural data for the control and alcohol-exposed group.

	Heavy-Exposed (% of trials/ms)	Controls (% of trials/ms)	Statistics *t*-tests
Error trials			
Correct Go (%)	97.2 (0.0)	98.1 (0.0)	<1
Correct NoGo (%)	90.5 (0.1)	89.2 (0.1)	<1
Reaction time			
Correct Go (ms)	601.5 (77.1)	533.7 (133.4)	16.29*

* $p<0.0001$

5.3.3 Event-related Potentials

The midline (Fz, Cz, Pz) ERPs for each group under each condition are presented in Figure 5.1, followed by the topographical distribution of the P2, N2 and P3 component amplitudes in Figure 5.2. The ERP component latency and amplitude data are presented in Table 5.3.

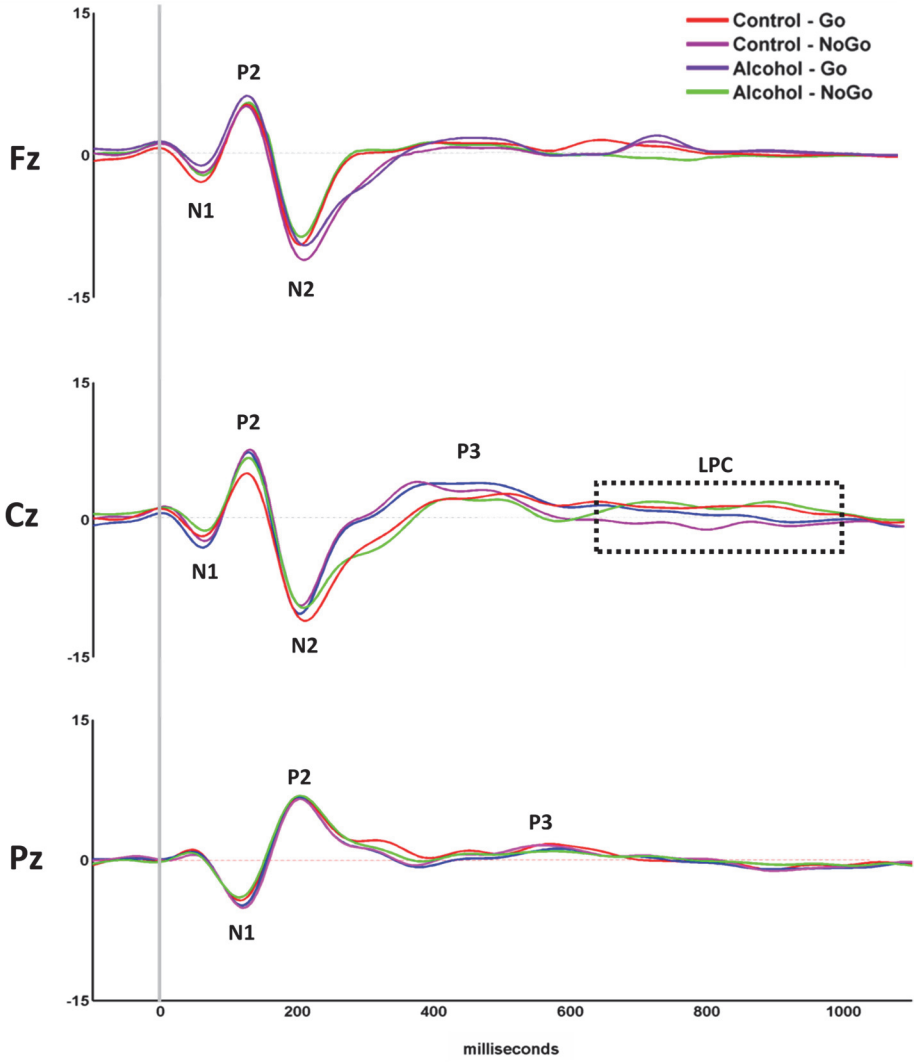

Figure 5.1: Grand average ERPs for each group under each condition along the midline (Frontal-Fz, Central-Cz, Parietal-Pz). Controls Go-condition light blue, controls NoGo-condition purple, alcohol exposed Go-condition green, and alcohol exposed NoGo-condition red. The P1-N1-P2-N2-P3-LPC waveform complex is visible along the mid-line electrodes.

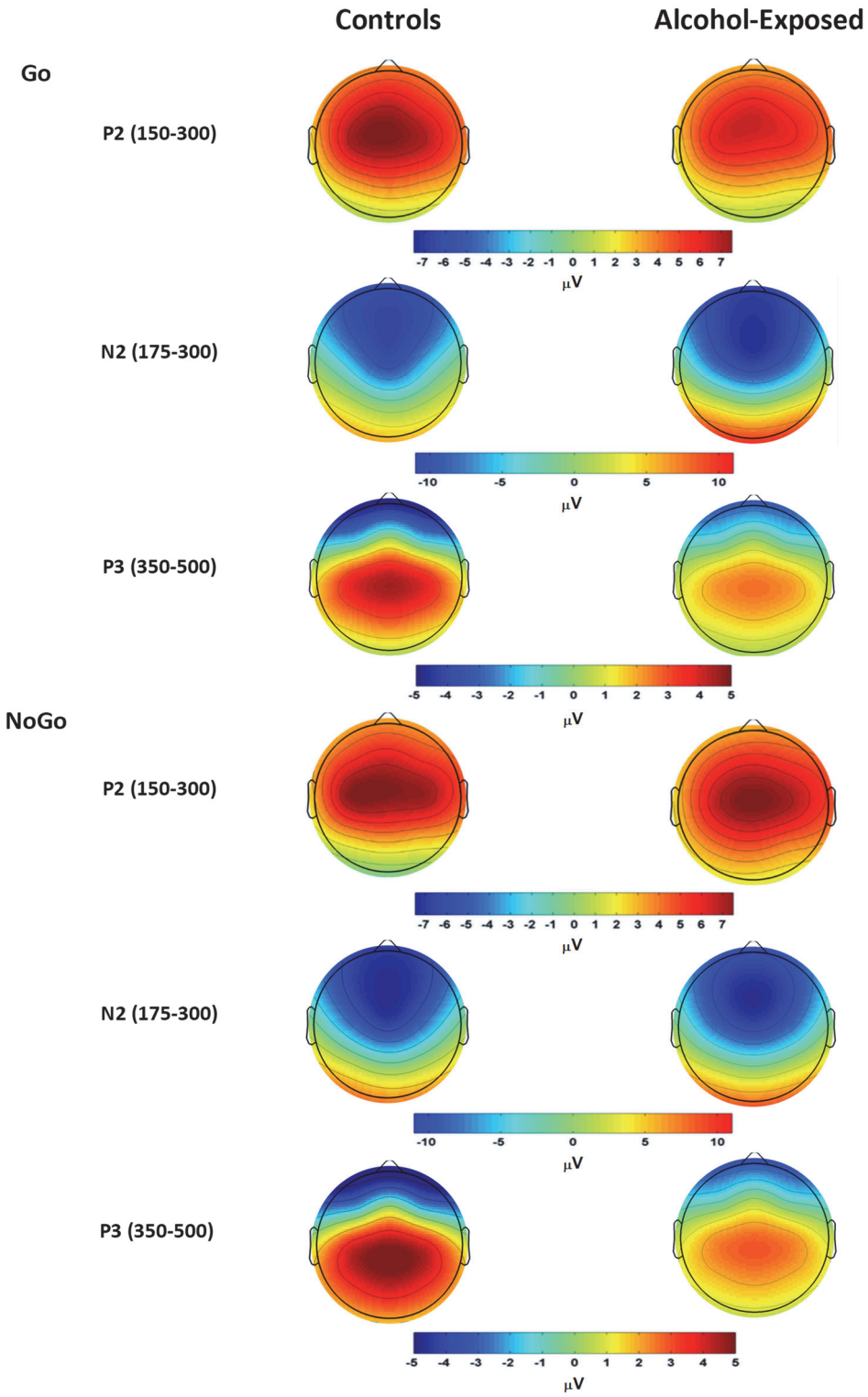

Figure 5.2: Topographical maps illustrating the N2 and the P3 ERP components. Colours on heatmaps represent amplitude changes relative to pre-stimulus baseline; the values are in microvolts (μV).

Table 5.3: ERP quantification: means and standard errors.

		Alcohol-Exposed		Control	
		Go	NoGo	Go	NoGo
P2					
	Latency (ms)	148.0 (12.1)	161.3 (10.5)	150.4 (25.2)	159.5 (13.2)
	Amplitude (uV)	5.1 (3.1)	6.1 (4.0)	7.1(3.2)	7.2(3.5)
N2					
	Latency (ms)	217.8 (23.4)	215.3 (22.5)	208.2 (23.9)	211.1 (18.2)
	Amplitude (uV)	-10.8 (3.4)	-11.8 (2.2)	-9.1 (3.2)	-11.0 (5.2)
P3					
	Latency (ms)	430.5 (30.5)	418.5 (17.8)	387.7 (32.4)	368.1 (13.2)
	Amplitude (uV)	3.0 (3.6)	3.1 (4.2)	4.3 (3.2)	4.8 (4.5)
LPC					
	Amplitude (uV)	2.00 (0.9)	2.2 (0.4)	1.0 (0.8)	0.43 (0.5)

There was a main effect for condition for P2 latency, with longer latencies in the NoGo- than the Go-condition for both groups, $F(1, 23) = 3.86$, $p < 0.05$. There was also a main effect for exposure group, with controls having significantly greater amplitude across both conditions, $F(1, 23) = 4.01$, $p < 0.05$. No significant interaction effects were observed. There was a main effect for exposure group for N2 latency, with the alcohol-exposed children having longer latencies than the controls, $F(1, 23) = 3.99$, $p < 0.05$. There was a significant condition x exposure group interaction for N2 amplitude, $F(1, 23) = 5.12$, $p < 0.05$. In the control group, the N-2 component was of a greater amplitude in the NoGo-condition (M = -11.00, SE = 5.2) compared to the Go-condition (M = -9.08, SE = 3.2, $p < 0.01$). This difference was not seen in for the exposed group: NoGo-condition (M = -11.82, SE = 2.23); the Go-condition (M = -10.75, SE = 3.4). There was also a significant group x condition interaction for P3 latency, $F(1, 23) = 9.86$, $p < 0.01$. In the exposed group, P3 latency was slower in the Go-condition (M = 430, SE = 30.5) than in the NoGo-condition (M = 418, SE = 17.8, $p < 0.01$) but no latency difference was seen in the control group. In addition, there was a signficant group x condition effect for P3 amplitude, $F(1, 23) = 7.16$, $p < 0.01$. In the control group, P3 amplitude was larger

in the Go-condition (M = 4.25, SE = 3.2) than in the No-condition (M = 4.75, SE = 4.5, $p < 0.05$) but no difference was seen in the FASD group. There was a main effect for exposure group for LPC amplitude, $F(1, 23) = 5.98$, $p < 0.05$, with the alcohol-exposed group exhibiting an LPC over the central region in both conditions; this effect was not seen in the control group.

Five ERP measures were affected by maternal alcohol consumption: P2 amplitude, P3 latency, P3 amplitude, N2 latency, and the LPC amplitude. None of the covariates reported in Table 5.1 were related to any of the ERP components at $p < 0.20$.

5.4 Discussion

The children with PAE whose ERP data were examined in this study performed as accurately as the healthy controls, indicating competent performance on this relatively simple auditory Go/NoGo response inhibition task. In contrast to the visual domain, in which no exposure group differences were seen on reaction time (Burden *et al.*, 2009, 2011), reaction time in the auditory domain was significantly slower in the alcohol-exposed compared to the control group. This finding is consistent with previous research showing that infants and children diagnosed with an FASD demonstrate slower processing speed (e.g., Jacobson *et al.*, 1993, 1994; Coles *et al.*, 2002; Burden *et al.*, 2005).

Despite similar performance accuracy on this task, the alcohol-exposed and control groups differed in latencies and amplitudes on several ERP components. As with the visual Go/NoGo paradigm, group differences were seen in early perceptual processing related to stimulus discrimination: lower P2 amplitude in the alcohol-exposed compared to the control group. However, in our study, these differences were seen as a difference across groups and not a group x condition effect—as in Burden *et al.*, 2009—wherein an enhanced P2 was only observed in the control group within the

Go-condition (Go>NoGo). P2 latency was observed as a significant main effect across conditions in this study: NoGo were slower versus Go.

The P2 component is believed to reflect discrimination between stimuli through perceptual facilitation, i.e. differentiating stimuli based on meaning as opposed to the conditions they represent ("X" vs all consonants other than "X" or 1000Hz vs 2000Hz sinusoidal tone). This component may have been affected by functional differences between groups within higher brain regions or by delivery of degraded representations of sensory inputs to higher brain regions in the alcohol-exposed group. Data from animal studies demonstrate dysfunction in auditory and visual pre-cortical pathways that is attributable to ethanol exposure (Church *et al.*, 1996; Pettigrew and Hutchinson, 2008; Rössig *et al.*, 1994; Scher *et al.*, 1998). PAE has also been linked to outer-ear disorders as late as early adulthood (Church and Gerkin, 1988). Using magnetoencephalography (MEG), Stephen *et al.* (2012) reported a functional deficit in younger preschool-aged children with FASD, i.e. a sluggish response from within the primary auditory regions in response to a repetitive tone. Stephen *et al.*'s observations were attributed to changes within peripheral auditory pathways. In our study, no main effect of alcohol-exposure was observed on P2 latency, the first major component downstream from the auditory cortices; the data from animal models of ethanol exposure indicate group differences in early auditory responses decrease as a function of cortical maturation—our participants were older than those of Stephen *et al.* So, while Stephen *et al.* highlight speed of nerve conduction at the periphery as an important biomarker for FASD at younger ages, we argue that these deficits translate, at a later stage of development, into issues around the quality of mental of representations, i.e. the delivery of degraded representations to higher brain regions for perceptual processing. Degraded representations may also account, in part, for the observed slower reaction times, which may be attributable to the increased time needed to execute compensatory top-down processing to aid in perceptual discrimination between simple stimuli.

The P2 differences across modalities may also be attributable to differences in experimental design: the visual task of Burden *et al.* (2009, 2011) had multiple Go stimuli (any consonant other than "X"), while the auditory task used a single tone at a set frequency (1000Hz). Differences in stimulus-response sets maintained in working memory—particularly related to memory load—lead to a different allocation of processing resources during task performance over-and-above modality-specific effects. Top-down mediated effects have been shown to modulate early ERP components in the visual and auditory domains (Alain *et al.*, 2001; Gazzaley et al, 2005). Thus, the effects of top-down modulations arising for stimulus-response set complexity and associated differential allocation of processing resources might also modulate early components, leading to differences in ERP responses across tasks.

In-line with our hypothesis and the finding in the Burden *et al.* (2009) visual Go/NoGo study, N2 amplitude was greater in the NoGo compared to the Go-condition for the control group but not for the alcohol-exposed group. In addition, alcohol-exposed participants showed significantly longer latencies under the NoGo-condition. The N2 effects related to alcohol exposure may reflect compensatory neurophysiological mechanisms—due to reduced cellular populations in key cortical regions—that drive performance in this paradigm, or dysregulation of neurotransmitter systems as demonstrated in some rodent models of response inhibition (Archibald *et al.*, 2001; Eagle and Baunez, 2010; Sowell *et al.*, 2001; 2002).

Alterations in the N2 may also reflect effects of PAE on connectivity among the pre-supplementary motor area (preSMA), anterior cingulate cortex (ACC), dorsolateral prefrontal cortex (DLPFC) and projections into the striatum. The N2 source generators have been shown to be frontally-oriented, both in human studies and animal models. Given that the DLPFC, a key area in decision-making processes, is known to be involved in Go/NoGo performance, the N2 component may reflect decision-making prompted by conflict between the on-line behavioural response (the prepotent motor response) and the demands of the environment (the cue to inhibit). Studies with the

macaca fuscata by Sasaki *et al.* (1989) have demonstrated a functional homologue of the human N2 ERP component, elicited in frontal regions on inhibition of a prepotent motor-response. Electrical stimulation of the area in subsequent testing had the effect of cancelling the pre-potent motor-response, while electrical stimulation of surrounding tissue had the effect of delaying the response. The interaction of the preSMA with frontally-oriented regions is key in conflict monitoring in humans during motor task performance (Chikazoe, 2010; Simmonds, Pekar, and Mostofsky, 2008). Thus, changes in neurophysiological function in frontally-oriented processes may explain the changes in the N2 component observed in the heavy-exposed group.

In contrast to the visual ERP studies, in which both the exposure and control groups exhibited the increased P3 amplitude in the NoGo-condition that is characteristic of normally developing samples, in the auditory task only the alcohol-exposed subjects exhibited longer latency and reduced amplitude of the P3 ERP component. The P3 is elicited in tasks involving working memory and attention allocation, the latter of which is crucial to response inhibition. Kaneko *et al.* (1996) also observed a reduced P3 in an auditory odd-ball paradigm in alcohol-exposed children relative to their Down syndrome group. Thus, contrasting our data with Burden *et al.* (2009) suggests that an alcohol-related deficit in attention allocation may influence response inhibition in the auditory but not in the visual domain—a modality specific effect.

The LPC that was observed in the Burden *et al.* (2009) visual study under the NoGo-condition within the alcohol-exposed group was also observed in the current study. However, it was elicited within the alcohol-exposed group under both the Go- and NoGo-conditions in this auditory study and had a different scalp topography, i.e. midline as opposed to left-hemisphere. Burden *et al.* interpreted the LPC as reflecting an increase in the need for cognitive effort to inhibit against prepotency within the heavy-exposed group. However, that explanation would not account for why the LPC is seen in both the Go- and NoGo-conditions in our auditory ERP task. Instead, we suggest that the increased LPC may be a manifestation of compensatory

neurophysiological function related to resetting of attentional control networks—after a behavioural response—in preparation for the next trial. The only remaining demand placed upon participants later on in the trial is to prepare for the next stimulus; this invariably involves reorientation of attentional resources.

The manifestation of the LPC only under the NoGo-condition during the visual ERP task may be related to the different size stimulus-response sets, which in that task consist of a variable number of Go stimuli. The different stimulus-response sets will place different demands on higher cognitive functioning during task performance, both in terms of memory load and attentional resources. The LPC may be manifest only under the NoGo-condition in the visual task due to increased attentional demands required to differentiate a number of Go stimuli relative to the NoGo cue. Relatively similar attention demands are required in the auditory task across conditions owing to one-on-one stimulus-response-correspondence under each condition, which may account for the elicitation of the LPC in the heavy-exposed group under both conditions.

Attentional control is believed to involve functional integration of frontal and parietal regions including the ACC, DLPFC, and regions around the inferior parietal sulcus (Wang *et al.*, 2010). The ACC is thought to be involved in sudden shifts in attention, while the DLPFC is known to be more involved in slower shifts (Onton *et al.*, 2005). Parietal hypoplasias as well as structural changes in the superior parietal lobules have been reported in FASD (Meintjes *et al.*, 2014; Sowell *et al.*, 2002). In heavily alcohol-exposed subjects, malformations of the orbital extending into the ventrolateral prefrontal regions have been observed (Sowell *et al.*, 2002). Due to morphological changes in cerebral structure, the LPC may reflect changes in functional and anatomical connectivity between the frontal and parietal regions, which is believed to be important in integrating information while attempting to achieve attentional control. If so, compensatory activations in the alcohol-exposed children might well alter the location and orientation of underlying dipole sources within the cerebral

cortex, leading to the manifestation of an unconventional scalp potential in the presence of an FASD. The extended reaction times observed in this study for the alcohol-exposed group under the Go-condition are also consistent with less efficient function in relation to the resetting of attentional networks.

Our ERP findings point to fetal alcohol-related effects in how the brain responds when there is a need to switch away from a prepotent response to an inhibited state. As in all human correlational studies, there are always unmeasured potential confounders. However, the observed effects remained significant after adjustment for the most likely potential confounding variables, including the Hollingshead Scale, which we have found in this and other cohorts from this community to be valid in relation to a large number of maternal and child measures, including maternal (r = 0.47; p = 0.003), and child IQ (r = 0.43, p < 0.001), at levels similar to those found in the U.S. These findings are, for the most part, also consistent across both the visual and auditory domains. Our data indicate fetal alcohol-related deficits in attention processing in response to stimulus onset and resetting of the attentional network in preparation for the next trial as well as impairment of conflict monitoring. It is important to note that these differences in processing were not due to differences in IQ or in ADHD diagnosis. Although the alcohol-exposed and control groups did not differ in behavioural performance on this simple response inhibition task, the differences in neural processing revealed by the ERP analysis point to specific deficits in attentional processing. These deficits are likely to contribute to the poorer performance commonly seen in more complex response-inhibition tasks in children with FASD.

Chapter 6
General Discussion

The aims of this research were to extend previously published PAE related ERP findings from a visual Go/NoGo study into the auditory domain and to investigate scalp-measured induced oscillatory activity during performance of the Go/NoGo task. Regarding the latter aim, the intention was to extend findings from adult samples into a normally-developing sample and to assess to what degree PAE affects the power of these oscillations. We also aimed to demonstrate that alcohol exposure related effects were not explained by other factors known to influence brain development, such as socio-economic conditions, comorbidity, and other teratogens. Across our tasks, equivalent inhibitory control was achieved between the experimental groups; however, group differences on reaction times, errors-of-omission within the visual task, and significant group differences on a number of electrophysiological measures were observed. These differences could not be accounted for by covariates and fixed-effects related to alternative teratogens, socio-economic factors, maternal characteristics, nor comorbid ADHD. We thus demonstrate that PAE affects a number of important component processes required for successful performance on the Go/NoGo response inhibition task.

6.1 Contemplating Prenatal Alcohol Exposure and Response Inhibition

In general, the Go/NoGo task is thought of as a measure of inhibitory-control; however, the task activates a number of component processes that in turn enable response inhibition. Thus, the structure of a single Go/NoGo trial can be decomposed into overlapping segments within which there are specific requirements for different forms of processing: stimulus-encoding, executive functions related to conflict monitoring, cognitive-control and decision-making, as well as motor-system dynamics related to executing and inhibiting an on-line motor program (Alegre *et al.*, 2004, 2006a; Burden *et al.*, 2009; Donkers & van Boxtel, 2004; Ipser, 2011; Mostofsky & Simmonds, 2008). In addition, the Go/NoGo task requires working memory contributions in order to maintain and access the stimulus-response pairings required for task performance. It also requires self-monitoring processes to evaluate performance in real-time to allow for adaptation in the instance of a performance error. Thus, response-inhibition in the context of the Go/NoGo task is a product of an interaction of a number of component processes. The studies presented herein demonstrated that such processes are affected in the instance of heavy PAE.

6.1.1 Implementations of the Go/NoGo Task

The Go/NoGo tasks used in this research were simple, i.e. they were not designed with the intent to challenge either experimental group. As such, the stimuli that represented either condition were distinctive and easy to perceive, there was a large inter-stimulus interval in both tasks, there was only a single stimulus defining the NoGo-condition in either task, the Go-condition required a simple button press with an index finger, and the participants were directly/explicitly cued in each trial, as opposed to more challenging implementations of response inhibition tasks that utilise anticipatory cues prior to signalling movement/inhibition (Kieffaber & Cho, 2010).

Research on executive functions within the FASD population have demonstrated that performance deficits are only observed when tasks become challenging; furthermore, performance deficits on such tasks are only apparent in the most heavy-exposed participants (Aragon, Klaberg, & Buckley, 2008; Burden *et al.*, 2005; Kodituwakku *et al.*, 2001). Thus, equivalent inhibitory control between groups observed in the auditory and visual tasks is expected given the simplicity of the implementations; however, changes in neocortical oscillatory dynamics that are phase-locked to stimulus onset (ERP/evoked power) and non-phase-locked induced power changes provide insight regarding the impact of PAE on component processes that support task performance.

6.1.2 Degraded Sensory Representations

In terms of stimulus processing occurring early on within the experimental trials, Gerhold *et al.*, (2017) demonstrated a significant change in P2 ERP component amplitude owing to PAE. The studies of Burden *et al.*, (2009, 2011) also demonstrated alcohol-related changes on this ERP component. The P2 is tied to early perceptual processes that enable discrimination between stimuli, but not discrimination between conditions which requires additional processing to access stimulus-response pairings stored in working memory. The changes in the P2 ERP component observed across visual and auditory studies indicate alcohol-related changes in early stages of stimulus processing independent of stimulus modality (visual vs auditory). A number of animal models of PAE demonstrate dysfunction in early pre-cortical sensory pathways (Church, Abel, Kaltenbach, & Overbeck, 1996; Pettigrew & Hutchinson, 1984; Scher *et al.*, 1998). At early stages of human development, PAE leads to longer latencies in magnetic field responses within the primary auditory cortex (Stephen *et al.*, 2012). Thus, due to poor encoding on the periphery in the instance of heavy PAE, it is likely that degraded sensory representations are delivered to higher brain regions. The degraded quality of sensory information creates a need for compensatory top-down

processing in order to discriminate between simple cues in the auditory and visual tasks, leading to changes in latency and amplitude of the P2 ERP component.

6.1.3 Impaired Detection of Conflict

We observed a number of ERP components and temporally overlapping induced oscillations occurring after P2 peak latency that were also affected by PAE. Of these features, the frontal-central N2 ERP component was observed in the earliest time-window. Within normally-developing samples, the N2 ERP component is characteristically observed with greater amplitude in the NoGo-condition compared to the Go-condition (Davis *et al.*, 2003; Johnstone *et al.*, 2005). Gerhold *et al.*, (2017) did not observe this effect within the heavy-exposed group, neither did Burden *et al.* (2009). The N2 ERP component has been linked to response inhibition and conflict-monitoring processes (Botvinick *et al.*, 2004). Owing to the early latency of this ERP component, and the fact that it precedes other oscillatory features linked to processes that enable inhibition of a motor response, it is more likely to reflect evaluative aspects of conflict-monitoring rather than actual inhibition. Thus, PAE affects processes related to a detection of conflict between the on-line motor program and inhibitory cues. Due to the simplicity of the tasks, the effect of disordered conflict monitoring was not apparent on the overall measure of inhibitory control.

6.1.4 Faulty Decision-Making and Deficits in Self-Monitoring

Using data from the visual task, we identified a decision-making linked induced frontal beta-ERS within the control group that was observed in a partially overlapping time-window to the N2 ERP component. The beta-ERS was elicited after the start of the N2 detection time-window and persisted for some time after the N2 detection period ended. The frontal beta-ERS was not observed within the heavy-exposed group—we observed a desynchronised hemispheric asymmetry. In addition, a significant association between performance accuracy and beta-power was observed

within the heavy-exposed group, where desynchronised frontal beta-power was associated with performance errors. In the control group, on a single trial basis, spectral power was consistently synchronised, even on error trials. If the beta-ERS was linked to decision-making, we would expect to see the association between beta-power and accuracy in both groups; however, in the control group beta power varied independently of accuracy. We thus proposed that the beta-ERS could be linked to processes running parallel to decision-making, rather than purely reflecting the decision-making process. Given the structure of a Go/NoGo trial, such a process would either be related to a form of self-monitoring and/or working memory processes involved in maintaining or retrieving the stimulus-response sets stored in working memory—although theta oscillations have been linked to working memory function (Onton, Delorme, & Makeig, 2005). As such, we proposed that PAE may lead to changes in self-monitoring processes related to decision-making, i.e. decreased metacognitive awareness or, more specifically, changes in inwardly directed attention levels. This self-monitoring is distinct from the phase-locked error-related negativity elicited on error trials within event-related tasks, as we demonstrated that ERP magnitude and induced power varied independently of each other.

Serotonin is known to be important in decision-making and is linked to reduced performance accuracy in the Go/NoGo task (Eagle *et al.*, 2008; Homberg, 2012). Rodent animal models of PAE have demonstrated underdeveloped serotonergic dependent frontal brain regions and changes to thalamocortical projections that are dependent on serotonin (Zhou *et al.*, 2005). In addition, such models demonstrate that Go/NoGo performance is affected by serotonergic depletion, but not experimental manipulations related to other neurotransmitter systems (Eagle *et al.*, 2008). Thus, heavy PAE can specifically affect circuitry involved in decision-making. Due to the correspondence between the beta-ERS and decision-making processes, either through a one-on-one correspondence, or through a parallel self-monitoring process, our results point to the fact that decision-making dimensions within the Go/NoGo are affected by PAE and

that the errors of heavy-exposed participants are linked to faulty decision-making, or are more likely due to impairment of inwardly directed attention towards the decision-making process.

6.1.5 Cognitive-Control and Dealing with Prepotency

We observed a significant frontal induced gamma-band ERS in the control group within the NoGo-condition. Within the heavy-exposed group, gamma-power was observed at baseline levels in both conditions. The gamma-ERS reached maximal differences between conditions towards the end of the N2 detection window, the maximal difference was reached after the onset of the beta-ERS; gamma power remained synchronised once the beta-ERS returned to baseline levels. This frontal gamma-ERS was previously observed within the Go/NoGo task and on other tasks that require participants to select against prepotency. The oscillatory bout is linked to cognitive-control processes (Kieffaber & Cho, 2010; Shibata *et al.*, 1999). These processes involve the reallocation and reorganisation of processing resources in order to deal with changes in task demands—the demands of having to inhibit a prepotent motor response. In terms of the temporal sequence of component processes that enable performance on the response-inhibition Go/NoGo task, cognitive-control processing follows decision-making. Our feature detection method identified a region of maximal differences between conditions (450ms – 850ms); however, the spectral power synchronised earlier-on within the NoGo trials (< 450ms). Previous research in normally-developed adults has shown that the gamma-ERS occurs even if inhibition is anticipated, thus it is in-line with known behaviours of the component to start to synchronise before a decision to inhibit is made, or even before the cue to inhibit appears if the cue is anticipated (Kieffaber & Cho, 2010).

We observed that the gamma-ERS was not present in the scalp-measured EEG of the heavy-exposed group. In clinical groups with dysfunctional frontal thalamocortical relay circuitry, the gamma-ERS is not observed in conditions that

require high levels of cognitive control and is associated with decreased performance accuracy (Cho *et al.*, 2006; Minzenberg *et al.*, 2010). PAE is associated with deficits on complex measures that require cognitive control, such as the Stroop Task and Wisconsin Card Sorting Task (Burden *et al.*, 2005; Connor *et al.*, 2000; Mattson *et al.*, 1999). There are a number of structural changes within the cerebral cortex, in terms of volume of grey-matter, but also changes in cortical white-matter related to regions and pathways involved in performance on executive-function tasks. Thus, cognitive-control processing is impaired in the heavy-exposed group, although the deficit does not affect overall inhibitory control due to the simplicity of the task.

In addition to the induced gamma-power dynamics, we also observed an increase in evoked theta power across experimental conditions within the control group, but not the FASD group. No group differences within the NoGo condition were observed at the FDR threshold (see Appendix E – Time-Frequency Contrasts by Group); however, relaxing the threshold did reveal a small magnitude effect at 6Hz. Thus, evoked theta followed the same response pattern as gamma, but the magnitude of this effect was smaller. Evoked theta power has been implicated in cognitive control processing, specifically in the detection of conflict (Cavanagh & Frank, 2014). This connection is seen less often in the instance of induced theta power (Cohen & Donner, 2013). As Andrew & Fein (2010a) argue that analysis of evoked power, over-and-above that of group ERP effects, does not offer any additional discriminatory power between groups, we did not enter into a detailed analysis thereof. We do however note that Burden *et al.*'s (2009) ERP results from the visual Go/NoGo experiment were in-line with our gamma findings: cognitive-control, specifically conflict-detection, is impaired in the instance of FASD, as evidenced by N2 ERP component interaction effects.

6.1.6 Alcohol-Related Attention Deficits

The P300 ERP component is linked to attention and working memory (Polich, 2007). In Burden *et al.* (2009), no P300 effects were reported; however, in the auditory ERP

study of Gerhold *et al.* (2017), the heavy-exposed group had reduced amplitude and longer latency P300s. Thus, our data indicates possible modality specific attention related deficits, or even deficits related to retrieval of stimulus-response pairings stored in working memory. We believe that the LPC observed in the Burden *et al.* (2009) and in Gerhold *et al.*, (2017) is related to top-down attention processing. Due to the latency of the late slow wave potential, it is likely to be related to attention allocation in preparation for the next trial; this, in contrast to Burden *et al.*'s (2009) interpretation of "increased cognitive effort". These results point to alcohol-related changes in attention processing later on in the trial that are independent of stimulus modality.

6.1.7 Performance Strategies, Arousal/Motivation, and Reduced Processing Efficiency

In terms of behavioural measures across both the auditory and visual task, both groups achieved equivalent levels of inhibitory control; however, slower reaction times were observed within the heavy-exposed group and more errors-of-omission were made by the controls within the visual task. In terms of reaction times, two factors can contribute to extended reaction times within the Go/NoGo task: (1) conscious choices regarding how to approach task-performance in order to meet the aims of the task (performance strategies); and (2) factors related to the central nervous system's capacity to efficiently process and transmit information—these are factors outside of conscious awareness and control.

In terms of conscious performance strategies, participants could potentially be encoding a "target" letter or tone as a single inhibitory stimulus-response pair, and then simply waiting for the occurrence of the symbol or tone, i.e. a "target-detection" strategy. This would be an especially efficient approach in the visual task where there are multiple Go-condition cues. We would expect participants that select such a strategy to be more accurate in the NoGo-condition, but would be prone to make more

errors-of-omission. They would also likely produce faster reaction times due to more efficient processing that does not require each trial to be allocated equal processing resources, in contrast to a participant that considers each and every symbol/tone without selecting a "target". Our observations within the control group performing the visual task were in-line with these expectations. The Go/NoGo task does not constrain the participant's choice of performance strategy beyond the general demands of the task; thus, different approaches can be utilised to achieve the goals of the task (see Ipser, 2011, Chapter 5). Different performance strategies used by either group may make the task more or less challenging, by reducing cognitive-load and/or reorganising the allocation of processing resources in more or less efficient configurations. In this regard, the relationship between performance and arousal as well as the connection between arousal and motivation are applicable (Broadbent, 1965; Mendl, 1999; Yerkes & Dodson, 1908). The differences in task difficulty experienced by either groups would also have had an impact on metabolite utilisation in neural tissue, as studies point to the fact that different patterns of regional blood flow arise due to different levels of task-related difficulty (Mostofsky & Simmonds, 2008).

In the instance of reduced processing efficiency driving increased reaction times within the heavy-exposed group, the fact that there are structural changes in the cerebral cortex and cerebral white-matter fibre tracts (see Fan *et al.*, 2016), the slower reaction times could not be wholly attributable to conscious factors related to task performance, but rather to less efficient information-processing capacity within the nervous systems of heavy-exposed participants. As lipid is an insulator and enables nerve conduction, decreased myelination of cortical fibre tracts, as suggested by Fan *et al.*, (2016), would lead to less efficient transmission of information via the affected fibre tracts. Decreased efficiency in information processing is observed throughout development in heavy-exposed populations (Burden *et al.*, 2005; Jacobson et al., 1993; Jacobson et al., 1994;).

It is likely that the two factors work in combination to yield slower reaction times within the Go/NoGo task. Without experimental manipulations or related control variables, it is not possible to attribute variability in reaction times to either conscious or central nervous system processing efficiencies.

6.1.8 Spectral Estimator Dependent Outcomes

We found differences in analytical outcomes in the beta and gamma analyses when using either STFT or AIC-AAR spectral estimates. The divergence between the two spectral estimators, despite using the same window length for the sliding window, is related to a number of estimation bias-variance trade-offs. Within finite samples, AIC has a tendency to over-parametrise—select an overly complex model (De Waele, 2003). This over parametrisation brings into effect different estimation bias-variance trade-offs relative to those of the STFT estimates, consequently yielding divergent spectral estimates in the time-frequency domain. In addition, the small sample properties of either estimator also affect estimation bias-variance trade-offs: on a single-trial basis, the STFT estimates are inconsistent, while the AR estimate is consistent but biased. These estimator dependent statistical bias-variance trade-offs lead to different specifications of components in time and frequency owing to the relationship between estimation bias and resolution. Over-and-above these points, the use of Gaussian tapering in the STFT and rectangular windowing in the AAR approach lead to further differences in signal component representations in time and frequency, primarily due to weighting on the leading and trailing edges of the analytical window, that in turn affect overall datum-points available for the spectral estimates within the sliding analytical window. Due to these differences, we observed that spectral power estimates differ enough to affect analytical outcomes. The scalp maps derived using either estimator also provide slightly different spatial representations across the scalp due to the estimation bias-variance trade-offs specific to each method.

6.2 Clinical and Societal Relevance

Evidence points to the fact that specific component processes that enable motor-response inhibition are linked to narrow-band oscillatory phenomena during performance of the Go/NoGo task. This suggests a potential avenue for clinical management of FASD, whereby different forms of transcranial stimulation of the neocortex may prove a viable treatment option (Hsu, Zanto, Schouwenburg, & Gazzaley, 2017, Lefaucher *et al.,* 2014). Transcranial stimulation targeting narrow bands in high-frequencies—beta and gamma—could potentially enhance neocortical response-inhibition processing by targeting sub-component processes, i.e. in terms of stimulating cortical networks that implement subcomponent processes like cognitive-control and decision-making. The efficacy of such an intervention has yet to be explored, but in the future may well provide an avenue to enhance response-inhibition performance, with effects generalising to areas of daily life that depend on such cognitive-capacities, such as academic performance, performance in competitive sports, and occupational achievement.

Translation of alcohol-related findings within the educational context should lead to the formation of teaching styles and methods that work synergistically with impaired executive function, specifically that of compromised attention, cognitive-control and decision-making processes. As such, short informational segments presented on tablets and laptops that communicate key concepts, where the teacher acts as a coach/facilitator instead of being the point of focus, could be utilised in place of classroom-textbook learning; the suggested approach reduces the need for sustained attention and the necessity to inhibit distractors is minimised. The latter is achieved through high energy media content that exploits brightness and colour transitions from scene to scene, that utilises a mixture of sounds—natural speech, natural sound, synthesised sound, and music—to consistently re-engage the learner's neocortical-deep brain systems. There is a growing body of studies that support the feasibility of such an approach (Vecchiato, Cherubino, Trettel, & Babiloni, 2013). In

addition, as has been demonstrated in studies of optimisation of cognitive function, computer games that apply key concepts and recapitulate such concepts at increasing levels of complexity, can be used to re-engage and hold cognitive systems in optimal states for information processing, while optimising cognitive performance on an implicit level during game play (Jyoti, Anguera, & Gazzaley, 2016; Rolle, Anguera, Skiner, Vyotek, & Gazzaley, 2017). Of course, much work would need to be done to explore transfer effects from the classroom into daily-life with in the FASD population, and at later stages of development into measures of occupational achievement.

6.3 Limitations and Future Research

As was pointed out in the visual beta and gamma studies, the sample size for the visual task was relatively small in comparison to the auditory task; however, the effects that the studies sought to replicate were observed using samples of 7 – 10 participants. Thus, the overall power in the induced oscillatory studies in relation to known effect-sizes was fairly high. Our main aims in the studies were to replicate the effects in a normally-developing sample and assess whether PAE affected the power of the scalp-measured oscillatory bouts. In terms of achieving these aims, we had adequate power within our analyses. We extended the previous findings in a normally developing sample: the effects were highly significant and in the hypothesised direction. Our heavy-exposed group in these studies was larger than the control group, so if the oscillatory bouts were elicited in this group, we were more likely to observe them. In both studies, the effects were clearly visible in the control group, but not in the heavy-exposed group.

We were limited in our approach to the auditory data, as the data contained high-frequency artefact. This artefact was not myogenic and neither was it related to electrical lines noise—notch filtering did not reduce its presence in the signals; neither did it display a myogenic spatial topography. In addition, it was present in a fairly broad band within a high-frequency range (> 40Hz). Due to hair-types that challenged

the research assistant during data-acquisition (characteristically African hair types), the conductive bridge between the EGI electrode and the scalp was compromised in many of the auditory recordings. We did assess regional power measures across participants that participated in both the auditory and visual tasks in the lower bands (< 30Hz) and we did not find significant differences across the regions of the scalp; however, in the higher frequencies, the noise did lead to significant differences. This limitation arising from the data-acquisition phase when using the EGI system placed limitations on the extent on which we could analyse the auditory data. The BioSemi system used a conductive gel (as opposed to a saline electrolyte) that yielded a more robust conductive bridge between the participant's scalp and the recording electrodes, and thus provided excellent quality data within the sample, allowing for extensive analysis across a broad frequency band.

Future experimental designs that build on this research should implement a number of important changes:

- The tasks should be implemented with increasing levels of complexity. For example, three levels of complexity could be used, wherein complexity could be operationalised by: decreasing the inter-stimulus intervals within the task, placing constraints on the time for an allowable response, and using multiple inhibitory cues or using anticipatory (implicit) inhibitory cues.

Given the implementation of the above point, behavioural performance metrics (reaction times and error rates), regional oscillatory power measures, as well as ERP magnitudes and latencies can then be assessed for alcohol related effects at increasing levels of complexity. Such a research design is in-line with the FASD literature which points to the fact that deficits are only observed in the FASD population when tasks are challenging, and only in the most heavy-exposed participants.

In-line with the inverted-U hypothesis related to task performance, experimental manipulations related to increasing complexity would lead to changes in task-related arousal; thus:

- there is a need for a measure of autonomic nervous system arousal in order to quantify the arousal/motivation dimension of the task. These changes could be measured using either: respiratory rates, galvanic-skin response, heart-rate variability, or pupillary dilation.

At least one of the above measures should be used as a covariate to control for confounding, or test for mediating effects related to arousal induced changes in behaviour and neocortical oscillatory dynamics. Research has shown that regional metabolite utilisation changes as a function of task difficulty, thus implementing such a control is important for future research.

6.4 Conclusions

This thesis presented the first studies to address the impact of PAE on induced oscillatory activity related to decision-making and cognitive-control during performance on the Go/NoGo task. It is also the first research to extend Go/NoGo beta- and gamma-ERS findings into a normally-developing sample. In addition, the ERP study confirmed that ERP waveform morphology is affected by PAE. While alcohol-related changes in electro-cortical oscillatory dynamics were observed, they did not translate into deficits of inhibitory control owing to the simplicity of the tasks. However, slower reaction times were observed in the heavy exposed group, which are likely to reflect group specific performance strategies as well as less efficient information processing within the central nervous systems of prenatally exposed participants. Overall, the thesis demonstrates that component processes that enable response inhibition during the Go/NoGo task are compromised in the instance of PAE. These alcohol-related effects are independent of socio-economic circumstances,

maternal characteristics, comorbid ADHD, and the effects of other teratogens, such as childhood lead exposure and prenatal cigarette smoke exposure.

Methodologically, the thesis contributes to our understanding of Akaike-parametrisation in the context of adaptive autoregressive spectral estimation. We demonstrated the effect of estimation bias-variance trade-offs on spectral quantities, and how a unique set of trade-offs in the instance of parametric modelling can lead to changes in signal component's specification in time and frequency, owing to the relationship between estimation bias and resolution. The divergence between parametric and non-parametric spectral estimates were prevalent in the condition and group contrasts used for feature identification. Differences across spectral estimators were also apparent in the context of the fixed-effects models used in the gamma and beta studies. As such, we recommend that EEG researchers need to exercise a critical understanding of the statistical properties of the spectral estimation routine(s) used in their research in order to arrive at robust inferences and conclusions.

In closing, PAE can lead to remarkable changes in electro-cortical oscillatory dynamics that may not necessarily manifest as observable deficits on simple tasks. However, given previously published research, we expect that as tasks become more challenging, it is likely that the observed deficits related to component processes that enable Go/NoGo task performance will result in observable performance deficits in heavy-exposed participants.

References

Adams, J., & Weakliem, D. (2011). August B. Hollingshead "Four Factor Index of Social Status": from unpublished paper to citation classic. *Yale Journal of Sociology, 8,* 11-20.

Akaike, H. (1974). A new look at the statistical model identification. *IEEE Transactions on Automatic Control, 19*, 716–723.

Alain, C., Arnott, S. R., & Picton, T. W. (2001). Bottom–up and top–down influences on auditory scene analysis: Evidence from event-related brain potentials. *Journal of Experimental Psychology: Human Perception and Performance, 27*, 1072–1089.

Alegre, M., Gurtubay, I. G., Labarga, A., Iriarte, J., Valencia, M., & Artieda, J. (2004). Frontal and central oscillatory changes related to different aspects of the motor process: a study in Go/NoGo paradigms. *Experimental Brain Research, 159*, 14–22.

Alegre, M., Imirizaldu, L., Valencia, M., Iriarte, J., Arcocha, J., & Artieda, J. (2006a). Alpha and beta changes in cortical oscillatory activity in a Go/NoGo randomly-delayed-response choice reaction time paradigm. *Clinical Neurophysiology, 117*, 16–25.

Alegre, M., Lázaro, D., Valencia, M., Iriarte, J., & Artieda, J. (2006b). Imitating versus non-imitating movements: Differences in frontal electroencephalographic oscillatory activity. *Neuroscience Letters, 398*, 201–205.

Allen, D. P., & MacKinnon, C. D. (2010). Time-frequency analysis of movement-related spectral power in EEG during repetitive movements: a comparison of methods. *Journal of Neuroscience Methods, 186*, 107.

Anderson, C. W., Stolz, E., Shamsunder, S., & others. (1998). Multivariate autoregressive models for classification of spontaneous electroencephalographic signals during mental tasks. *IEEE Transactions on Biomedical Engineering, 45*, 277–286.

Andrew, C., & Fein, G. (2010a). Event-related oscillations versus event-related potentials in a P300 task as biomarkers for alcoholism. *Alcoholism: Clinical and Experimental Research, 34*, 669–680.

Andrew, C., & Fein, G. (2010b). Induced theta oscillations as biomarkers for alcoholism. *Clinical Neurophysiology, 121*, 350–358.

Annett, M. (1970). The growth of manual preference and speed. *British Journal of Psychology, 61*, 545–558.

Archibald, S. L., Fennema-Notestine, C., Gamst, A., Riley, E. P., Mattson, S. N., & Jernigan, T. L. (2001). Brain dysmorphology in individuals with severe prenatal alcohol exposure. *Developmental Medicine and Child Neurology, 43*, 148–154.

Aragon A. S., Kalberg, W. O., Buckley, D. (2008). Neuropsychological study of FASD in a sample of American Indian children: processing simple versus complex information. *Alcoholism: Clinical and Experimental Research*, 32, 2136–2148

Astolfi, L., Cincotti, F., Mattia, D., Marciani, M. G., Baccala, L. A., de Vico Fallani, F., et al. (2007). Comparison of different cortical connectivity estimators for high-resolution EEG recordings. *Human Brain Mapping, 28*, 143–157.

Astolfi, L., Toppi, J., Wood, G., Kober, S., Risetti, M., Macchiusi, L., et al. (2013). Advanced methods for time-varying effective connectivity estimation in memory processes. In B. Wheeler Chairperson (Chair), *35th Annual International Conference of the IEEE Engineering in Medicine and Biology Society (EMBC)* (pp. 2936–2939). Retrieved from http://ieeexplore.ieee.org.ezproxy.uct.ac.za/document/6610155/

Baccalá, L. A., & Sameshima, K. (2001). Partial directed coherence: a new concept in neural structure determination. *Biological Cybernetics, 84*, 463–474.

Bauer, L. O. (2001). CNS recovery from cocaine, cocaine and alcohol, or opioid dependence: a P300 study. *Clinical Neurophysiology, 112*, 1508-1515.

Begleiter, H., Porjesz, B., Bihari, B., & Kissin, B. (1984). Event-related brain potentials in boys at risk for alcoholism. *Science, 225*,1493–1496.

Benikos, N., Johnstone, S. J., & Roodenrys, S. J. (2013). Varying task difficulty in the Go/NoGo task: The effects of inhibitory control, arousal, and perceived effort on ERP components. *International Journal of Psychophysiology, 87*, 262–272.

Benjamini, Y., & Yekutieli, D. (2001). The control of the false discovery rate in multiple testing under dependency. *The Annals of Statistics, 29*, 1165–1188.

Bergmeir, C., & Benítez, J. M. (2012). On the use of cross-validation for time series predictor evaluation. *Information Sciences, 191*, 192–213.

BioSemi [ActiveTwo EEG system]. (2017). Retrieved from https://www.biosemi.com/index.htm

Botvinick, M. M., Braver, T. S., Barch, D. M., Carter, C. S., & Cohen, J. D. (2001). Conflict monitoring and cognitive control. *Psychological Review, 108*, 624–652.

Bowman, R. S., Stein, L. I., & Newton, J. R. (1975). Measurement and interpretation of drinking behavior. I. On measuring patterns of alcohol consumption. II. Relationships between drinking behavior and social adjustment in a sample of problem drinkers. *Journal of Studies on Alcohol, 36*, 1154–1172.

Broadbent, D. E. (1965). A reformulation of the Yerkes-Dodson law. *British Journal of Mathematical and Statistical Psychology, 18*, 145–157.

Brown, J. W. (2013). Beyond conflict monitoring: cognitive control and the neural basis of thinking before you act. *Current Directions in Psychological Science, 22*, 179–185.

Brunner, C., Billinger, M., Seeber, M., Mullen, T. R., & Makeig, S. (2016). Volume Conduction Influences Scalp-Based Connectivity Estimates. *Frontiers in Computational Neuroscience, 10,* 1-4.

Burden, M. J., Jacobson, S. W., & Jacobson, J. L. (2005). Relation of prenatal alcohol exposure to cognitive processing speed and efficiency in childhood. *Alcoholism: Clinical and Experimental Research, 29*, 1473–1483.

Burden, M. J., Andrew, C., Saint-Amour, D., Meintjes, E. M., Molteno, C. D., Hoyme, H. E., et al. (2009). The effects of fetal alcohol syndrome on response execution and inhibition: an event-related potential study. *Alcoholism: Clinical and Experimental Research, 33*, 1994–2004.

Burden, M. J., Westerlund, A., Muckle, G., Dodge, N., Dewailly, E., Nelson, C. A., et al. (2011). The effects of maternal binge drinking during pregnancy on neural correlates of response inhibition and memory in childhood. *Alcoholism: Clinical and Experimental Research, 35*, 69–82.

Cavanagh, J. F. & Frank, M. J. (2014). Frontal theta as a mechanism for cognitive control. Trends in cognitive sciences, 18, 414-421.

Cecil, K. M., Brubaker, C. J., Adler, C. M., Dietrich, K. N., Altaye, M., Egelhoff, J. C., et al. (2008). Decreased brain volume in adults with childhood lead exposure. *PLoS Medicine, 5*, 741-750.

Cheung, B. L. P., Riedner, B., Tononi, G., & Van Veen, B. D. (2010). Estimation of cortical connectivity from EEG using state-space models. *IEEE Transactions on Biomedical engineering, 57*, 2122–2134.

Chikazoe, J. (2010). Localizing performance of Go/NoGo tasks to prefrontal cortical subregions. *Current Opinion in Psychiatry, 23*, 267–272.

Cho, R. Y., Konecky, R. O., & Carter, C. S. (2006). Impairments in frontal cortical gamma synchrony and cognitive control in schizophrenia. *Proceedings of the National Academy of Sciences of the United States of America, 103*, 19878–19883.

Chudley, A. E., Conry, J., Cook, J. L., Loock, C., Rosales, T., LeBlanc, N., & Public Health Agency of Canada's National Advisory Committee on Fetal Alcohol Spectrum Disorder. (2005). Fetal alcohol spectrum disorder: Canadian guidelines for diagnosis. *Canadian Medical Association Journal, 172*, 1–21.

Church, M. W., & Gerkin, K. P. (1988). Hearing disorders in children with fetal alcohol syndrome: Findings from case reports. *Paediatrics, 82*, 147-154.

Church, M. W., Abel, E. L., Kaltenbach, J. A., & Overbeck, G. W. (1996). Effects of prenatal alcohol exposure and aging on auditory function in the rat: Preliminary results. *Alcoholism: Clinical and Experimental Research, 20*, 172-179.

Cohen, M. X. (2014). *Analyzing Neural Time Series Data: Theory and Practice*. Cambridge: The MIT Press.

Cohen, M. X., & Donner, T. H. (2013). Midfrontal conflict-related theta-band power reflects neural oscillations that predict behaviour. Journal of Neurophysiology, 110, 2752-2763.

Coles, C. D., Platzman, K. A., Lynch, M. E., & Freides, D. (2002). Auditory and visual sustained attention in adolescents prenatally exposed to alcohol. *Alcoholism: Clinical and Experimental Research, 26*, 263-271.

Connor, P. D., Sampson, P. D., Bookstein, F. L., Barr, H. M., & Streissguth, A. P. (2000). Direct and indirect effects of prenatal alcohol damage on executive function. *Developmental Neuropsychology, 18*, 331–354.

Costa, A. H., & Hengstler, S. (2011). Adaptive time–frequency analysis based on autoregressive modelling. *Signal Processing, 91*, 740–749.

Crocker, N., Vaurio, L., Riley, E. P., & Mattson, S. N. (2011). Comparison of verbal learning and memory in children with heavy prenatal alcohol exposure or attention-deficit/hyperactivity disorder. *Alcoholism: Clinical and Experimental Research, 35*, 1114–1121.

Davis, E. P., Bruce, J., Snyder, K., & Nelson, C. A. (2003). The X-trials: neural correlates of an inhibitory control task in children and adults. *Journal of Cognitive Neuroscience, 15*, 432–443.

De Guio, F., Mangin, J.-F., Rivière, D., Perrot, M., Molteno, C. D., Jacobson, S. W., et al. (2014). A study of cortical morphology in children with fetal alcohol spectrum disorders. *Human Brain Mapping, 35*, 2285–2296.

De Waele, S. (2003). Automatic inference form finite time observation of stationary stochastic signals (Doctoral dissertation). Retrieved from http://www.dcsc.tudelft.nl/Research/PhDtheses/index.html

Delorme, A., & Makeig, S. (2004). EEGLAB: an open source toolbox for analysis of single-trial EEG dynamics including independent component analysis. *Journal of Neuroscience Methods, 134*, 9–21.

Delorme, A., Mullen, T., Kothe, C., Akalin Acar, Z., Bigdely-Shamlo, N., Vankov, A., et al. (2011). EEGLAB, SIFT, NFT, BCILAB, and ERICA: new tools for advanced EEG processing. *Computational Intelligence and Neuroscience, 2011*, 1-12.

Dentico, D., Cheung, B. L., Chang, J.-Y., Guokas, J., Boly, M., Tononi, G., & Van Veen, B. (2014). Reversal of cortical information flow during visual imagery as compared to visual perception. *NeuroImage, 100*, 237–243.

Diwadkar, V., Meintjes, E. M., Goradia, D., Dodge, N. C., Molteno, C. D., Jacobson, S. W., & Jacobson, J. L. (2013). Differences in cortico-striatal-cerebellar activations during working memory in syndromal and non-syndromal children with prenatal alcohol exposure. *Human Brain Mapping, 34*, 1931-1945.

Donkers, F. C. L., & van Boxtel, G. J. M. (2004). The N2 in Go/NoGo tasks reflects conflict monitoring not response inhibition. *Brain and Cognition, 56*, 165–176.

Durka, P. J., Zygierewicz, J., Klekowicz, H., Ginter, J., & Blinowska, K. J. (2004). On the statistical significance of event-related EEG desynchronization and

synchronization in the time-frequency plane. *IEEE Transactions on Biomedical Engineering, 51*, 1167–1175.

Eagle, D. M., Bari, A., & Robbins, T. W. (2008). The neuropsychopharmacology of action inhibition: cross-species translation of the stop-signal and Go/NoGo tasks. *Psychopharmacology, 199*, 439–456.

Eagle, D. M., & Baunez, C. (2010). Is there an inhibitory-response-control system in the rat? Evidence from anatomical and pharmacological studies of behavioral inhibition. *Neuroscience & Biobehavioral Reviews, 34*, 50–72.

Efron, B., & Tibshirani, R. (1986). Bootstrap methods for standard errors, confidence intervals, and other measures of statistical accuracy. *Statistical Science, 1*, 54–75.

Engel, A. K., & Fries, P. (2010). Beta-band oscillations—signalling the status quo? *Current Opinion in Neurobiology, 20*, 156–165.

Hoyme, H. E., May, P. A., Kalberg, W. O., Kodituwakku, P., Phillip Gossage, J., Trujillo, P. M., et al. (2005). A practical clinical approach to diagnosis of fetal alcohol spectrum disorders: clarification of the 1996 institute of medicine criteria. *Pediatrics, 115*, 39–47.

EGI System 200 Technical Manual [Electronic version]. (2001). USA: Electrical Geodesics Inc.

Fan, J., Byrne, J., Worden, M. S., Guise, K. G., McCandliss, B. D., Fossella, J., & Posner, M. I. (2007). The relation of brain oscillations to attentional networks. *The Journal of Neuroscience, 27*, 6197–6206.

Fan, J., Jacobson, S. W., Taylor, P. A., Molteno, C. D., Dodge, N. C., Stanton, M. E., et al. (2016). White matter deficits mediate effects of prenatal alcohol exposure on cognitive development in childhood. *Human Brain Mapping, 37*, 2943–2958.

Florian, G., & Pfurtscheller, G. (1995). Dynamic spectral analysis of event-related EEG data. *Electroencephalography and Clinical Neurophysiology, 95*, 393–396.

Fryer, S. L., Mattson, S. N., Jernigan, T. L., Archibald, S. L., Jones, K. L., & Riley, E. P. (2012). Caudate volume predicts neurocognitive performance in youth with heavy prenatal alcohol exposure. *Alcoholism: Clinical and Experimental Research, 36*, 1932–1941.

Gabor, D. (1946). Theory of communication. Part 1: the analysis of information. *Journal of the Institution of Electrical Engineers - Part III: Radio and Communication Engineering, 93*, 429–441.

Gazzaley, A., Cooney, J. W., McEvoy, K., Knight, R. T., & D'Esposito, M. (2005). Top-down enhancement and suppression of the magnitude and speed of neural activity. *Journal of Cognitive Neuroscience, 17*, 507–517.

Gerhold, M. M., Jacobson, S. W., Jacobson, J. L., Molteno, C. D., Meintjes, E. M., & Andrew, C. M. (2017). An ERP study of response inhibition in the auditory domain in children with fetal alcohol spectrum disorders. *Alcoholism: Clinical and Experimental Research, 41*, 96–106.

Glavinovic, M. I., Gooria, P., Aristizabal, F., & Taghirad, H. (2008). Parametric spectral analysis of nonstationary fluctuations of excitatory synaptic currents. *Biological Cybernetics, 98*, 145–169.

Gohlke, J. M., Griffith, W. C., & Faustman, E. M. (2008). Computational models of ethanol-induced neurodevelopmental toxicity across species: Implications for risk assessment. *Developmental and Reproductive Toxicology, 83*, 1–11.

Gross, J., Kujala, J., Hamalainen, M., Timmermann, L., Schnitzler, A., & Salmelin, R. (2001). Dynamic imaging of coherent sources: Studying neural interactions in the human brain. *Proceedings of the National Academy of Sciences of the United States of America, 98*, 694–699.

Handy, T. (2004). *Event-related potentials: a methods handbook*. Cambridge: A Bradford Book.

Hastie, T., Tibshirani, R., & Friedman, J. H. (2009). *The elements of statistical learning data mining, inference, and prediction*. New York: Springer.

Haykin, S. S. (1996). *Adaptive filter theory*. New Jersey: Prentice Hall.

Hoaglin, D. C., Iglewicz, B., & Tukey, J. W. (1986). Performance of some resistant rules for outlier labeling. *Journal of the American Statistical Association, 81*, 991–999.

Hoaglin, D. C., & Iglewicz, B. (1987). Fine-tuning some resistant rules for outlier labeling. *Journal of the American Statistical Association, 82*, 1147–1149.

Hollingshead, A. B. (1975). *Four Factor Index of Social Status*. Retrieved from http://ubir.buffalo.edu/xmlui/handle/10477/1879

Hollingshead, A. B. (2011). Four factor index of social status. *Yale Journal of Sociology, 8*, 21-51.

Holm, S. (1979). A simple sequentially rejective multiple test procedure. *Scandinavian Journal of Statistics, 6*, 65–70.

Homberg, J. R. (2012). Serotonin and decision making processes. *Neuroscience & Biobehavioral Reviews, 36*, 218–236.

Hoyme H.E., May P.A., Kalberg W.O., Kodituwakku P., Gossage J.G., Trujillo P.M., Buckley D.G., Miller J.H., Aragon A.S., Khaole N., Viljoen D.L., JonesK.L., Robinson L.K. (2005). A practical clinical approach to diagnosis of fetal alcohol spectrum disorders: clarification of the 1996 Institute of Medicine criteria. *Pediatrics, 115*, 39-47.

Hsu, W-Y., Zanto, T. P., Schouwenburg, M. R., & Gazzaley, A. (2017). Enhancement of multitasking performance and neural oscillations by transcranial alternating current stimulation. PLOS ONE, 12, e0178579.

Hu, L., Xiao, P., Zhang, Z. G., Mouraux, A., & Iannetti, G. D. (2014). Single-trial time–frequency analysis of electrocortical signals: Baseline correction and beyond. *NeuroImage, 84*, 876–887.

IBM [SPSS 24]. (2017). Retrieved from http://www-03.ibm.com/software/products/en/spss-statistics

IBM SPSS, Technote. (2016, September 7). Final Hessian matrix not positive definite or failure to converge warning. Retrieved from http://www-01.ibm.com/support/docview.wss?uid=swg21480810

Ikeda, A., Lüders, H. O., Collura, T. F., Burgess, R. C., Morris, H. H., Hamano, T., & Shibasaki, H. (1996). Subdural potentials at orbitofrontal and mesial prefrontal areas accompanying anticipation and decision making in humans: a comparison

with Bereitschaftspotential. *Electroencephalography and Clinical Neurophysiology, 98*, 206–212.

Ipser, J. (2011). *The relationship between impulsivity, affect and a history of psychological adversity: a cognitive-affective neuroscience approach* (Doctoral dissertation). Retrieved from https://open.uct.ac.za/handle/11427/11554

Jacobson, S. W., Jacobson, J. L., Sokol, R. J., Martier, S. S., & Ager, J. W. (1993). Prenatal alcohol exposure and infant information processing ability. *Child Development, 64*, 1706-1721.

Jacobson, S. W., & Jacobson, J. L., & Sokol, R. J. (1994). Effects of fetal alcohol exposure on infant reaction time. *Alcoholism: Clinical and Experimental Research, 18*, 1125-1132.

Jacobson, S. W., Chiodo, L. M., Sokol, R. J., & Jacobson, J. L. (2002). Validity of maternal report of prenatal alcohol, cocaine, and smoking in relation to neurobehavioral outcome. *Pediatrics, 109*, 815–825.

Jacobson, S. W., Stanton, M. E., Molteno, C. D., Burden, M. J., Fuller, D. S., Hoyme, H. E., et al. (2008). Impaired eyeblink conditioning in children with fetal alcohol syndrome. *Alcoholism: Clinical and Experimental Research, 32*, 365–372.

Jacobson, S. W., Stanton, M. E., Dodge, N. C., Pienaar, M., Fuller, D. S., Molteno, C. D., et al. (2011). Impaired delay and trace eyeblink conditioning in school-age children with fetal alcohol syndrome. *Alcoholism: Clinical and Experimental Research, 35*, 250–264.

Johnstone, S. J., Pleffer, C. B., Barry, R. J., Clarke, A. R., & Smith, J. L. (2005). Development of inhibitory processing during the Go/NoGo Task: a behavioral and

event-related potential study of children and adults. *Journal of Psychophysiology, 19*, 11–23.

Jones, K. L., & Smith, D. W. (1973). Recognition of the fetal alcohol syndrome in early infancy. *Lancet, 302*, 999–1001.

Jurcak, V., Tsuzuki, D., & Dan, I. (2007). 10/20, 10/10, and 10/5 systems revisited: their validity as relative head-surface-based positioning systems. *NeuroImage, 34*, 1600–1611.

Jyoti, M., Anguera, J. A., & Gazzaley, A. (2016). Video Games for Neuro-Cognitive Optimization. Neuron, 90, 214-218.

Kaneko, W. M., Ehlers, C. L., Philips, E. L., & Riley, E. P. (1996). Auditory event-related potentials in fetal alcohol syndrome and Down's syndrome children. *Alcoholism: Clinical and Experimental Research, 2*, 35–42.

Kaplan, A. Y., Fingelkurts, A. A., Fingelkurts, A. A., Borisov, S. V., & Darkhovsky, B. S. (2005). Nonstationary nature of the brain activity as revealed by EEG/MEG: Methodological, practical and conceptual challenges. *Signal Processing, 85*, 2190–2212.

Karch, S., Segmiller, F., Hantschk, I., Cerovecki, A., Opgen-Rhein, M., Hock, B., et al. (2012). Increased gamma oscillations during voluntary selection processes in adult patients with attention deficit/hyperactivity disorder. *Journal of Psychiatric Research, 46*, 1515–1523.

Keirn, Z., Aunon, J. I., & others. (1990). A new mode of communication between man and his surroundings. *IEEE Transactions on Biomedical Engineering, 37*, 1209–1214.

Kiebel, S. J., Tallon-Baudry, C., & Friston, K. J. (2005). Parametric analysis of oscillatory activity as measured with EEG/MEG. *Human Brain Mapping, 26*, 170–177.

Kieffaber, P. D., & Cho, R. Y. (2010). Induced cortical gamma-band oscillations reflect cognitive control elicited by implicit probability cues in the preparing-to-overcome-prepotency (POP) task. *Cognitive, Affective & Behavioural Neuroscience, 10*, 431–440.

Kirmizi-Alsan, E., Bayraktaroglu, Z., Gurvit, H., Keskin, Y. H., Emre, M., & Demiralp, T. (2006). Comparative analysis of event-related potentials during Go/NoGo and CPT: Decomposition of electrophysiological markers of response inhibition and sustained attention. *Brain Research, 1104*, 114–128.

Klimesch, W. (1999). EEG alpha and theta oscillations reflect cognitive and memory performance: a review and analysis. Brain Research. *Brain Research Reviews, 29*, 169–195.

Klimesch, W. (2012). Alpha-band oscillations, attention, and controlled access to stored information. *Trends in Cognitive Sciences, 16*, 606–617.

Klimesch, W., Sauseng, P., & Hanslmayr, S. (2007). EEG alpha oscillations: the inhibition-timing hypothesis. *Brain Research Reviews, 53*, 63–88.

Kodali, V. N., Jacobson, J. L., Lindinger, N. M., Dodge, N. C., Molteno, C. D., Meintjes, E. M., & Jacobson, S. W. (2017). Differential recruitment of brain regions during response inhibition in children prenatally exposed to alcohol. *Alcoholism: Clinical and Experimental Research, 41*, 334–344.

Kodituwakku, P. W. (2009). Neurocognitive profile in children with fetal alcohol spectrum disorders. *Developmental disabilities research reviews, 15*, 218–224.

Kodituwakku, P. W., Handmaker, N. S., Cutler, S. K., Weathersby, E. K., & Handmaker, S. D. (1995). Specific impairments in self-regulation in children exposed to alcohol prenatally. *Alcoholism: Clinical and Experimental Research, 19*, 1558–1564.

Lefaucher, J-P., Andre-Obadia, N., Antal, A., Ayache, S. S. Baeken, C., & Benninger, D. H., et al. (2014). Evidence-based guidelines on the therapeutic use of repetitive transcranial magnetic stimulation (rTMS). Clinical Neurophysiology, 125, 2150-2206.

Lezak, M. D. (2004). *Neuropsychological assessment*. New York: Oxford University Press.

Liddle, P. F., Kiehl, K. A., & Smith, A. M. (2001). Event-related fMRI study of response inhibition. *Human Brain Mapping, 12*, 100–109.

Luck, S. J. (2012). *The oxford handbook of event-related potential components*. New York: Oxford University Press.

Makeig, S., Debener, S., Onton, J., & Delorme, A. (2004). Mining event-related brain dynamics. *Trends in Cognitive Sciences, 8*, 204–210.

Marple, S. L. (1986). *Digital spectral analysis: with applications*. New Jersey: Prentice Hall.

The MathWorks, Inc. [MATLAB]. (2015). Retrieved from https://www.mathworks.com/products/matlab.html

The MathWorks, Inc. [Parallel Computing Toolbox]. (2015). Retrieved from https://www.mathworks.com/products/matlab.html

The MathWorks, Inc. [Statistics Toolbox]. (2015). Retrieved from https://www.mathworks.com/products/matlab.html

Mattson, S. N., & Riley, E. P. (1998). A review of the neurobehavioral deficits in children with fetal alcohol syndrome or prenatal exposure to alcohol. *Alcoholism: Clinical and Experimental Research, 22*, 279–294.

Mattson, S. N., Goodman, A. M., Caine, C., Delis, D. C., & Riley, E. P. (1999). Executive functioning in children with heavy prenatal alcohol exposure. *Alcoholism: Clinical and Experimental Research, 23*, 1808–1815.

May, P. A., Gossage, J. P., Marais, A. S., Adnams, C. M., Hoyme, H. E., Jones, K. L., Robinson, L. K., Khaole, N. C. O., Snell, C., Kalberg, W. O., Hendricks, L., Brooke, L., Stellavato, C., & Viljoen, D. (2007). The epidemiology of fetal alcohol syndrome and partial FAS in a South African community. *Drug and Alcohol Dependency, 88*, 259-271.

May, P. A., Blankenship, J., Marais, A. S., Gossage, J. P., Kalberg, W. O., Barnard, R., De Vries, M., Robinson, L. K., Adnams, C. M., Buckley, D., Manning, M., Jones, K. L., Parry, C., Hoyme, H. E., & Seedat, S. (2013). Approaching the prevalence of the full spectrum of fetal alcohol spectrum disorders in a South African population-based study. *Alcoholism: Clinical and Experimental Research, 37*, 818-830.

McLeod, A. I., & Li, W. K. (1983). Diagnostic checking ARMA time series models using squared-residual autocorrelations. *Journal of Time Series Analysis, 4*, 269–27.

Meintjes, E. M., Jacobson, J. L., Molteno, C. D., Gatenby, J. C., Warton, C., Cannistraci, C. J., et al. (2010). An FMRI study of number processing in children with fetal alcohol syndrome. *Alcoholism: Clinical and Experimental Research, 34*, 1450–1464.

Meintjes, E. M., Narr, K. L., van der Kouwe, A. J. W., Molteno, C. D., Pirnia, T., Gutman, B., Woods, R. P., Thompson, P. M., Jacobson, J. L., & Jacobson, S. W. (2014). A tensor-based morphometry analysis of regional differences in brain volume in relation to prenatal alcohol exposure. *NeuroImage: Clinical, 5*, 152-160.

Mendl, M. (1999). Performing under pressure: stress and cognitive function. *Applied Animal Behaviour Science, 65*, 221–244.

Mima, T., Simpkins, N., Oluwatimilehin, T., & Hallett, M. (1999). Force level modulates human cortical oscillatory activities. *Neuroscience Letters, 275*, 77–80.

Minzenberg, M. J., Firl, A. J., Yoon, J. H., Gomes, G. C., Reinking, C., & Carter, C. S. (2010). Gamma oscillatory power is impaired during cognitive control Independent of medication status in first-episode schizophrenia. *Neuropsychopharmacology, 35*, 2590–2599.

Mostofsky, S. H., & Simmonds, D. J. (2008). Response inhibition and response selection: two sides of the same coin. *Journal of Cognitive Neuroscience, 20*, 751–761.

Mullen, T. R. (2014). *The dynamic brain: modelling neural dynamics and interactions from human electrophysiological recordings* (Doctoral dissertation). Retrieved from http://gradworks.umi.com/36/39/3639187.html

Mullen, T., Delorme, A., Kothe, C., & Makeig, S. (2010). An electrophysiological information flow toolbox for EEGLAB. *Biological Cybernetics, 83*, 35–45.

Nunez, P. L., & Srinivasan, R. (2005). *Electric fields of the brain: the neurophysics of EEG*. New York: Oxford University Press.

Okazaki, M., Kaneko, Y., Yumoto, M., & Arima, K. (2008). Perceptual change in response to a bi-stable picture increases neuromagnetic beta-band activities. *Neuroscience Research, 61*, 319–328.

Omlor, W., Patino, L., Hepp-Reymond, M.-C., & Kristeva, R. (2007). Gamma-range corticomuscular coherence during dynamic force output. *NeuroImage, 34*, 1191–1198.

Onton, J., Delorme, A., & Makeig, S. (2005). Frontal midline EEG dynamics during working memory. *NeuroImage, 27*, 341–356.

Oostenveld, R., Fries, P., Maris, E., Schoffelen, J.-M., Oostenveld, R., Fries, P., et al. (2010). FieldTrip: Open source software for advanced analysis of MEG, EEG, and invasive electrophysiological data. *Computational Intelligence and Neuroscience*, e156869.

Oppenheim, A. V., & Schafer, R. W. (2009). *Discrete-time signal processing*. Upper Saddle River: Prentice Hall.

Pardey, J., Roberts, S., & Tarassenko, L. (1996). A review of parametric modelling techniques for EEG analysis. *Medical Engineering and Physics, 18*, 2–11.

Pelham, W. E., Evans, S. W., Gnagy, E. M., & Greenslade, K. E. (1992). Teacher ratings of DSM–III–R symptoms for the disruptive behaviour disorders: prevalence, factor analyses, and conditional probabilities in a special education sample. *School Psychology Review, 21* ,285–299.

Pettigrew, A. G., & Hutchinson, J. (2008). Effects of alcohol on functional development of the auditory pathway in the brainstem of infants and chick embryos. *Ciba Foundation Symposium, 105*, 26-46.

Pfefferbaum, A., Ford, J. M., Weller, B. J., & Kopell, B. S. (1985). ERPs to response production and inhibition. *Electroencephalography and Clinical Neurophysiology, 60*, 423–434.

Pfurtscheller, G. (1981). Central beta rhythm during sensorimotor activities in man. *Electroencephalography and Clinical Neurophysiology, 51*, 253–264.

Pfurtscheller, G. (1992). Event-related synchronization (ERS): an electrophysiological correlate of cortical areas at rest. *Electroencephalography and Clinical Neurophysiology, 83*, 62–69.

Pfurtscheller, G. (2006). The cortical activation model (CAM). In C. N. and W. Klimesch (Ed.), *Progress in Brain Research* (Vol. 159, pp. 19–27). Retrieved from http://www.sciencedirect.com/science/article/pii/S0079612306590028

Pfurtscheller, G., & Neuper, C. (1994). Event-related synchronization of mu rhythm in the EEG over the cortical hand area in man. *Neuroscience Letters, 174*, 93–96.

Pfurtscheller, G., Stancák, A., & Neuper, C. (1996). Post-movement beta synchronization. A correlate of an idling motor area? *Electroencephalography and Clinical Neurophysiology, 98*, 281–293.

Pfurtscheller, G., Neuper, C., Andrew, C., & Edlinger, G. (1997). Foot and hand area mu rhythms. *International Journal of Psychophysiology, 26*, 121–135.

Pfurtscheller, G., & Lopes da Silva, F. L. (1999). Event-related EEG/MEG synchronization and desynchronization: basic principles. *Clinical Neurophysiology, 110*, 1842–1857.

Pfurtscheller, G., Neuper, C., & Krausz, G. (2000). Functional dissociation of lower and upper frequency mu rhythms in relation to voluntary limb movement. *Clinical Neurophysiology, 111*, 1873–1879.

Polich, J. (2007). Updating P300: An integrative theory of P3a and P3b. *Clinical Neurophysiology, 118*, 2128–2148.

Popova, S., Lange, S., Probst, C., Gmel, G., & Rehm, J. (2017). Estimation of national, regional, and global prevalence of alcohol use during pregnancy and fetal alcohol syndrome: a systematic review and meta-analysis. *The Lancet Global Health, 5*, 290-299.

Priestley, M. B. (1981). *Spectral analysis and time series: multivariate series, prediction and control*. Cambridge: Academic Press.

Principe, J. C., & Brockmeier, A. J. (2015). Representing and decomposing neural potential signals. *Current Opinion in Neurobiology, 31*, 13–17.

Psychology Software Tools, Inc. [E-Prime 2.0]. (2012). Retrieved from http://www.pstnet.com

Ridley, J. (1935). Studies of interference in serial verbal reactions. *Journal of Experimental Psychology, 18*, 643–662.

Rolle, C., Anguera, J. A., Skinner, S. N., Voytek, B., & Gazzaley, A. (2017). Enhancing Spatial Attention and Working Memory in Younger and Older Adults. Journal of Cognitive Neuroscience, 29, 1483-1497.

Roskies, A. L. (1999). The binding problem. *Neuron, 24*, 7–9, 111–125.

Rössig, C., Wässer, S., & Oppermann, P. (1994). Audiologic manifestations in fetal alcohol syndrome assessed by brainstem auditory-evoked potentials. *Neuropaediatrics, 25*, 245-249.

Sanei, S., & Chambers, J. A. (2007). *EEG signal processing*. New Jersey: John Wiley & Sons.

Sasaki, K., Gemba, H., & Tsujimoto, T. (1989). Suppression of visually initiated hand movement by stimulation of the prefrontal cortex in the monkey. *Brain Research, 495*, 100–107.

Sattler. (1992). Assessment of Children: WISC-III and WPPSI-R Supplement. Barnes & Noble. http://www.barnesandnoble.com/w/assessment-of-children-jerome-m-sattler/1101

Scher, M. S., Richardson, G. A., Robles, N., Geva, D., Goldschmidt, L., Dahl, R. E., & Sclabassi, R. J., et al. (1998). Effects of prenatal substance exposure: altered maturation of visual evoked potentials. *Paediatric Neurology, 18*, 236-243.

Schlögl, A. (2006). A comparison of multivariate autoregressive estimators. *Signal Processing, 86*, 2426–2429.

Schlögl, A., Flotzinger, D., & Pfurtscheller, G. (1997). Adaptive autoregressive modeling used for single-trial EEG classification. *Biomedical Engineering, 42*, 162–167.

Schlögl, A., & Supp, G. (2006). Analyzing event-related EEG data with multivariate autoregressive parameters. In Christa Neuper and Wolfgang Klimesch (Ed.), Progress in Brain Research (Vol. 159, pp. 135–147). Retrieved from http://www.sciencedirect.com/science/article/pii/S0079612306590090

Schomer, D. L., & Lopes da Silva, F. L. (2012). *Niedermeyer's electroencephalography: basic principles, clinical applications, and related fields*. Philadelphia: Lippincott Williams & Wilkins.

Schwarz, G. (1978). Estimating the dimension of a model. *The Annals of Statistics, 6*, 461–464.

Shibata, T., Shimoyama, I., Ito, T., Abla, D., Iwasa, H., Koseki, K., et al. (1999). Event-related dynamics of the gamma-band oscillation in the human brain: information processing during a GO/NOGO hand movement task. *Neuroscience Research, 33*, 215–222.

Simmonds, D. J., Pekar, J. J., & Mostofsky, S. H. (2008). Meta-analysis of Go/NoGo tasks demonstrating the fMRI activation associated with response inhibition is task-dependent. *Neuropsychologia, 46*, 224-232.

Singer, W. (2001). Consciousness and the binding problem. *Annals of the New York Academy of Sciences, 929*, 123–146.

Snedecor, G. W., & Cochran, W. G. (1989). *Statistical methods*. Iowa: Iowa State University Press.

Sörnmo, L., & Laguna, P. (2005). *Bioelectrical signal processing in cardiac and neurological applications*. Cambridge: Academic Press.

Sowell, E. R., Thompson, P. M., Mattson, S. N., Tessner, K. D., Jernigan, T. L., Riley, E. P., & Toga, A. W. (2002). Regional brain shape abnormalities persist into adolescence after heavy prenatal alcohol exposure. *Cerebral Cortex, 12*, 856–865.

Sowell E. R., Thompson P. M., Mattson S. N., Tessner K. D., Jernigan T. L., Riley E. P., & Toga A.W. (2001). Voxel-based morphometric analyses of the brain in children and adolescents prenatally exposed to alcohol. *Neuroreport, 12*, 515–23.

Spohr, H. L., & Steinhausen, H. C. (2008). Fetal alcohol spectrum disorders and their persisting sequelae in adult life. *Deutsches Ärzteblatt International*, 105, 693–698.

Stephen, J. M., Kodituwakku, P. W., Kodituwakku, E. L., Romero, L., Peters, A. M., Sharadamma, N. M., Caprihan, A., & Coffman, B. A. (2012). Delays in auditory processing identified in preschool children with FASD. *Alcoholism: Clinical and Experimental Research, 36*, 1720-1727.

Suffczynski, P., Kalitzin, S., Pfurtscheller, G., & Lopes da Silva, F. H. (2001). Computational model of thalamocortical networks: dynamical control of alpha rhythms in relation to focal attention. *International Journal of Psychophysiology, 43*, 25–40.

Sugiura, N. (1976). Further analysts of the data by Akaike' s information criterion and the finite corrections. *Communications in Statistics (Theory and Methods), 7*, 13-26.

Tallon-Baudry, C., Bertrand, O., Delpuech, C., & Pernier, J. (1996). Stimulus specificity of phase-locked and non-phase-locked 40 Hz visual responses in human. *The Journal of Neuroscience, 16*, 4240–4249.

Tarvainen, M. P., Hiltunen, J. K., Ranta-aho, P. O., & Karjalainen, P. A. (2004). Estimation of nonstationary EEG with Kalman smoother approach: an application to event-related synchronization (ERS). *IEEE Transactions on Biomedical Engineering, 51*, 516–524.

Thakor, N. V., & Shanbao Tong. (2004). Advances in quantitative electroencephalogram analysis methods. *Annual Review of Biomedical Engineering, 6*, 453-NaN-3.

Ting, C.-M., Salleh, S.-H., Zainuddin, Z. M., & Bahar, A. (2011). Spectral estimation of nonstationary eeg using particle filtering with application to event-related desynchronization (ERD). *IEEE Transactions on Biomedical Engineering, 58*, 321–331.

Twisk, J. W. R. (2006). *Applied multilevel analysis: a practical guide for medical researchers*. Cambridge University Press.

Van Veen, B. D., Van Drongelen, W., Yuchtman, M., & Suzuki, A. (1997). Localization of brain electrical activity via linearly constrained minimum variance spatial filtering. *IEEE Transactions on Biomedical Engineering, 44*, 867–880.

Vecchiato, G., Cherubino, P.,Trettel, A., & Babiloni, F. (2013). Neuroelectrical brain imaging tools for the study of the efficacy of TV advertising stimuli and their application to neuromarketing. New York: Springer Science & Business Media.

Viana-Wackerman, P. C., Erikson, F. F., Esser, G, Schmidt, M. H., & Laucht, M. et al (2007). Lower P300 amplitude in eight-year-old offspring of alcoholic fathers with a delinquent history. *European Archive of Psychiatry and Clinical Neuroscience, 4,* 211-216.

Wang, L., Li, Y., Metzak, P., He, Y., & Woodward, T. S. (2010). Age-related changes in topological patterns of large-scale brain functional networks during memory encoding and recognition. *NeuroImage, 50*, 862–872.

Wang, N., Zhang, L., & Liu, G. (2015). EEG-based research on brain functional networks in cognition. *Biomedical Materials and Engineering, 26*, 1107-1114.

Wang, Y., Veluvolu, K. C., & Lee, M. (2013). Time-frequency analysis of band-limited EEG with BMFLC and Kalman filter for BCI applications. Journal of *Neuroengineering and Rehabilitation, 10*, 109.

Wattendorf, D. J., & Muenke, M. (2005). Fetal alcohol spectrum disorders. *American Family Physician, 72*, 279–285.

Yerkes, R. M., & Dodson, J. D. (1908). The relation of strength of stimulus to rapidity of habit-formation. *Journal of Comparative Neurology and Psychology, 18*, 459–482.

Yuan, W., Holland, S. K., Cecil, K. M., Dietrich, K. N., Wessel, S. D., Altaye, M., et al. (2006). The impact of early childhood lead exposure on brain organization: a functional magnetic resonance imaging study of language function. *Pediatrics, 118*, 971–977.

Zetterberg, L. H. (1969). Estimation of parameters for a linear difference equation with application to EEG analysis. *Mathematical Biosciences, 5*, 227–275.

Zhang, Z. G., Hung, Y. S., & Chan, S. C. (2011). Local polynomial modelling of time-varying autoregressive models with application to time-frequency analysis of event-related EEG. *IEEE Transactions on Biomedical Engineering, 58*, 557–566.

Zhou, F. C., Sari, Y., & Powrozek, T. A. (2005). Fetal alcohol exposure reduces serotonin innervation and compromises development of the forebrain along the serotonergic pathway. *Alcoholism: Clinical and Experimental Research, 29*, 141–149.

Appendix A

Compare Peaks AIC-AAR

We extracted multiple cross-sections from the time-varying AIC-AAR spectral estimates to assess the frequency domain represenation of the simulated data prior to the application of preprocessing procedures. One of these cross-sections taken at 1.25 seconds from Condition 1 is presented in the Figure A.1 below.

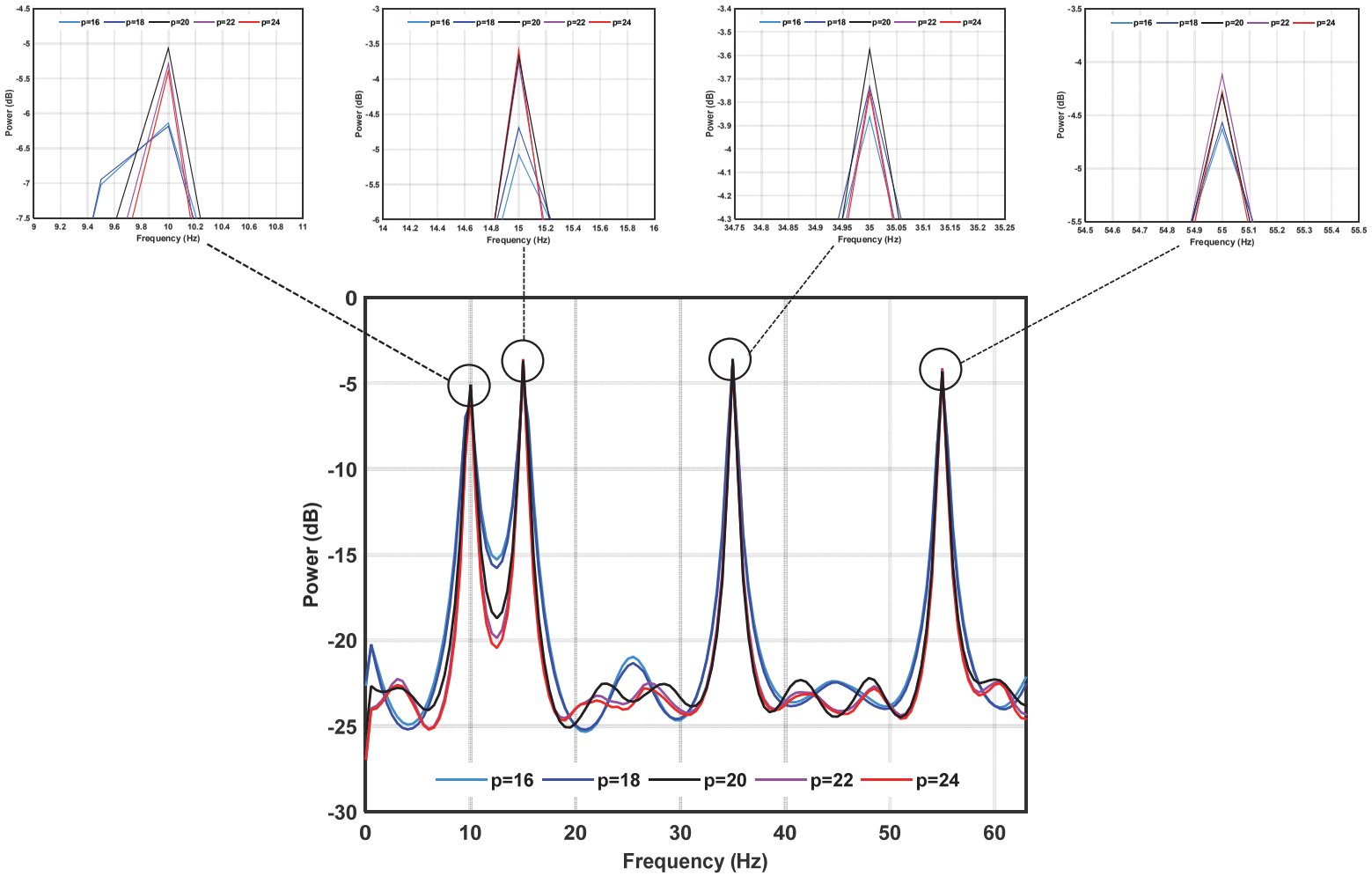

Figure A.1: A cross-section of the AIC-AAR time-frequency representation from Condition 1.The estimates from different model orders are overlaid in the main panel. In the upper panels, the peaks of each component are magnified to assess peak location.

Appendix B

Statistical Thresholds Applied to Simulated Data

We tested four procedures to correct for increases in the Type I error rate due to multiple comparisons within the time-frequency condition contrasts. The procedures tested were:

- Bonferonni correction,
- Bonferonni-Holm's correction (Holm, 1979),
- Durka *et al.*'s (2004) False Discovery Rate (FDR) correction procedure, and
- Benjamini and Yekutieli (2001) correction procedure implemented in EEGLAB (Delorme & Makeig, 2004)

The details of these methods are provided in the respective publications and have been widely applied across a broad range of studies; they are also available in a number commercial and open-source software suites.

Our simulations reflect known properties of these procedures: the Bonferonni correction being the most conservative, while the Bejamini and Yekutieli's (2001) procedure implemented in EEGLAB provides the least stringent statistical threshold (see Figure B.1 and Figure B.2 below for the resultant simulated significance contrasts for STFT and AIC-AAR estimates respectively). Due to the varying thresholds produced by these procedures, a consideration when applying such methods would be the magnitude of effect(s) for a set of given comparisons. Where the effect-sizes are large, one would opt for a conservative approach such as the Bonferonni correction;

however, in the instance of small effect-sizes, one may use a less stringent approach to guard against overcorrecting and generating Type II statistical errors. Our simulations pose an example of large effect-sizes due to the sinusoidals being compared to regions of noise (5 dB) in the corresponding time-frequency region of the associated condition.

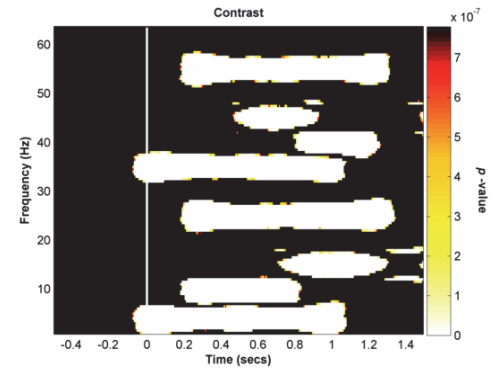

(a) Bonferonni (*FDR* = 7.7809e-07)

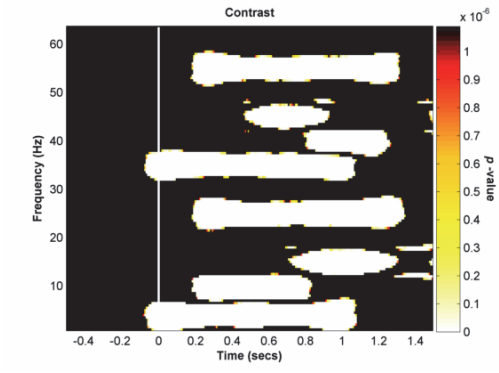

(b) Bonferonni-Holms (*FDR* = 1.0905e-06)

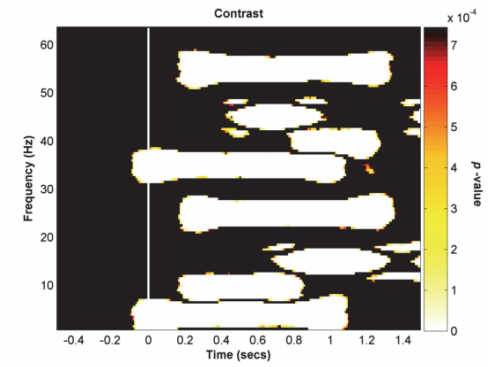

(c) Durka et al (*FDR* = 7.4442e-04)

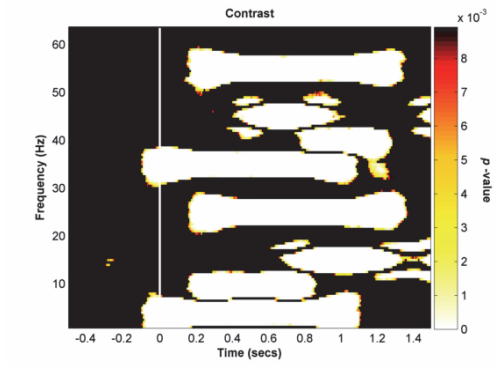

(d) Delorme and Makieg (*FDR* = 0.0089)

Figure B.1: Masked probability contrasts for the STFT estimator. (a) Threshold set using Bonferonni correction; (b) threshold set using Bonferonni-Holm's correction; (c) threshold set using Durka *et al.*'s correction, and (d) EEGLAB's correction procedure.

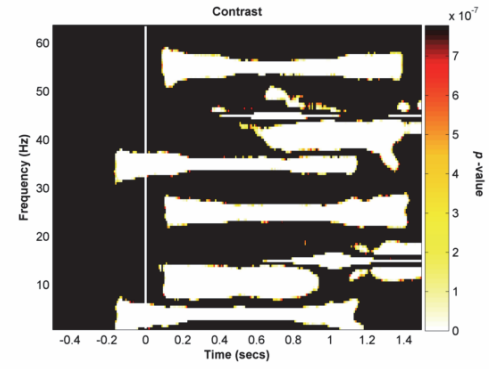

(a) Bonferonni (*FDR* = 7.7809e-07)

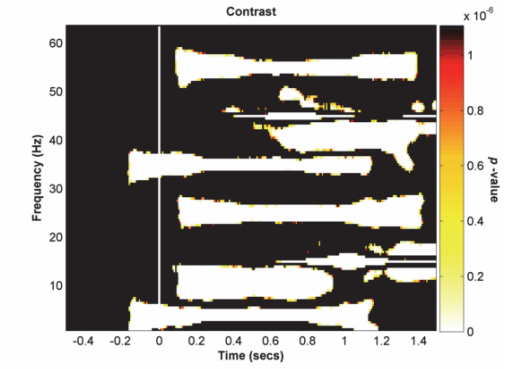

(b) Bonferonni-Holms (*FDR* = 6.8839e-06)

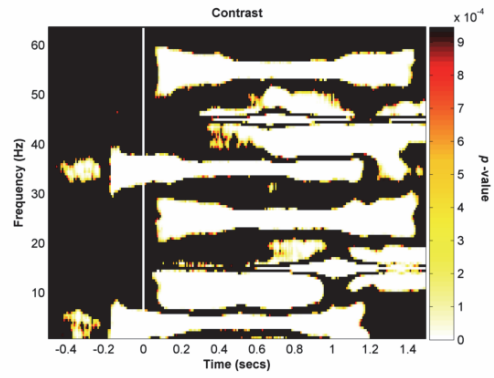

(c) Durka et al (*FDR* = 9.4569e-04)

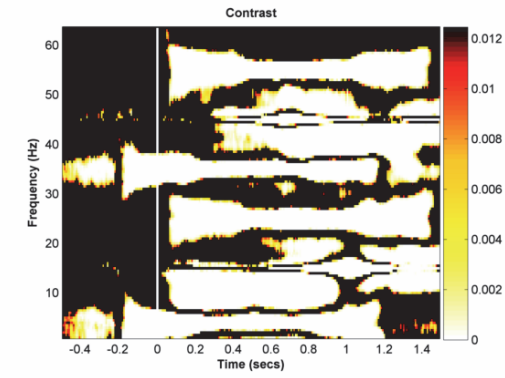

(d) Delorme and Makieg (*FDR* = 0.0125)

Figure B.2: Masked probability contrasts for the AIC-AAR estimator. (a) Threshold set using Bonferonni correction; (b) threshold set using Bonferonni-Holm's correction; (c) threshold set using Durka *et al*'s correction, and (d) EEGLAB's correction procedure.

Appendix C

Model Order, Estimation Bias, and Resolution

As model order is the only free parameter in an AR-model, optimal selection is crucial. The functional significance of model-order selection is the trade-off in estimation bias and variance and how this trade-off affects resolution and dynamic range in the resultant time-varying spectra. For AR spectral estimates, the relationship between bias and variance is defined heuristically compared to the formal descriptions of Fourier-based estimates (Sörnmo & Laguna, 2005).

Lower-models orders yield highly biased spectra with low variability. In these instances, closely spaced components cannot be resolved; the dynamic range of the estimate is greatly reduced. As estimation bias is related to dynamic range and spectral resolution, the resolution of the resultant spectra are also affected.

Higher-order models provide a reduction in estimation bias; however, this comes at the cost of increased variability. Higher model orders also provide greater dynamic range with enhanced frequency resolution associated with the reduction in bias. In the instances where overfitting occurs due to too high a model order, component peaks split and shift apart. Spurious peaks may also arise within the context of highly variable spectra.

In order to assess the impact of the above-mentioned trade-offs at different model orders in the region of those selected by AIC-C and AIC, we generated a number of TFD's with different model orders. We also included a representation generated using a *short-time Fourier transform* (STFT) for comparison. Time-frequency representations are presented in Figure C1 below.

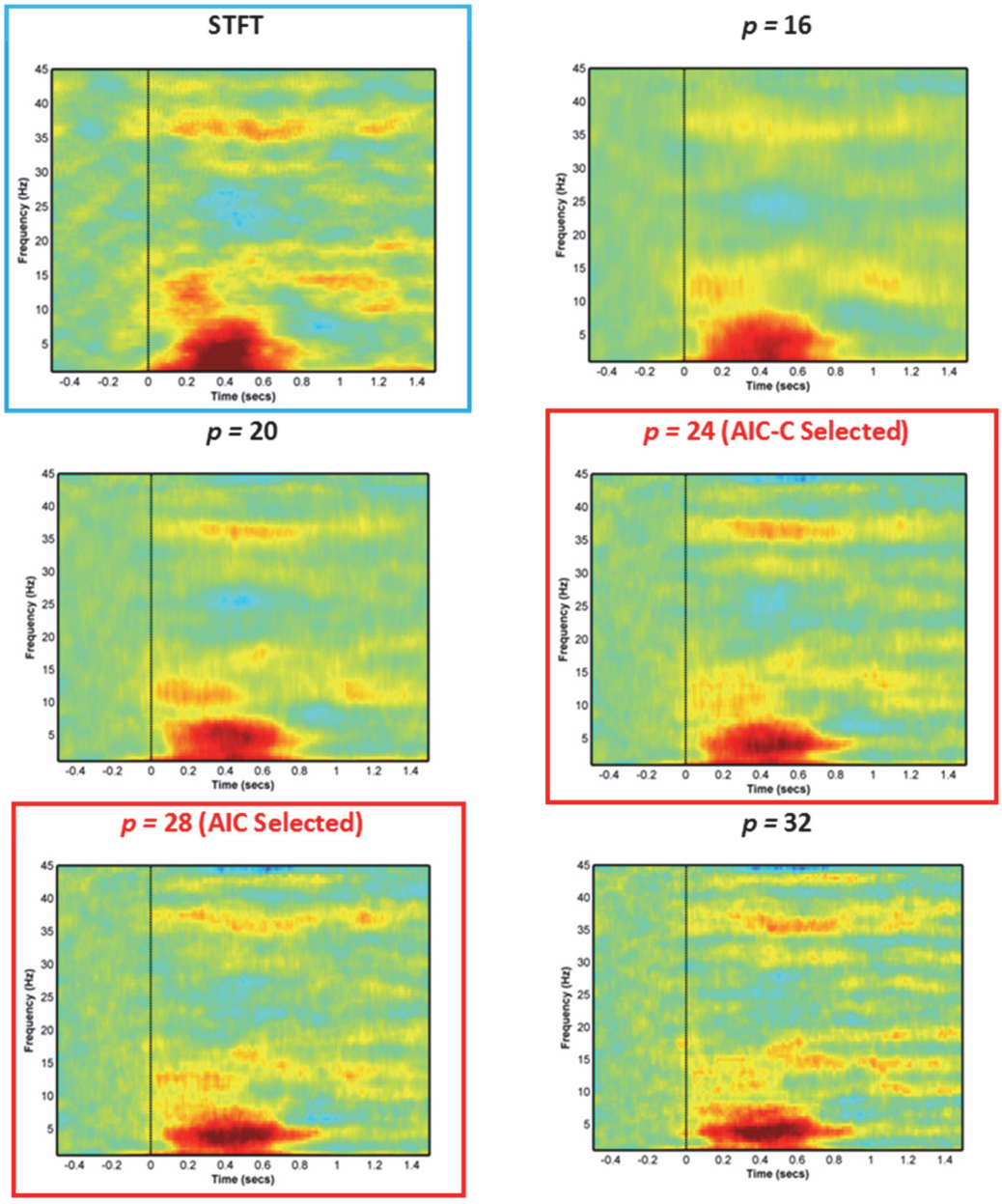

Figure C.1: TFDs generated using non-parametric (STFT) and parametric spectral estimators taken from electrode Fz for a control subject under the Go-condition. The STFT is presented in the top left panel surrounded by a blue box. The other panels provide AIC-AAR based representations at different model orders. Highlighted TFRs are generated based on model-orders chosen in the section 2.3.4.2.

Based on the information presented in Figure C1, we can observe the components present within the STFT TFD in all AIC-AAR models. At $p = 16$, there is less variability in the TFD and the dynamic range appears to be reduced relative to the STFT TFD. The

AIC and AIC-C selected TFDs appear more variable with greater dynamic range and contain the components present in the STFT representation; however, components specification in time and frequency are different owing to differences in tapering, estimation bias-variance, and consequential changes in time-frequency resolution. For example, in the AIC-AAR distributions the low-frequency delta/theta oscillation appears more well-defined in frequency and has a longer duration in comparison to the STFT. This is partly owing to the use of a rectangular window; however, with increasing model order the effect is more pronounced. At model orders > 30, the components start to split and the TFD becomes highly variable indicating over-fitting, this suggests a higher order model (greater than 28) may start to introduce spurious effects in the AAR-based TFRs

Appendix D

Statistical Thresholds Applied to Empirical Data

We tested four procedures to correct for increases in the Type I error rate due to multiple comparisons within the time-frequency condition contrasts. The procedures tested were:

- Bonferonni correction,
- Bonferonni-Holm's correction (Holm, 1979),
- Durka *et al.*'s, (2004) False Discovery Rate (FDR) correction procedure, and
- Benjamini and Yekutieli's (2001) correction procedure implemented in EEGLAB (Delorme & Makeig, 2004)

The details of these methods are provided in the respective publications and have been widely applied across a broad range of studies; they are also available in a number commercial and open-source software suites. The empirical contrasts shown herein have smaller effect-sizes in comparison to the simulated data, as such Bonferonni, Bonferonni-Holms, and Durka *et al.*—the more stringent of the four correction procedures—overcorrect and result in Type II errors. EEGLAB's fdr.m function yielded no significant regions, thus, we used a threshold of 0.01 as suggested on the EEGLAB Wiki (Delorme & Makeig, 2004).

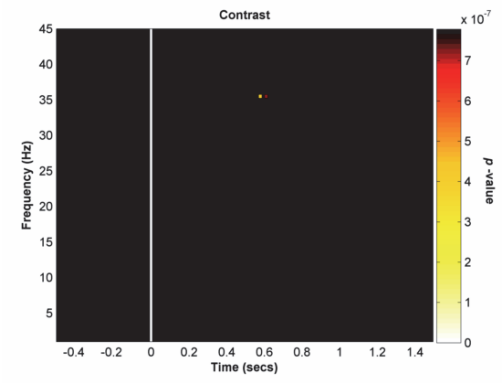

(a) Bonferonni (*FDR* = 7.7809e-06)

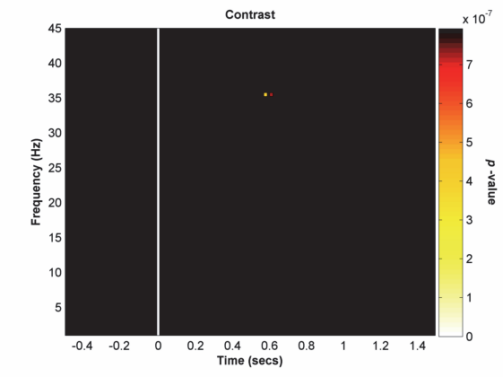

(b) Bonferonni-Holms (*FDR* = 6.8839e-06)

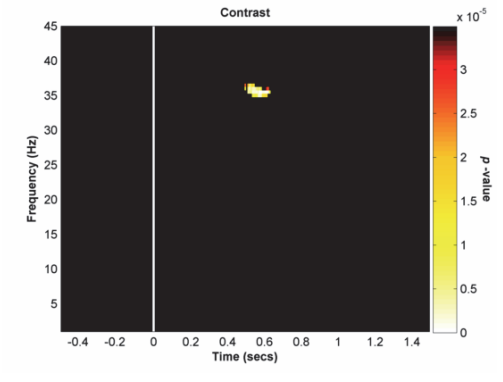

(c) Durka et al (*FDR* = 3.4915e-05)

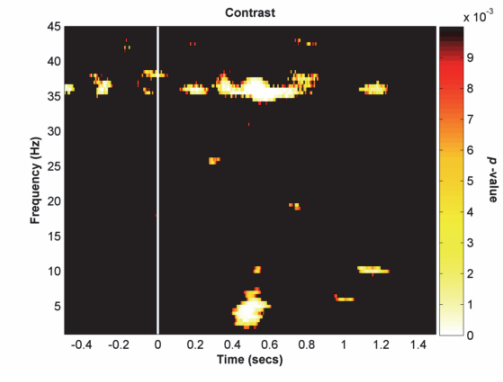

(d) Delorme and Makieg (*FDR* = 0.01)

Figure D.1: Masked probability contrasts for the STFT estimator. (a) Threshold set using Bonferonni correction; (b) threshold set using Bonferonni-Holm's correction; (c) threshold set using Durka *et al*.'s correction, and (d) EEGLAB's correction procedure.

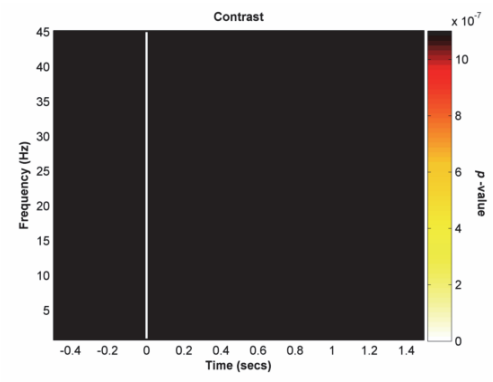

(a) Bonferonni (*FDR* = 7.7809e-06)

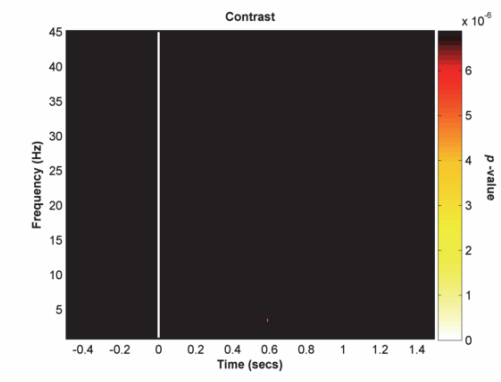

(b) Bonferonni-Holms (*FDR* = 6.8839e-06)

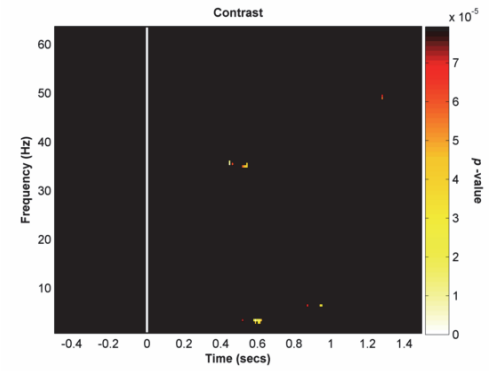

(c) Durka et al (*FDR* = 7.9328e-05)

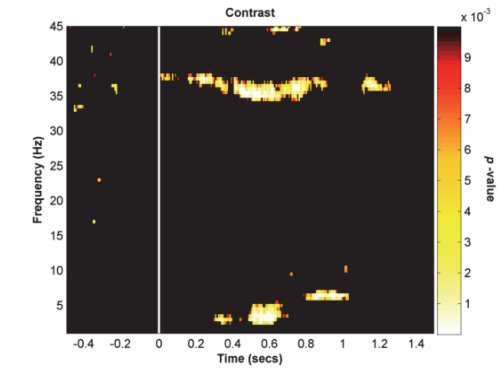

(d) Delorme and Makieg (*FDR* = 0.01)

Figure D.2: Masked probability contrasts for the AIC-AAR estimator. (a) Threshold set using Bonferonni correction; (b) threshold set using Bonferonni-Holm's correction; (c) threshold set using Durka *et al*'s correction, and (d) EEGLAB's correction procedure.

Appendix E

Time-Frequency Contrasts by Group

We generated group time-frequency contrasts using the methods outlined in Chapter 2, these contrast are presented in Figure E.1. The contrasts demonstrate regions of interest wherein the two experimental groups differed in either condition. In the Go-condition group contrast, one can observe greater beta power within the control group; this relative increase in oscillatory power is also observed across other electrodes within the frontal region within the same band. Our analysis in Chapter 4 focuses on the oscillation as a frontal regional feature. Within the NoGo-condition group contrast, one observes greater gamma and beta oscillatory power within the control group, as well as a late decrease in beta power. Unlike the beta feature, the gamma feature was spatially confined to the Fz electrode. Our analysis in Chapter 3 focuses on the oscillation as a frontal mid-line feature. A late beta feature differentiates the groups in the NoGo condition; however, this feature is not analysed, as little is known about its role in Go/NoGo task performance. The same features were identified with the AIC-AAR estimator, although with slight differences in time and frequency as well as magnitude of differences.

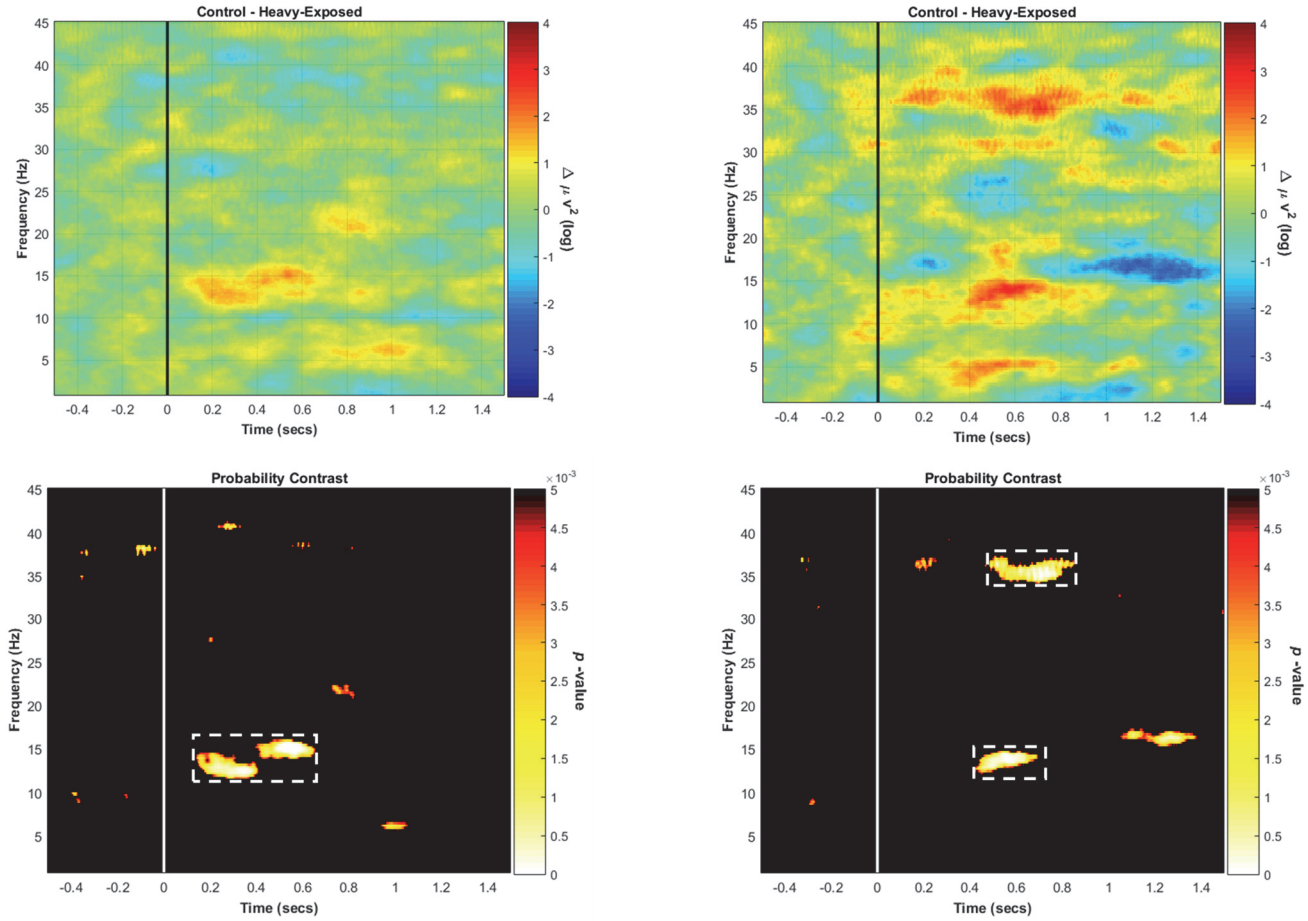

Figure E.1: Group contrasts at the Fz electrode using the STFT time-frequency representations. (Left) Go-condition group contrast: (Right) NoGo-condition group contrast. Regions of significant differences in the probability contrast are highlighted with a white-box (FDR = .005). The same features were identified with the AIC-AAR estimator, although with slight differences in time and frequency as well as magnitude of differences.